MULTIDISCIPLINARY CENTER FOR EARTHQUAKE ENGINEERING RESEARCH
A National Center of Excellence in Advanced Technology Applications

ISSN 1520-295X

Experimental Study on the Seismic Design and Retrofit of Bridge Columns Including Axial Load Effects

by

Anindya Dutta, Tatiana Kokorina and John B. Mander
University at Buffalo, State University of New York
Department of Civil, Structural and Environmental Engineering
Ketter Hall
Buffalo, New York 14260-4300

Technical Report MCEER-99-0003

February 22, 1999

This research was conducted at University at Buffalo, State University of New York and was supported by the Federal Highway Administration under contract number DTFH61-92-C-00106.

NOTICE

This report was prepared by the University at Buffalo, State University of New York as a result of research sponsored by the Multidisciplinary Center for Earthquake Engineering Research (MCEER) through a contract from the Federal Highway Administration. Neither MCEER, associates of MCEER, its sponsors, University at Buffalo, State University of New York, nor any person acting on their behalf:

a. makes any warranty, express or implied, with respect to the use of any information, apparatus, method, or process disclosed in this report or that such use may not infringe upon privately owned rights; or

b. assumes any liabilities of whatsoever kind with respect to the use of, or the damage resulting from the use of, any information, apparatus, method, or process disclosed in this report.

Any opinions, findings, and conclusions or recommendations expressed in this publication are those of the author(s) and do not necessarily reflect the views of MCEER or the Federal Highway Administration.

MULTIDISCIPLINARY CENTER FOR EARTHQUAKE ENGINEERING RESEARCH
A National Center of Excellence in Advanced Technology Applications

Experimental Study on the Seismic Design and Retrofit of Bridge Columns Including Axial Load Effects

by

Anindya Dutta[1], Tatiana Kokorina[1] and John B. Mander[2]

Publication Date: February 22, 1999
Submittal Date: September 12, 1998

Technical Report MCEER-99-0003

Task Number 106-F-2.1

FHWA Contract Number DTFH61-92-C-00106

1 Research Assistant, Department of Civil, Structural and Environmental Engineering, University at Buffalo, State University of New York
2 Associate Professor, Department of Civil, Structural and Environmental Engineering, University at Buffalo, State University of New York

MULTIDISCIPLINARY CENTER FOR EARTHQUAKE ENGINEERING RESEARCH
University at Buffalo, State University of New York
Red Jacket Quadrangle, Buffalo, NY 14261

Preface

The Multidisciplinary Center for Earthquake Engineering Research (MCEER) is a national center of excellence in advanced technology applications that is dedicated to the reduction of earthquake losses nationwide. Headquartered at the University at Buffalo, State University of New York, the Center was originally established by the National Science Foundation in 1986, as the National Center for Earthquake Engineering Research (NCEER).

Comprising a consortium of researchers from numerous disciplines and institutions throughout the United States, the Center's mission is to reduce earthquake losses through research and the application of advanced technologies that improve engineering, pre-earthquake planning and post-earthquake recovery strategies. Toward this end, the Center coordinates a nationwide program of multidisciplinary team research, education and outreach activities.

MCEER's research is conducted under the sponsorship of two major federal agencies, the National Science Foundation (NSF) and the Federal Highway Administration (FHWA), and the State of New York. Significant support is also derived from the Federal Emergency Management Agency (FEMA), other state governments, academic institutions, foreign governments and private industry.

The Center's FHWA-sponsored Highway Project develops retrofit and evaluation methodologies for existing bridges and other highway structures (including tunnels, retaining structures, slopes, culverts, and pavements), and improved seismic design criteria and procedures for bridges and other highway structures. Specifically, tasks are being conducted to:

- assess the vulnerability of highway systems, structures and components;
- develop concepts for retrofitting vulnerable highway structures and components;
- develop improved design and analysis methodologies for bridges, tunnels, and retaining structures, which include consideration of soil-structure interaction mechanisms and their influence on structural response;
- review and recommend improved seismic design and performance criteria for new highway systems and structures.

Highway Project research focuses on two distinct areas: the development of improved design criteria and philosophies for new or future highway construction, and the development of improved analysis and retrofitting methodologies for existing highway systems and structures. The research discussed in this report is a result of work conducted under the existing highway structures project, and was performed within Task 106-F-2.1, "Seismic Retrofit of Shear-Critical Bridge Columns" of that project as shown in the flowchart on the following page.

The overall objective of this task was to develop retrofit procedures for reinforced concrete bridge columns and their connections. This report extends the Control and Repairability of Damage (CARD) column design philosophy for new structures that uses replaceable fuse bars in the plastic hinge zone (see technical report NCEER-97-0013) for the design of new structures. The work reported herein resulted in the development of a new philosophy, ReCARD (Retrofit,

Control and Repairability of Damage) that uses the same fuse-bar concept adopted in CARD designs. Fuse-bars are spliced into existing non-ductile columns that have vulnerable hinge zone details. This type of retrofit permits relatively rapid and cost-effective repairs following a damaging earthquake. Both the CARD and ReCARD details are examined to verify that they have adequate fatigue life under realistic seismic loading, including the effects of variable axial loads that arise from a combination of the framing action of multiple column pier bents and vertical ground motions.

SEISMIC VULNERABILITY OF EXISTING HIGHWAY CONSTRUCTION
FHWA Contract DTFH61-92-C-00106

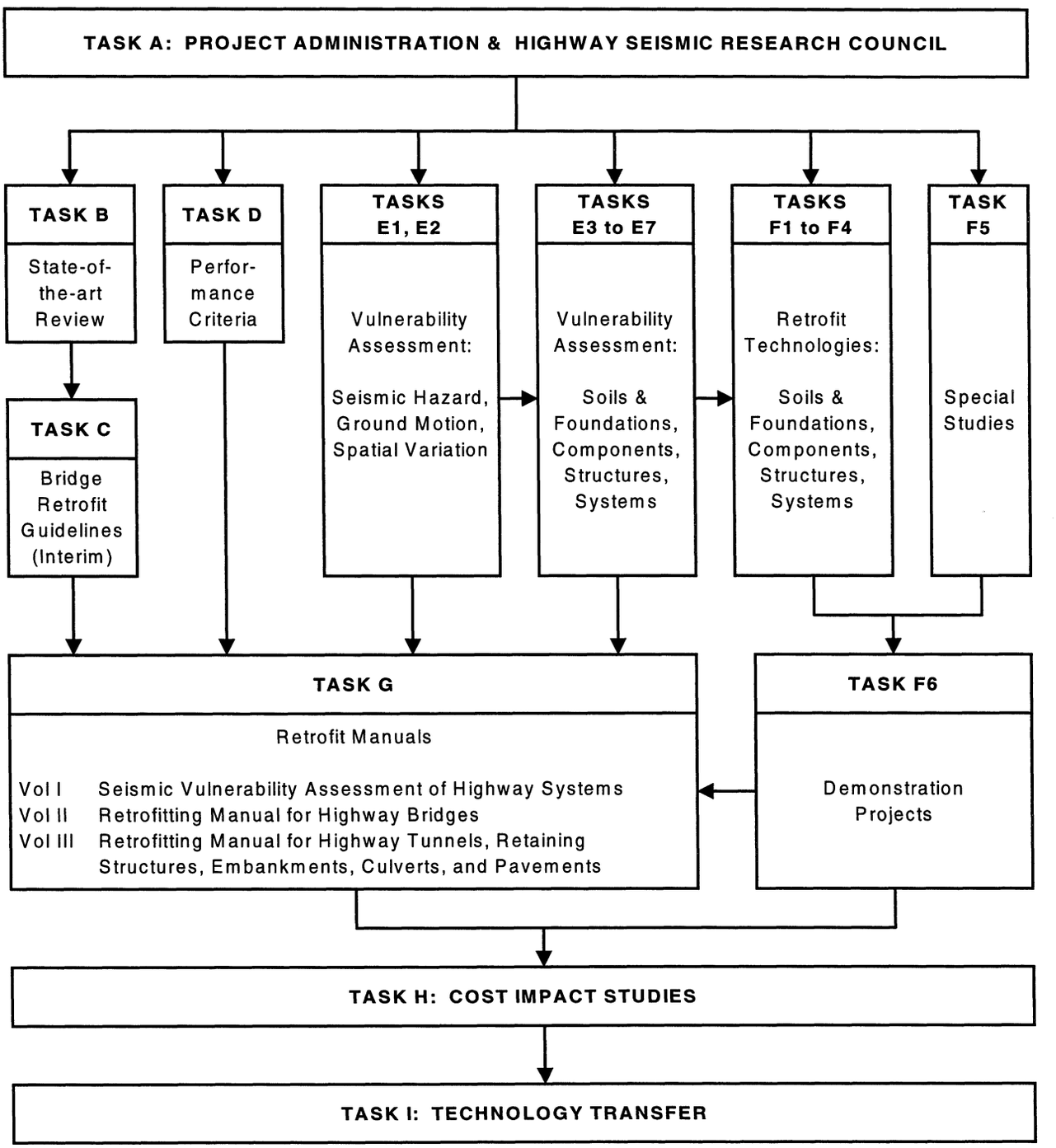

ABSTRACT

This research is concerned with validation of alternative theories for seismic design and retrofit of bridge structures. The intent of these methodologies is to not only maintain life safety of bridges in a strong earthquake, but also to control damage while accommodating large seismically-induced deformations in order to maintain post-earthquake serviceability.

The primary purpose of this research endeavor is to verify that both Control and Repairability of Damage (CARD) and Retrofit, Control and Repairability of Damage (ReCARD) sacrificial fuse-bar plastic hinge details have adequate fatigue life under realistic seismic loading –including the effects of variable axial loads that arise from a combination of the framing action of multiple column pier bents and vertical ground motion.

As a secondary purpose, a new technique called Quasi-Earthquake Displacement (QED) Experimentation is developed to verify the CARD and ReCARD construction details. The experimental technique uses a non-linear time-history computational simulation to predict seismic displacements (and forces) in a prototype structure. These earthquake-induced actions are scaled to permit laboratory experiments to be conducted on reduced scale subassemblages of the prototype structure.

It is concluded that reinforced concrete bridge columns that possess sacrificial /replaceable fuse-bars have sufficient cyclic capacity under the most adverse seismic loading conditions (including large axial load variation) to sustain a strong foreshock, mainshock and aftershock.

ACKNOWLEDGEMENTS

This research was carried out at the Department of Civil, Structural and Environmental Engineering, State University of New York at Buffalo.

Financial support is gratefully acknowledged from the Multidisciplinary Center for Earthquake Engineering Research through contract with the Federal Highway Administration on Seismic Vulnerability of Existing Highway Construction, FHWA Contract No. DTFH61-00106, Task 106-F-2.1.

Mr Jim Shea of Master Builders is thanked for his generous donation of specimens and valuable tips during the mix design of concrete.

TABLE OF CONTENTS

LIST OF ILLUSTRATIONS

LIST OF TABLES

SECTION 1
INTRODUCTION

Recent earthquakes, particularly the 1989 Loma Prieta and 1994 Northridge earthquakes in California, and the 1995 Kobe earthquake in Japan have caused extensive damage to a considerable number of bridge structures that were ostensibly designed for nominal seismic forces. The post-earthquake serviceability of many damaged bridges were jeopardized. This was due to the prevailing ductile design philosophy that permits damage while aiming to preserve safety to life and limb. Consequently, the foundation of the ductile design philosophy has been seriously questioned. For example, Mander and Cheng (1997) advocate a new philosophy called Damage Avoidance Design (DAD). This approach is especially suited to precast/prestressed construction where dry-joint connections are used instead of conventional plastic hinges. The DAD philosophy is a radical departure from the conventional wisdom of hysteretic energy dissipation (damage) and may not always be tenable to design engineers even though conventional ductile design may be untenable from an owner's point of view. To this end, Cheng and Mander (1997) developed an alternative design philosophy called Control and Repairability of Damage (CARD). The ductile design philosophy can be maintained, but it is the detailing of the plastic hinge zones that has been improved to permit repair of earthquake-induced damage.

The CARD philosophy introduced by Cheng and Mander (1997) was primarily aimed at new construction, whereby it is possible to design structures that serve two specific needs: Firstly, columns are designed to be strong enough to withstand the expected shaking, with damage incurred only at specific locations. Secondly, since the damage location is predefined, it is possible to quickly repair the column following an event and restore full operational serviceability.

Cheng (1997) proposed that the CARD philosophy could also be extended for use in retrofit purposes. Thus the notion of ReCARD – Retrofit Control and Repairability of Damage

was born. From experimental results on near full-size bridge columns with lap splices at the base, Cheng (1997) showed that it is possible to restrict and localize damage and then repair that damage so that the column remains fully functional by using some careful detailing strategies.

The purpose of this report is twofold. First, the Cheng and Mander (1997) CARD column design philosophy for new structures that uses replaceable fuse bars in the plastic hinge zone is extended to incorporate retrofit of existing structures. Thus a ReCARD philosophy is advanced that uses the same fuse-bar concept adopted in CARD designs. Fuse-bars are spliced into existing non-ductile columns that have faulty hinge zone details; such a retrofit permits repairs following a damaging earthquake.

The second purpose of this report is to verify that both CARD and ReCARD details have adequate fatigue life under realistic seismic loading – including the effects of variable axial loads that arise from a combination of the framing action of multiple column pier bents and vertical ground motions.

Following this introductory section, the report is divided into eight sections. Section 2 deals with the previous work and a basic overview of CARD philosophy and its extension to ReCARD principles. Section 3 deals with the experimental approach adopted in the laboratory testing of near full size specimens. These specimens are introduced in Section 4. Section 5 describes the constant amplitude results on the retrofitted columns. The Quasi-Earthquake Displacement (QED) experimentation that is developed as part of the current program is introduced in Section 6. Results from the QED tests on specimens incorporating CARD and ReCARD details are presented in Section 7. Section 8 presents a discussion comparing the theoretical and experimental fatigue life of these specimens. Finally a summary and references cited in this research are presented in Sections 9 and 10, respectively.

SECTION 2
RESEARCH OVERVIEW

2.1 BACKGROUND

In the United States there is a large inventory of bridges that were built before the era of modern seismic design. An evaluation of these bridges in the light of current understanding has revealed major flaws with respect to reinforcement detailing. Since it is not economically feasible to demolish and replace all substandard existing structures and start afresh, the concept of seismic retrofitting has become an issue both for researchers as well as the practicing engineering community.

One of the most common detailing deficiencies found in existing bridge columns is the presence of lap splices in the potential plastic hinge zones. These bridges were typically designed with compression lap splices consisting of twenty longitudinal bar diameters ($20 d_b$). Due to insufficient lap length, tensile bond failure in the lap splice is likely to occur in a strong earthquake following the spalling of the cover concrete. This may also mark the end of usable life of the bridge column since the residual strength and energy dissipation capacity following bond failure is negligible.

In their attempts to seismically retrofit such bridge columns researchers have primarily aimed at increasing transverse confinement of the longitudinal rebar using a variety of techniques. The foremost amongst these techniques is the use of steel jackets (Priestley et al. 1996). Other methods such as composite jackets including fiberglass as well as carbon fiber that can be used to confine the potential plastic hinge zones have also been investigated (Priestley et al. 1996; Xiao et al. 1997) and these are beginning to find increasing acceptance in the field. Although retrofit techniques currently in vogue are effective in rehabilitating existing structures by increasing the inelastic (plastic) deformation capacity, this is generally associated with an

increase (albeit a modest increase) in the strength capacity. Any accidental or intentional flexural strengthening action in columns will raise the shear demand on those columns as well as the adjacent elements (cap beams and/or superstructures) and connections. Such strengthening will generally cause damage to both the column elements and connections or other undesirable elements (superstructure or foundation beams) that maybe irreparable following a strong earthquake.

It is extremely unfortunate that the present state-of-the-art seismic design/retrofitting procedures are not intended to limit and/or avoid structural damage, but merely to ensure life-safety. Moreover, post-earthquake serviceability is generally not possible owing to lack of repairability strategies. As stated in the research of Chai (1996), a possible ultimate limit state exists, particularly for large jacket thickness, where failure of a steel jacketed column may be governed by the fracture of the longitudinal reinforcement instead of the ultimate compressive strain of the concrete. The failure in low cycle fatigue of the longitudinal reinforcement (see for example Chai et al. 1991) is impossible to repair as the damage generally penetrates well into the pile cap beam connection. Even though the longitudinal reinforcement might not have fractured in an event, the degree of damage incurred and the extent of the fatigue life consumed are pertinent questions that cannot be answered—i.e. after an earthquake it is not possible to make an assessment of the remaining fatigue life, if any.

The problems discussed above can be explained with the use of fragility curves illustrated in figure 2-1. These curves show the expected performance and damage states of a hypothetical column before and after retrofit by either steel or composite fiber jacketing. As an example it may be presumed that for the unretrofitted column, the damage states of interest are cracking/spalling of the cover concrete which marks the onset of any visible damage and last but not the least, some form of a life safety limit state signifying impending collapse. The various median PGAs are typical of non-seismically designed bridge columns found in the United States. Thus the boundary between cracking of cover concrete and the life safety limit state can be conceived of damage states that are repairable following a seismic event. The retrofitted column

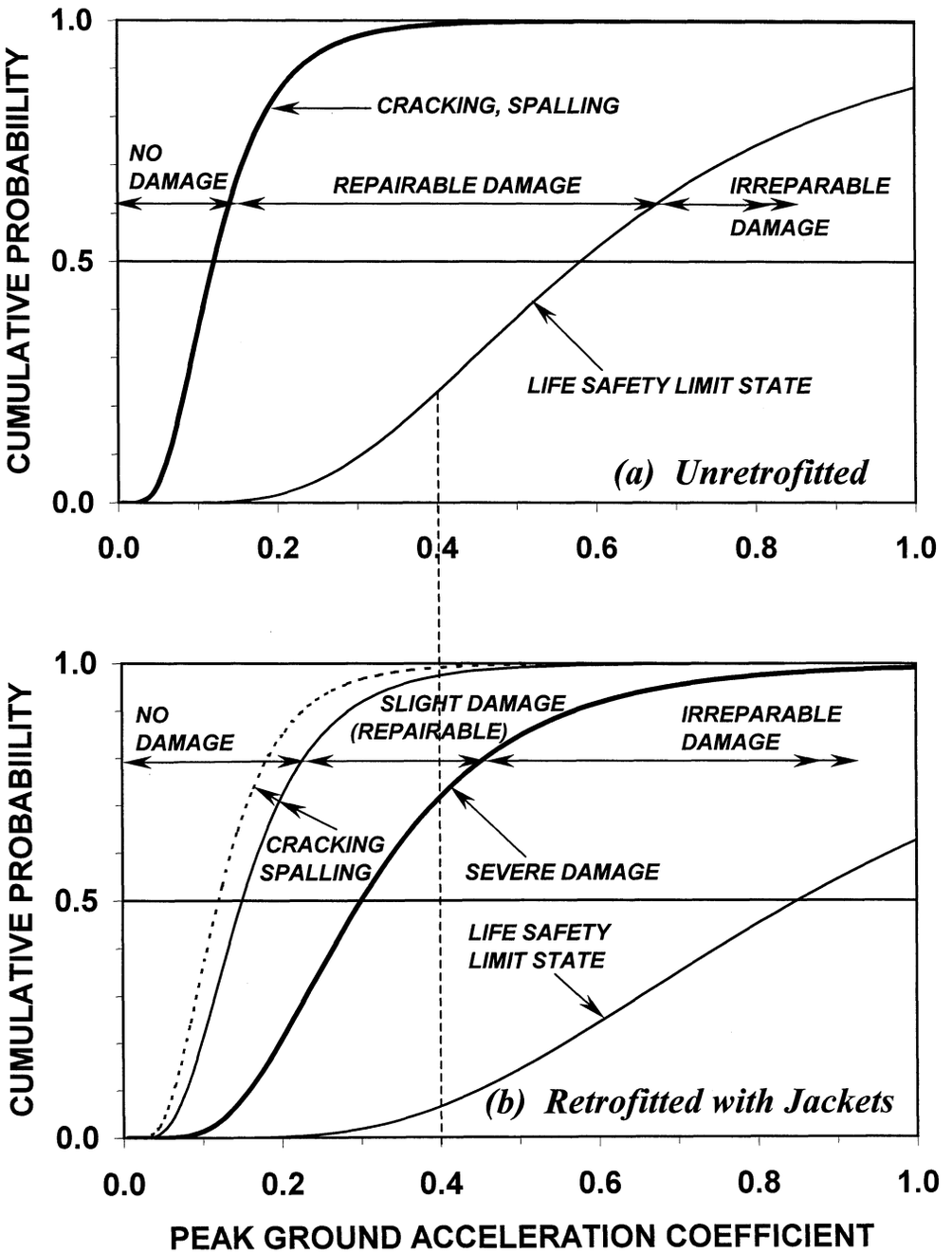

Figure 2-1 Fragility Curves for a Hypothetical Bridge Column before and after Retrofit with Steel/Epoxy Jacketting.

shown in figure 1-1b however reveals some interesting information. The median PGA for onset of damage improves by a small amount when compared to the curve for the unretrofitted column (in dotted lines). The fragility curve corresponding to the life-safety (collapse) limit state will shift considerably due to the effect of increased transverse confinement. However a new damage state in between these two cases will be introduced corresponding to some form of severe damage (e.g. fatigue fracture of the longitudinal reinforcing bars) that will effectively mark the boundary between repairable and irrepairable damage states. It can also be seen that for a peak ground acceleration of 0.4, there is about 20% probability that the life safety limit state can be mobilized for the unretrofitted column. Although for the retrofitted column there is even a lesser probability for the same limit state, there is unfortunately about 75% probability that severe damage will occur at the same level of ground shaking.

Although an engineer may choose to "do nothing" when it comes to retrofitting, there are cases when it is necessary to retrofit a bridge especially when post-earthquake functionality is an issue. This arises when there is little or no redundancy with respect to alternate routes in a transportation network or if the bridge itself is critical for maintaining lifeline usage following a major seismic event. Under such circumstances it may be desirable that the structure incur no or limited damage in the event of a maximum credible earthquake. However, any earthquake induced damage should ideally be repairable with minimum disruption of traffic flow. Unfortunately such performance objectives are outside the purview of current retrofitting techniques and is the major motivation for the current research program.

2.2 A Move Towards a New Direction

As discussed in the previous section, any suitable design or retrofit program should ensure easy repairability without interfering with the functionality of the structural system. Design and retrofitting strategies currently in vogue are effective in improving the overall performance but may lead to unwanted failure modes that often lead to irreparable damage. Thus for a critical bridge it is necessary to adopt a technique that can not only control damage while accommodating large seismically-induced displacements, but also ensure quick repairability

to restore post-earthquake serviceability. To this end Cheng and Mander (1997) and Mander and Cheng (1997) have proposed several new design philosophies referred to as CARD (Control and Repairability of Damage) and DAD (Damage Avoidance Design). Cheng (1997) extended these for retrofit of structures ReCARD (Retrofit Control and Repairability of Damage) and ReDAD (Retrofit Damage Avoidance Design). This subsection presents a brief overview of the two philosophies CARD and ReCARD that form the basis of the current research.

2.2.1 Control and Repairability of Damage (CARD)

Cheng and Mander (1997) proposed a technique for new construction that addresses the issue of easy repairability. Salient features of this design paradigm referred to as CARD (Control and Repairability of Damage) are explained schematically in figure 2-2. As can be observed from figure 2-2, the design basis of relocated hinge zones is to ensure that damage is limited and controlled entirely within plastic hinge zones which are specially detailed to permit repair and restoration following a strong earthquake. All other portions of the structure remain uncracked and essentially elastic at all times. The CARD philosophy thus uses a "weakening" concept: the hinge zone becomes a sacrificial fuse that is repairable. The weakening is achieved by machining the longitudinal reinforcement to a smaller diameter thereby creating a "fuse-bar" which is replaceable. This weakening also protects the rest of the structural system from damage. Through a series of experiments on near-full size prestressed-precast concrete bridge columns Cheng and Mander (1997) illustrated that such structures can not only accommodate large seismic deformations (see figure 2-3) without collapse, but can also be rapidly repaired to restore the bridge function to full service immediately after an earthquake. The current research builds on this design paradigm and also applies it for the purpose of retrofitting deficient structures with a special emphasis on bridge columns with lap splice details and/or inadequate transverse reinforcement in the potential plastic hinge zones.

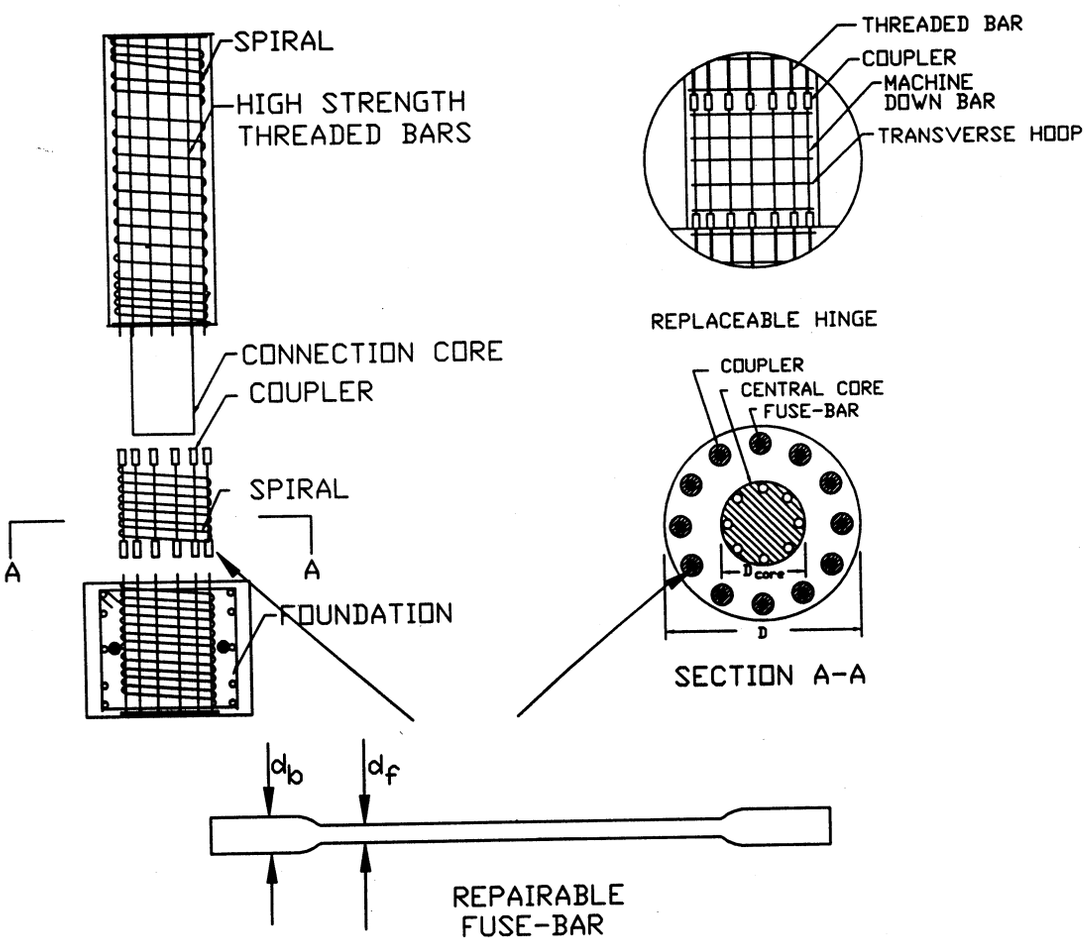

Figure 2-2 Salient Features of CARD Proposed by Cheng and Mander (1997).

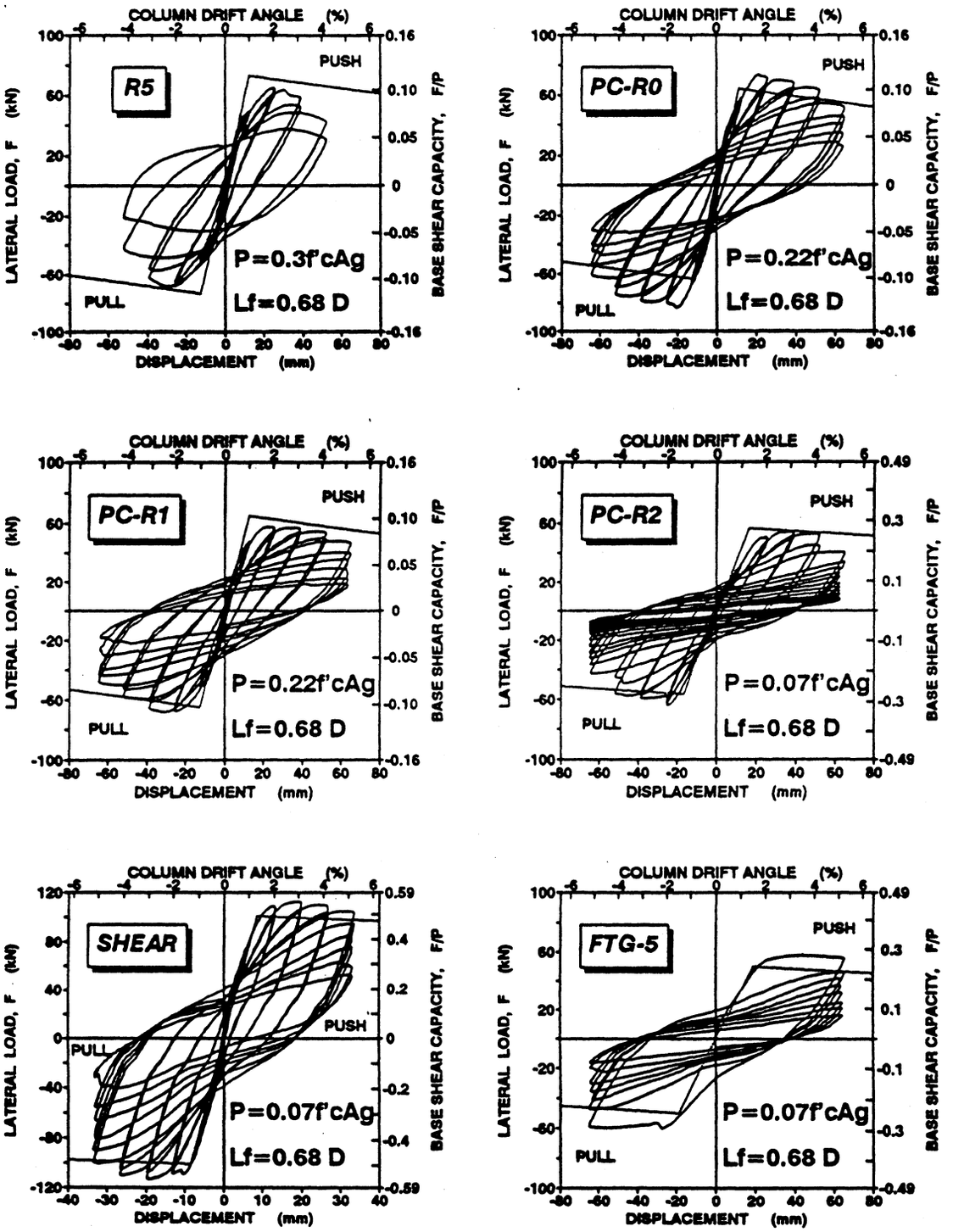

Figure 2-3 **Experimental Results of Cheng and Mander (1997) Illustrating the CARD Philosophy.**

2.2.2 Retrofit Control and Repairability of Damage (ReCARD)

In a follow-up to the CARD philosophy, Cheng (1997) proposed a methodology for retrofitting deficient structures based on the principles of damage control. As this is applied to existing structures, the philosophy is aptly named ReCARD – Retrofit Control and Repairability of Damage. Based on the experimental results on three-quarter scale lap spliced columns (figure 2-4), it was concluded that it is possible to control damage within the lap splice itself and obtain an adequate level of performance with some prudent detailing strategies. Since strengthening the lap splice might cause irreparable damage to other locations (e.g. in the foundation through low cycle fatigue of the longitudinal reinforcement), the splice was turned into a fuse-like entity by lowering the lap length from $20d_b$ to $10d_b$ (d_b = longitudinal bar diameter). Premature bond failure was prevented by providing extra transverse confinement that ensured delayed failure but not transferred to any other location – a principle advocated by the CARD philosophy.

2.3 Further Concept Development on ReCARD

The ReCARD philosophy proposed by Cheng (1997) is essentially an extension of the CARD principle to retrofit deficient structures. Although it was shown that the basic ideals of CARD are met satisfactorily by ReCARD, Cheng's application was somewhat limiting. It is considered that Cheng's post-earthquake repair of damaged columns with lap splice might be a satisfactory approach for bridges in low to moderate zones of seismicity, but a lack of redundancy in single column bents for bridges, particularly in high seismic risk zones, necessitates an approach in which the strength capacity can be maintained at large ductilities for several cycles of loading. Therefore, an approach is needed that is competitive with a conventional retrofit that uses steel jacketing, but without the fundamental flaw of that method.

A probable solution lies in incorporation of the detailing features of CARD for the purpose of retrofitting deficient structures. In other words the same fuse-bar concept can be

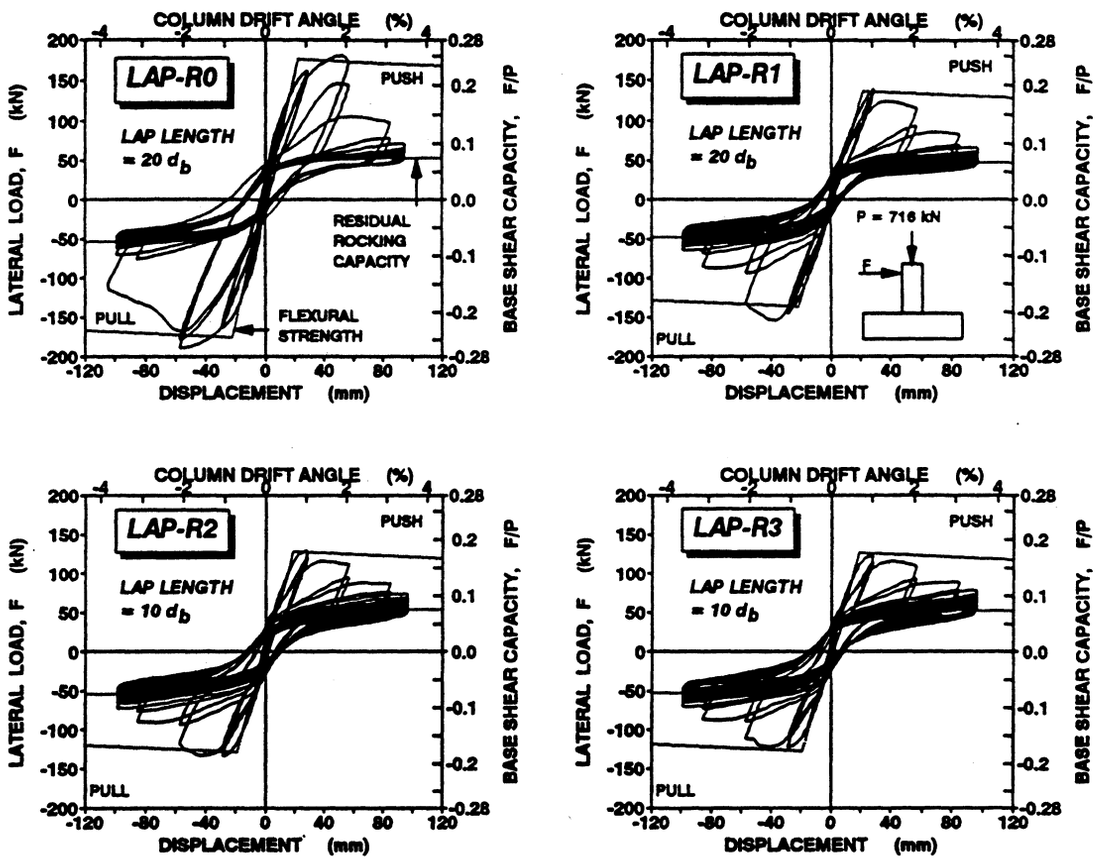

Figure 2-4 Experimental Results of Cheng (1997) Illustrating the ReCARD Philosophy.

used (see figure 2-5) that will relocate and restrict damage in specialized locations which can be capacity designed to ensure superior performance under strong ground shaking.

The design basis of relocated hinge zones is to ensure that damage can be limited and controlled entirely within plastic hinge zones which are specially detailed, while all other portions of the structure remain uncracked and essentially elastic at all times. However, since an existing column will have continuous longitudinal reinforcement, the sacrificial plastic hinges with the fuse-bars need to be installed in a manner such that they carry the entire tensile force when the column is subjected to reversal cyclic loading. This will ensure that the performance of the column is governed by the behavior of the fuses only i.e. usable fatigue life of the column is determined by the fatigue life of the fuse-bars. One way to achieve this is to discontinue the existing reinforcement in the column by cutting it at the center of the "to be installed" hinge and then introducing the fuse between the main column and the foundation as shown in figure 2-6. Specially sized rectangular plates can be used to transfer the tensile forces between the main column bars to the fuse-bars and back to the foundation. The whole assembly can be prepared in the shop and field welded after removing an adequate amount of concrete from the cover and behind the longitudinal bars. The artificial hinges can be further confined by transverse reinforcement so that adequate shear resistance is obtained. For extremely squat columns, such as those commonly found in highway bridge approach ramps, sacrificial hinges can be included at probable plastic hinge locations and the remaining portion of the column can be jacketed by either steel or composite fiber jacketing so that they remain undamaged and "capacity protected" against shear failures. The column failure mode can be changed from that of brittle shear to a more ductile flexural mode. Details of this retrofit design concept are discussed in the next subsection.

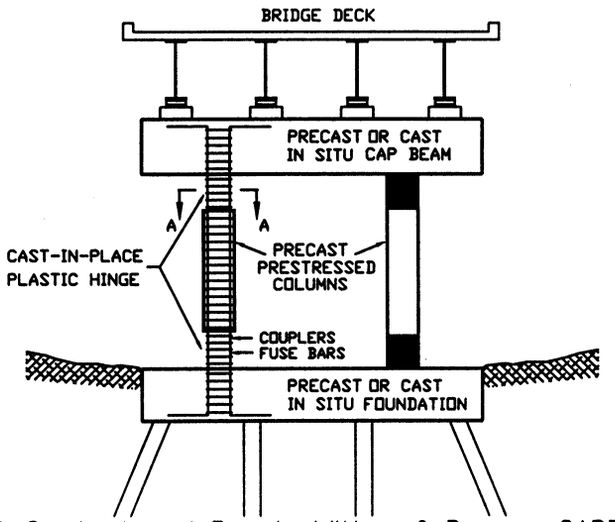

(a) Control and Repairability of Damage CARD Design Details for New Structures

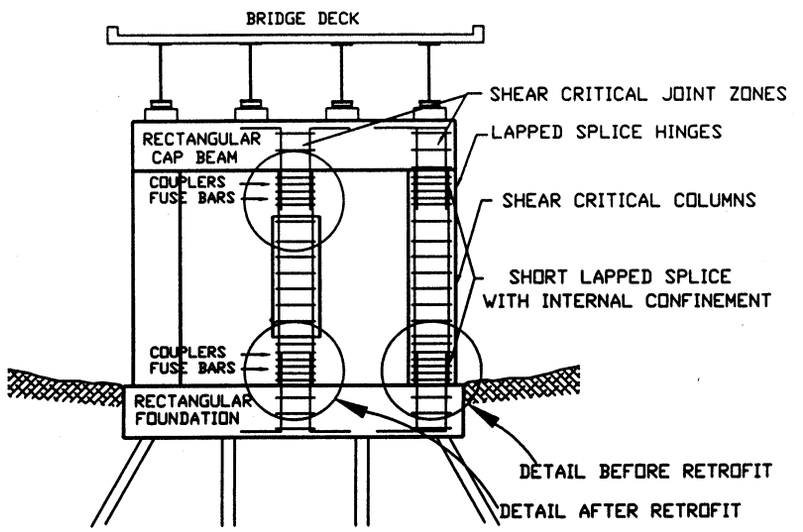

(b) Retrofit, Control and Repairability of Damage ReCARD for Existing Structures

Figure 2-5 Strategies to Ensure Post-Earthquake Serviceability.

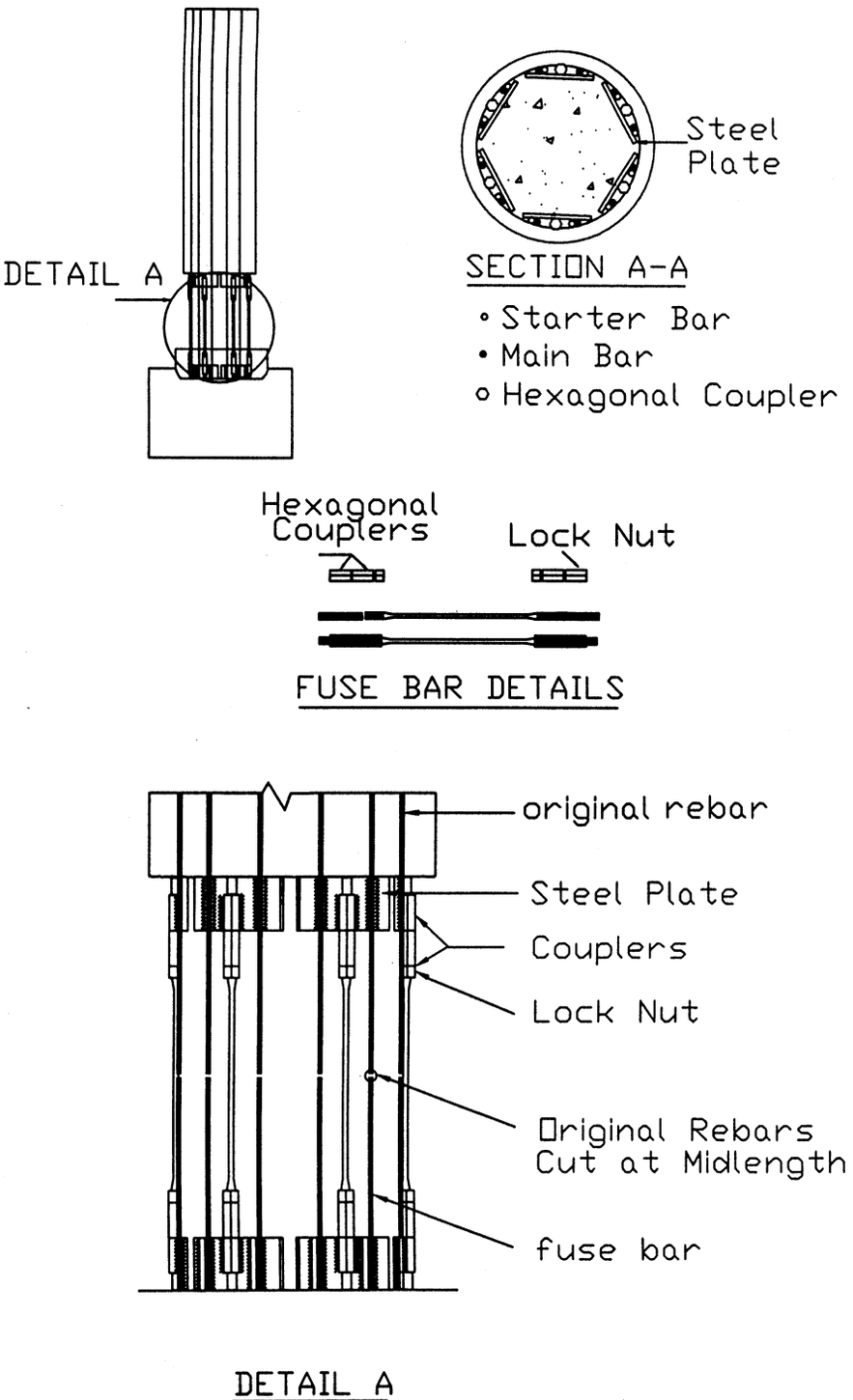

Figure 2-6 Retrofitting Strategy for Zones of High Seismicity.

2.4 RETROFIT DESIGN

2.4.1 Fuse-Bar Design for Plastic Hinge Zones

In order to weaken the plastic hinge for controlling and limiting damage to the hinge zone, the longitudinal reinforcement in that zone needs to be weakened. This is achieved by machining the longitudinal bars to a smaller diameter. This approach ensures the longitudinal reinforcement outside the plastic hinge zone remains elastic at all times. It is necessary to ensure that the upper bound ultimate tensile stress over the reduced area is less than the specified yield force on the root thread diameter of the threadbar, thus

$$\frac{\pi}{4} d_f^2 f_{su} < 2 \frac{\pi}{4} d_b^2 f_y \qquad \text{(2-1)}$$

where d_f = reduced fuse-bar diameter and d_b = diameter of the two longitudinal steel rebars that connect into the single fuse-bar, f_{su} = an upper bound ultimate strength of the fuse-bar steel, and f_y = dependable yield stress of the starter bar steel or column steel whichever is less. This reduces to

$$\frac{d_f}{d_b} < \sqrt{\frac{2 f_y}{f_{su}}} \qquad \text{(2-2)}$$

For design purposes, it is proposed $d_f = 0.95\, d_b$. Although this is on the conservative (low) side, it should ensure that outside the fuse zone the steel remains elastic at all times. Moreover, the existing steel yield strength (f_y) can only be assumed based on the specified minimum and the ultimate tensile strength of the replacement steel (f_{su}) could conceivably be somewhat greater than that of the original fuse bars. This ratio (when $d_f = 0.95 d_b$) implies from equation (2-2) that $f_y > 0.45 f_{su}$ and ensures an acceptable margin of safety for all likely replacement scenarios.

2.4.2 Determination of Fuse-Bar Length

It was shown by Dutta (1995) that the maximum plastic curvature obtainable from a well-detailed reinforced concrete column of incipient fatigue of the longitudinal reinforcement is given by

$$\phi_p D = 0.16 \frac{D}{D'} (2N_f)^{-0.5} \tag{2-3}$$

where ϕ_p = plastic curvature, D = overall depth (diameter for circular section), D' = distance between the extreme tension and compression bars (pitch circle diameter for circular section) and $2N_f$ = number of reversals to fatigue fracture. Multiplying this equation by the normalized fuse length (L_f/D) and using the well-known moment-area theorem, the plastic hinge rotation angle can be expressed as

$$\theta_p = (\phi_p D)\left(\frac{L_f}{D}\right) = 0.16 \frac{D}{D'} \frac{L_f}{D} (2N_f)^{-0.5} \tag{2-4}$$

In the preceding equation the number of cycles to fatigue failure (N_f) depends upon the demand imposed on the structural element by the particular seismic event. However, based on the analysis of typical ground motions, Chang and Mander (1994b) concluded that such demand is linked to the fundamental period of the structure and is given by

$$N_f = 7T^{-1/3} \quad ; \quad but \quad 4 \le N_f \le 20 \tag{2-5}$$

Rearranging equation (2-4), the normalized fuse length

$$\frac{L_f}{D} = \frac{\theta_p}{0.16} \frac{D'}{D} (2N_f)^{0.5} \tag{2-6}$$

Assuming that for typical bridge columns $D'/D \approx 0.8$ and $\theta_p = 0.03$ *rad.*, the upper and lower bounds of the fuse length is given by

$$0.43 < \frac{L_f}{D} < 0.95 \qquad (2\text{-}7)$$

corresponding to N_f = 4 and 20, respectively. It is thus evident that the fuse-bar length is related to the fatigue life of the column hinge. If the fuse length provided is less than required, the plastic hinge will fail prematurely. If necessary, an improved fatigue life can be obtained by lengthening the machined portion of the fuse bar. Based on studies investigating this parameter (L_f/D), Cheng and Mander (1997) concluded that for most column aspect ratios, good performance can be obtained when $L_f = 0.67\,D$.

2.4.3 Determination of the Plate and Weld Size

The required size of the plate (height and thickness) is linked directly to the force it is required to transmit. Assuming the electrode used is of the E70XX type and the plate is welded to both sides of the coupler, then as per AISC LRFD (1995)

$$2(l_w \times 0.707 \times s_w \times \phi F_w) = \frac{\pi}{4} d_f^2 f_{su} \qquad (2\text{-}8)$$

where l_w = length of the weld in mm, s_w = size of the weld in mm, ϕF_w = 217 *MPa* for E70XX electrode, d_f = diameter of fuse bar in mm and f_{su} = ultimate strength of the fuse bar (MPa). Thus rearranging and solving for l_w:

$$l_w = 0.56 \frac{d_f^2}{s_w} \frac{f_{su}}{217} \qquad (2\text{-}9)$$

As per the requirements of AISC LRFD (1995), the minimum plate thickness is given by

$$t_{plate} = size\ of\ weld + 1.6\,mm \qquad (2\text{-}10)$$

2.4.4 Design of Transverse Reinforcement

It was shown by Dutta and Mander (1998) that transverse reinforcement is required in a reinforced concrete beam-column element mainly for three purposes. They are

(i) confinement of core concrete

(ii) confinement of the longitudinal reinforcement, i.e., antibuckling reinforcement

(iii) shear resistance

Accordingly they proposed the following equations for volumetric ratios of transverse reinforcement for circular sections.

Confinement of Core Concrete

$$\rho_{s_{con}} = 0.008 \frac{f_c'}{U_{sf}} \left[12 \left(\frac{P_e}{f_c' A_g} + \rho_t \frac{f_y}{f_c'} \right) \left(\frac{A_g}{A_{cc}} \right)^2 - 1 \right] \qquad \text{(2-11)}$$

Antibuckling

$$\rho_s = 0.025 \frac{D}{s} \frac{s}{d_b} \rho_t \frac{f_y}{f_{yh}} \qquad \text{(2-12)}$$

Shear Resistance

$$\rho_s \geq 0.75\Lambda \frac{\rho_t}{\phi} \frac{f_{su}}{f_{yh}} \frac{A_g}{A_{cc}} \left[1 - \left(\frac{0.65 - P_e / \phi f_c' A_g}{0.65 + 1.2 \rho_t f_{su} / f_c'} \right) \right] \qquad \text{(2-13)}$$

In the above equations

A_{cc} = area of the core concrete

A_g = gross area of the concrete section

D = diameter of the section

P_e = applied axial load

U_{sf} = strain energy/unit volume of longitudinal reinforcement = $110\,MJ/m^3$

d_b = diameter of the longitudinal reinforcement

f'_c = unconfined compression strength of concrete (MPa)

f_{su} = ultimate strength of longitudinal reinforcement (MPa)

f_y = yield strength of longitudinal reinforcement (MPa)

f_{yh} = yield strength of transverse reinforcement (MPa)

s = spacing of the transverse reinforcement

ϕ = undercapacity factor for shear = 0.85

Λ = 1 for fixed free columns and 2 for fixed-fixed columns

ρ_t = volumetric ratio of longitudinal reinforcement

$\tan\alpha = D/L$ = pitch circle diameter/height of the column

$\tan\theta$ = tangent of the crack angle such that

$$\theta = \tan^{-1}\left(\frac{\rho_v n + \xi \frac{\rho_v}{\rho_t}\frac{A_v}{A_g}}{1 + \rho_v n}\right)^{1/4} > \alpha \qquad \textbf{(2-14)}$$

with $\rho_v = 0.5\,\rho_s$ provided, n = modular ratio = $E_{steel}/E_{concrete}$, ξ = 0.5704 for fixed-fixed and 1.5704 for fixed-free end conditions and A_v = effective shear area normally assumed to be $A_v = 0.8A_g$.

Using the principles of capacity design, transverse reinforcement should be provided corresponding to the greatest amount required from these three criterion.

2.5 CLOSURE

The issue of controlling damage and maintaining post earthquake serviceability is not addressed by any of the current seismic design codes. However, this can be extremely important for a bridge that lies in a major highway system network with little or no redundancy. The requirement of easy repairability is equally valid for new construction as well as retrofit of existing columns. In this section a new technique for retrofitting bridge columns with inadequate lap splices is advanced that caters to this specific requirement. The concept is based on the CARD and ReCARD philosophies proposed by Cheng and Mander (1997) with modifications to suit the requirements of high seismic zones.

SECTION 3
EXPERIMENTAL APPROACH

3.1 INTRODUCTION

This section describes the experimental apparatus, instrumentation, data acquisition system, and testing procedures of the experiments. As was stated earlier, the three-quarter scale bridge column retrofitted with sacrificial fuse bars required testing under reversed cyclic loading with the purpose of observing the efficiency of the retrofitting technique. Moreover, to examine the effect of variation of axial load on a reinforced concrete beam-column element, another three-quarter scale prestressed concrete CARD specimen and a further repair of the retrofitted column was also tested under realistic seismic input. A new method for application of lateral load was investigated as a part of the current research which is also discussed in detail in the following subsections.

3.2 IMPROVEMENTS IN THE EXPERIMENTAL INFRASTRUCTURE

Experimental investigations of the seismic performance of column components have been widely undertaken by various researchers. Different testing configurations are adopted depending on the nature of the available equipment. For a few of the different types of column tests conducted see for example, Mander et al. 1984, Yok Lung Wong 1990 and Sheikh et al. 1990. Figure 3-1 presents a typical test set up that has been used at the University at Buffalo over the last decade (see for example Cheng and Mander, 1997). The problem with most of the current test approaches is they do not correctly model $P-\Delta$ effects due to the inclination of the applied axial load with lateral displacement. Figure 3-2 shows the effect of axial load on the specimen and contrasts that with how the tests should be conducted to properly reflect the true $P-\Delta$ effects. From figures 3-1 and 3-2(a) it is evident that at the base of the column where the bending moments are the largest when under lateral load there is an additional secondary moment due to the column's deflected shape. This secondary moment is equal to $P \cdot \delta$ that arises

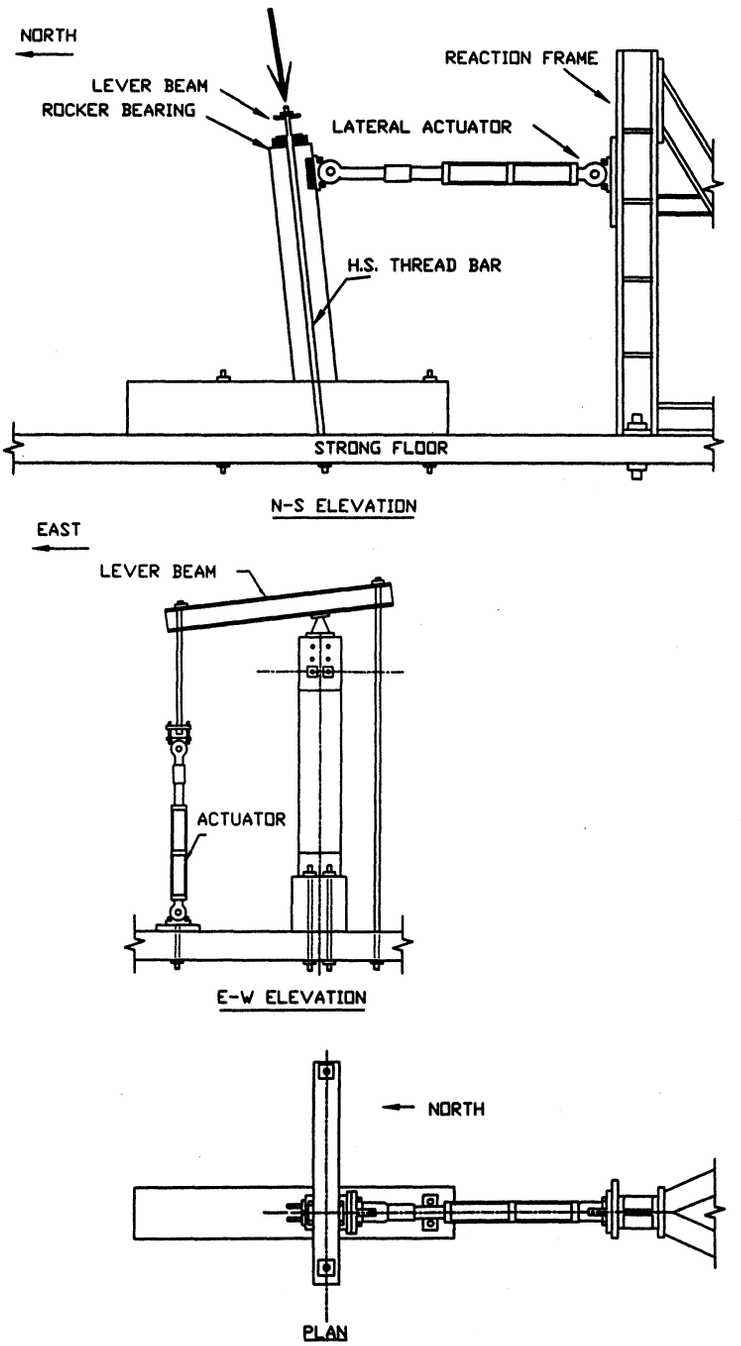

Figure 3-1 **Typical Test Setup used in the Laboratory Testing of Reinforced Concrete Beam-Column Subassemblages.**

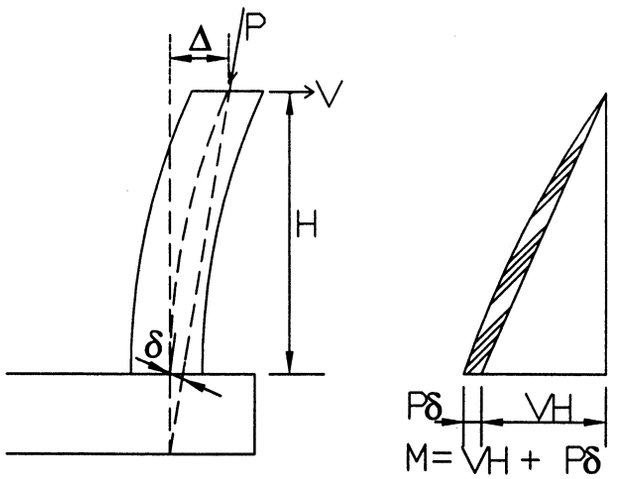

(a) Traditional Test Approach

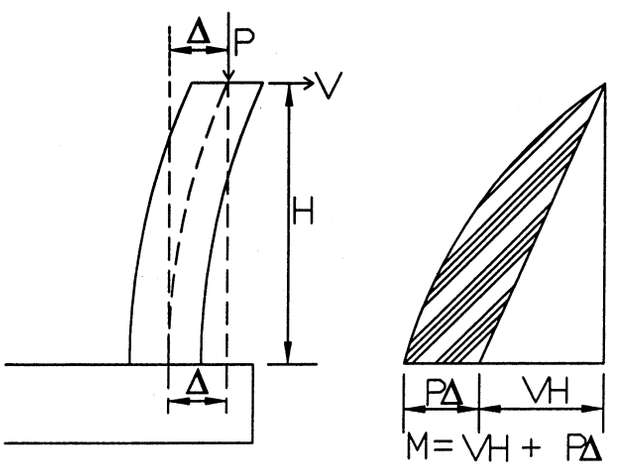

(b) Correct Approach Needed for Testing

Figure 3-2 Effects of $P-\Delta$ in The Conventional and Modified Setup.

from the deviation in the axial force vector from the bent column axis. The experimental $P \cdot \delta$ moment is less than the correct $P \cdot \Delta$ moment, where P should always be aligned vertically.

To rectify the experimental deficiency in the secondary $P \cdot \delta$ moments, it is necessary to ensure that the experimental axial load (as applied by an actuator system) be truly vertical. To this end the University at Buffalo strong-floor based column testing rig was modified as shown in figure 3-3. The vertical load is applied by a lever beam system connected to a secondary frame. This frame is then connected to a second (lower) actuator. The displacements of this actuator are slaved to the top actuator that is the primary driver in the experiment. The axial load is controlled by a vertical servo-hydraulic actuator ($250\,kN$) mounted on the secondary frame at the eastern end and a $35\,mm$ diameter high strength threadbar at the western end via a lever beam mounted on top of the column. The frame is supported by two $32\,mm$ diameter high strength threadbars at the western end and by two $25.4\,mm$ diameter bars of the same variety at the eastern end. These bars in turn pass through specially constructed H-beams with oversized tubular gaps along the web and anchored at the bottom via washers and locking nuts. The H-beams were supported on elastomeric bearings and prestressed to the laboratory strong floor.

Lateral load is applied to the specimen by a $500\,kN$ capacity $\pm 127\,mm$ stroke MTS servo-hydraulic actuator at a height of $2712\,mm$ from the top of the foundation beam. One end of the actuator is attached to the specimen through the actuator end plate and another end of the actuator is bolted to the extension and connected to the reaction frame.

A second "horizontal" actuator with a load capacity of $1100\,kN$ and $\pm 102\,mm$ displacement capacity is attached to the horizontal frame and traces the same displacement pattern (displacement "slaved") as the top actuator. This automatically ensures that the line of application of the axial load is kept vertical at all times thereby eliminating any possibilities of $P - \Delta$ error. This is illustrated in figure 3-4 which shows the proposed load application mechanism at its original and deflected positions, respectively.

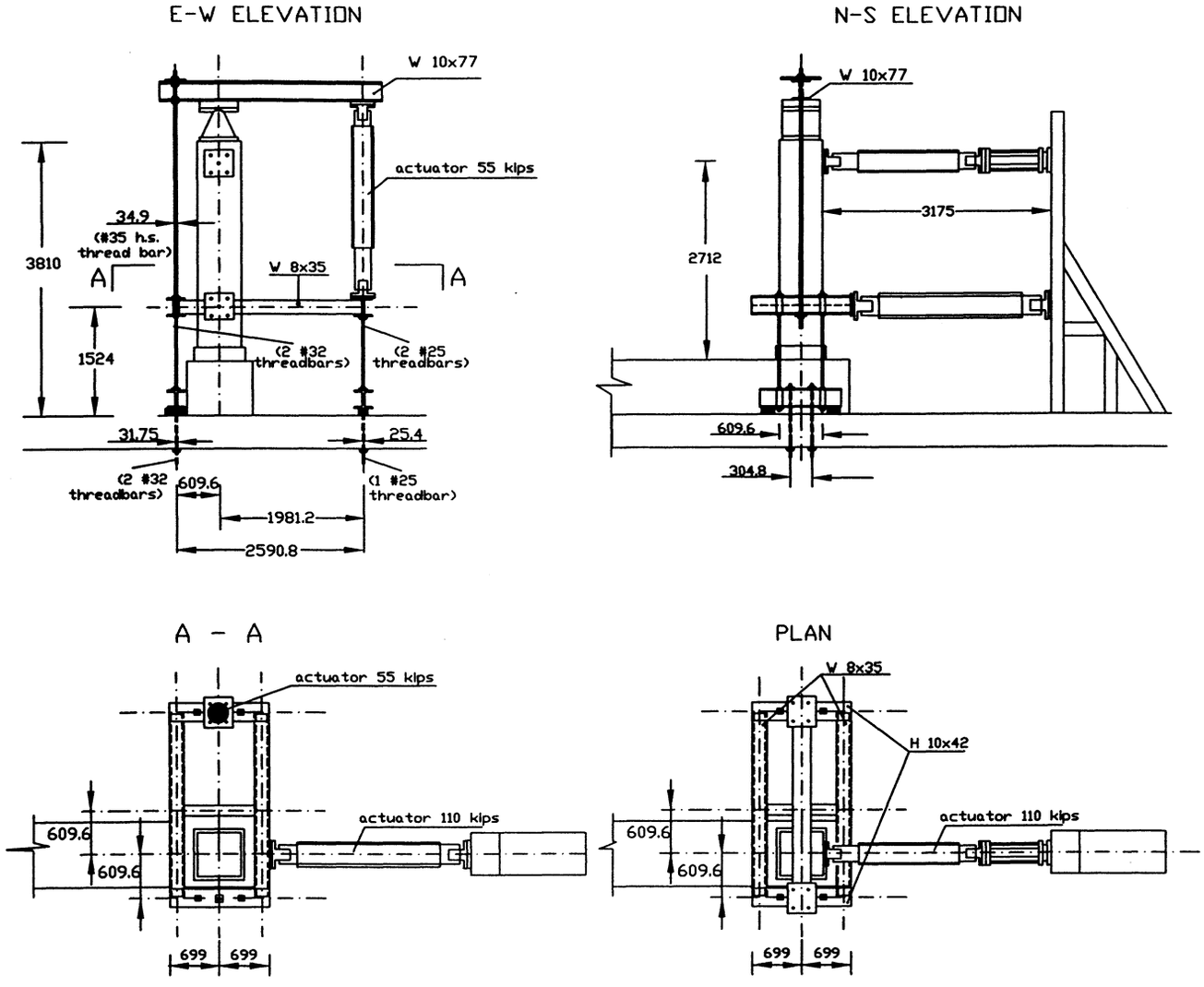

Figure 3-3Proposed Modifications in the Test setup for the Application of Axial Load.

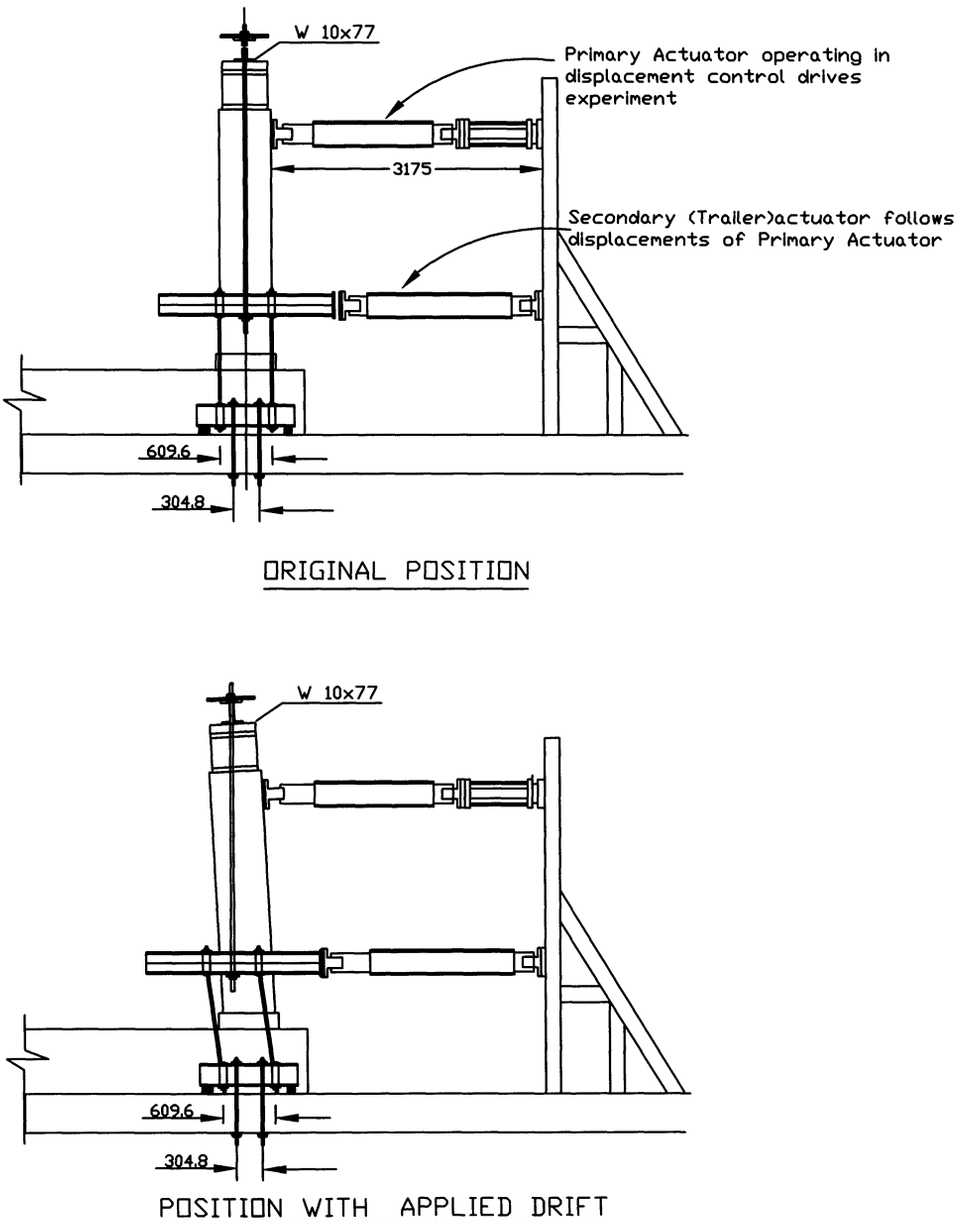

Figure 3-4 The Modified Test setup at (a) Neutral Position and (b) An Applied Drift.

To prevent sliding of the specimen under lateral load the foundation beam is anchored to the laboratory's 457 *mm* thick strong floor by applying prestress of 250 *kN* to each of the 25 *mm* diameter high strength threadbars. These threadbars pass through 76 *mm* steel pipes that are cast in the foundation beam giving a total hold-down prestress of 1000 *kN*. Therefore, by assuming a conservative value for the coefficient of friction of, say, 0.5 between the concrete specimen and the concrete strong floor, the dependable resistance against sliding is 500 *kN*. This is considerably greater than the lateral load capacity expected for the types of specimens to be tested in this research.

3.3 Accommodating Axial Load Changes

In the laboratory testing of structural concrete column components under simulated earthquake loading, there can be a number of ways in which the lateral load can be applied based on the orientation of the actuators. As will be shown, it is possible to accommodate the effect of tension uplift using a suitable control algorithm for the hydraulic actuator that applies the vertical load. The need to physically model the effect of tension uplift can be explained with reference to figure 3-5(a) which shows a typical twin column pier bent subjected to a lateral force of magnitude $2F$. From equilibrium considerations, the following equations are obtained:

$$V_b = \frac{2M_p}{L} = T \tag{3-1}$$

and by taking equilibrium about the base

$$2F \cdot H = 2M_p + T \cdot L \tag{3-2}$$

where V_b = cap beam shear force, T = tension tie down force to restrain overturning, M_p = plastic moments in the column, H = height of the column and L = distance between the centerline of the adjacent columns. By substituting equation (3-1) into (3-2) one obtains an explicit relation connecting F and T in terms of the geometric parameters. Thus,

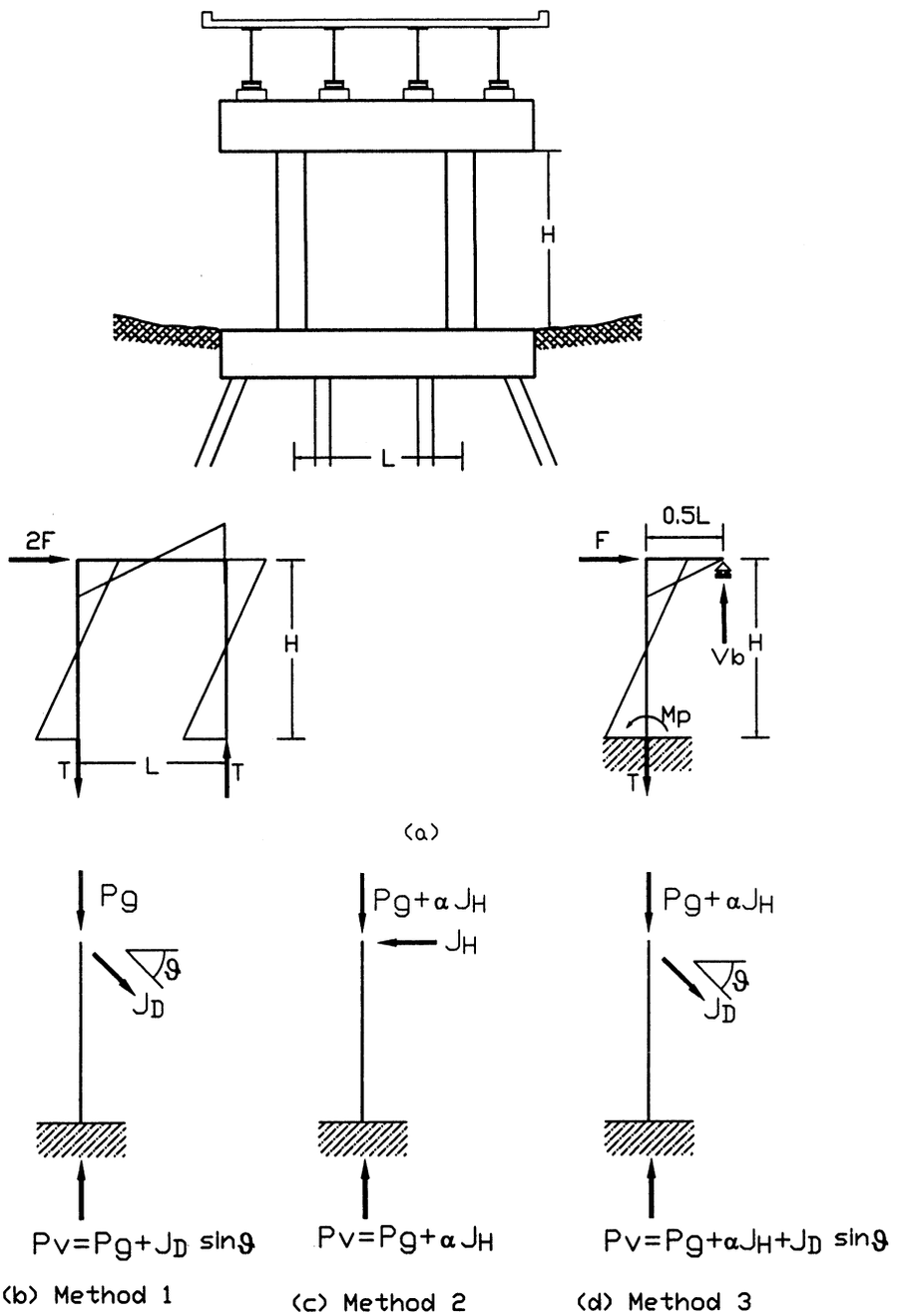

Figure 3-5 Methods of Applying Lateral and Vertical Loads to account for Tension Uplift.

$$T = F\frac{H}{L} \tag{3-3}$$

In the laboratory the effect of tension uplift can be incorporated by suitably aligning the horizontal actuator and using a suitable control signal for the vertical actuator. The various alternatives are described below.

Method 1: Inclined Actuator: The setup shown in figure 3-5(b) consists of an inclined actuator meant for applying the horizontal load in displacement control. The axial load P_g is applied through a vertical actuator that is held constant to simulate the constant gravity load. Lateral loading is applied by an actuator inclined at angle θ from the horizontal. The total reaction force in the column is the sum of the two actuator components:

$$P_V = P_g + J_D \sin\theta \tag{3-4}$$

where J_D = force applied by the "diagonally" oriented actuator. Note that when the force acts in the direction opposite to the direction shown in figure 3-5(b) it is taken as negative.

The main advantage of this setup is that it can directly accommodate vertical force changes including tension uplift. However, for high H/L ratios it is necessary to apply the horizontal force at a steep angle thereby sacrificing the horizontal displacement capability. Generally in a laboratory setup the proximity of the reaction frame inhibits provision of such steep angles.

Method 2: Horizontal Actuator with Variable Vertical Force: The setup shown in figure 3-5(c) is commonly used in laboratory testing. It consists of a horizontal actuator operating in displacement control and the vertical actuator operating in load control. If a variable axial load is necessary this can be accommodated as follows

$$P_V = P_g + \alpha \cdot J_H \tag{3-5}$$

where α is a proportionality factor that suitably adjusts the additional tension uplift force over and above the vertical component of the inclined actuator force. If the vertical actuator can only apply compression forces (due to the presence of tension-only tie down rods in the test set up) then this approach is limited so that $J_H < P_g L/H$.

Method 3: Hybrid Setup: Each of the first two methods have a disadvantage. Both of these disadvantages can be overcome by combining the two approaches as shown figure 3-5(d). The total vertical force is given by

$$P_V = P_g + \alpha J_D + J_D \sin\theta \tag{3-6}$$

Rearranging to solve for the axial load change (ΔT) gives:

$$\Delta T = T - J_D \sin\theta = J_D \left(\frac{H}{L}\right) \cos\theta - J_D \sin\theta = \alpha J_D \tag{3-7}$$

from which the actuator proportionality factor is given by

$$\alpha = \frac{H}{L} \cos\theta (1 - \tan\theta) \tag{3-8}$$

Clearly for a horizontal actuator (when $\theta = 0$), $\alpha = H/L$.

In this research Method 2 has been used for the variable amplitude tests with $\alpha = 0$; i.e. the axial load is held constant. For seismic simulations where the vertical load changes of a pier bent need to be accommodated, Method 3 has been used with $\theta = 28.2°$ and α is a variable that is changed by the computer software driving the test.

3.4 INSTRUMENTATION, DATA ACQUISITION AND PROCESSING

Forces, displacements and column curvatures were measured by load cells, displacement transducers and potentiometer, respectively. Figure 3-6 represents the instrumentation for the Variable Amplitude Tests and QED test on the ReCARD specimen. Four sonic transducers (T1 through T4) were used to monitor the transverse displacements relative to the fixed base. Out of the four transducers, three were attached to the specimen at various heights while one was connected to the horizontal frame. To measure the column curvatures, six potentiometers (three on each side) were used. Two potentiometers were mounted on each aluminum chassis; one covering the upper gauge length, the other covering the adjacent lower one. The chassis was bolted to a $9\,mm$ diameter threaded rod that was previously cast in the concrete during construction.

For the Quasi-Earthquake Displacement test on the CARD specimen, the instrumentation is presented in figure 3-7. Seven sonic transducers (T1 through T7) were used to monitor horizontal displacements. Seven pairs of potentiometers were used to measure column curvatures. Each potentiometer was mounted on an aluminum chassis that was attached to $9\,mm$ threaded rods previously cast into the specimen .

During each test, the instrument output was recorded by an Optimum Megadac 5533A Data Acquisition System in an ASCII format. The method for data analyses are outlined below:

Column drifts (θ) were calculated using the relation

$$\theta = \frac{T_1}{H} \tag{3-9}$$

where T_1 = displacement at the top sonic transducer and H = column height measured from the top of the foundation beam to the centerline of action of the lateral load actuator.

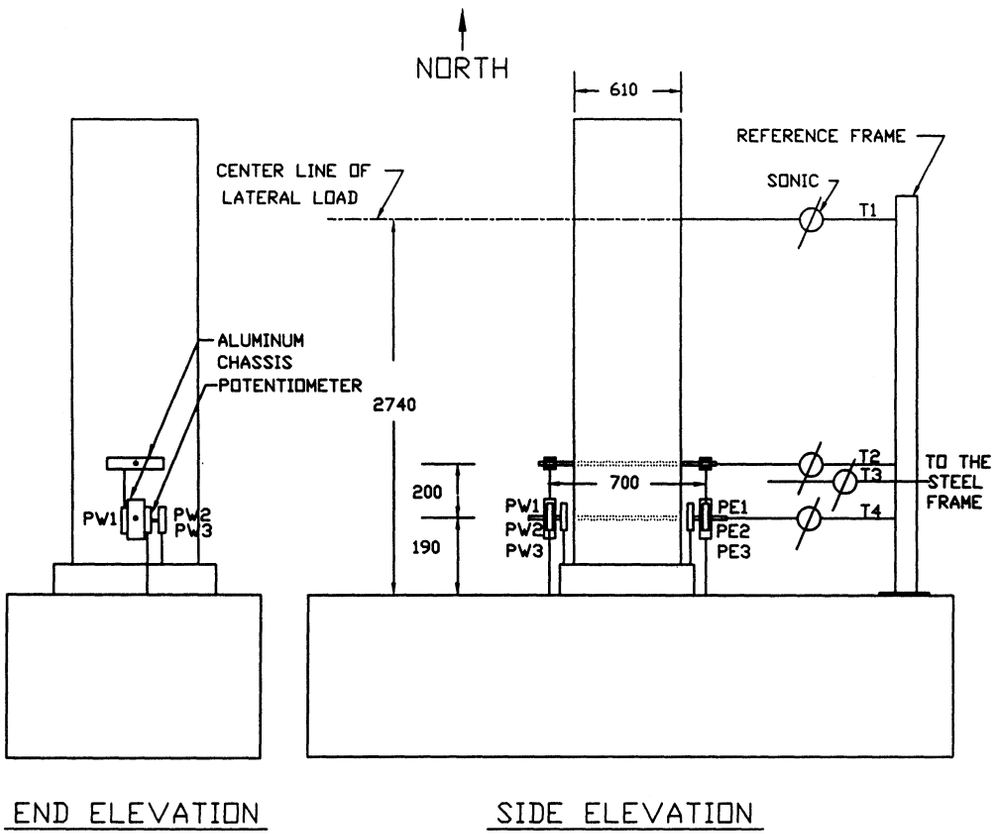

Figure 3-6 **Location of the Displacement Transducers and Linear Potentiometers for Variable Amplitude and QED Testing of the ReCARD Specimen.**

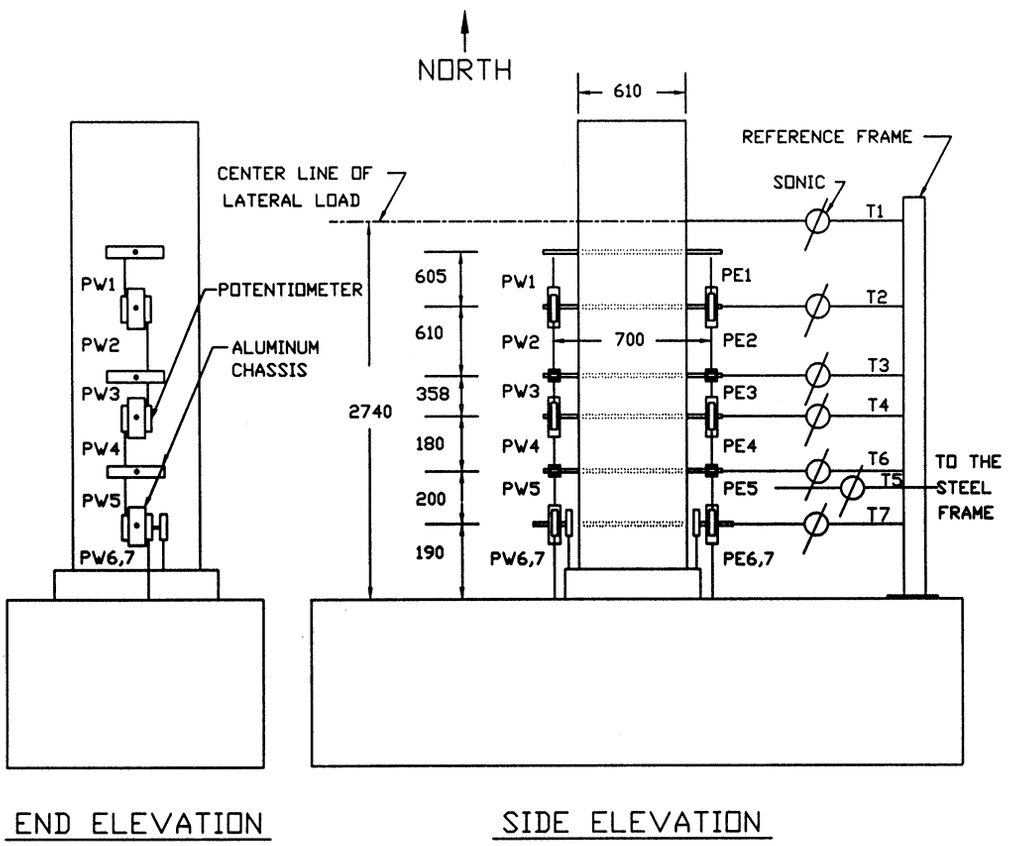

Figure 3-7 **Location of Displacement Transducers and Linear Potentiometers for the QED Testing of the CARD Specimen.**

Curvatures and strains (ϕ_i, ε_i) over the i-th gauge length were calculated from:

$$\phi_i = \frac{\Delta_{pi}}{L_{pi} L_{gi}} \tag{3-10}$$

and

$$\varepsilon_i = \frac{\Delta_{pi}}{L_{gi}} \tag{3-11}$$

where Δ_{pi} = algebraic difference of readings from the potentiometer pairs, L_{pi} = center-to-center distance between the potentiometer pairs, and L_{gi} = gauge length.

Hysteretic energy absorption (E_h) by the column per cycle is given by the area within the force-displacement loop. One cycle of loading is defined as one complete reversal between positive and negative drift amplitudes. The trapezoidal rule is used to find the hysteretical energy absorbed by the column resulting in

$$E_h = \sum_{i=1}^{n} \left(\frac{F_i + F_{i-1}}{2} \right) (x_i - x_{i-1}) \tag{3-12}$$

in which F_i = force in the i-th step and x_i = displacement of the same step.

The hysteretic energy absorption can be related to Elasto Perfectly Plastic (EPP) material by $E_h = \eta E_{EPP}$, where η = an efficiency factor, and E_{EPP} = the energy absorbed by a 100% perfect elasto-plastic system, defined as:

$$E_{EPP} = (M_n^+ + M_n^-)(\theta_p^+ + \theta_p^-) \tag{3-13}$$

where M_n^+, M_n^- = nominal moment capacities respectively in the push and pull direction and θ_p^+, θ_p^- = plastic component of the drift amplitude in the respective direction. The normalized energy is defined by dividing the energy in equation (3-12) by $(M_n^+ + M_n^-)$. Thus, by also dividing the EPP by $(M_n^+ + M_n^-)$ in equation (3-13), a comparison of the efficiency of energy absorbed by the column and a 100% EPP material can be obtained.

From the hysteretic energy absorbed by the column, two approaches for establishing the relationship between effective damping ratio and displacement ductility are proposed and described in what follows.

Cyclic Energy Absorption Efficiency (η)

One way to evaluate the equivalent damping ratio is by measuring the hysteretic performance using the concept of energy absorption efficiency with respect to an Elasto-Perfectly Plastic (EPP) system. By dividing the real cumulative energy absorbed by the piers (that is the area under the load-displacement hysteresis loop) by equation (3-13), the efficiency of energy absorption along cumulative plastic drift can be obtained from

$$\eta = \frac{E_{cycle}}{E_{EPP}} \tag{3-14}$$

where E_{cycle} = energy absorbed in an entire pier system over one complete loading cycle (between drifts θ_p^+ and θ_p^-). Generally, the values of η for a given loading cycle are initially constant until severe deterioration commences at the onset of either buckling of the longitudinal steel and/or spalling of the cover concrete.

Effective Viscous Damping Ratio (ξ_{eff})

One way to calculate the effective damping ratio ξ_{eff} is by directly calculating the equivalent damping ratio ξ_{eq} from the hysteresis area of the column. Therefore, the effective damping ratio is defined as

$$\xi_{eff} = \xi_0 + \xi_{eq} = \xi_0 + \frac{1}{2\pi}\frac{E_{cycle}}{F_{\max}\Delta_{\max}} \tag{3-15}$$

where ξ_0 = ordinary structural damping (usually taken as 5% of critical), ξ_{eq} = equivalent damping ratio of column, $F_{\max}$ = average maximum strength in forward and reverse loading direction and $\Delta_{\max}$ = average maximum displacements in both loading directions which can be

taken as $\mu \Delta_y$ where Δ_y is the yield displacement.

From the result of the calculation of the energy absorption efficiency for each bridge pier and assuming a bilinear hysteresis loop, the equivalent damping ratio ξ_{eq} for the bridge system can be derived as

$$\xi_{eq} = \frac{2\eta}{\pi} \frac{(1-\alpha)\left(1-\frac{1}{\mu}\right)}{(1-\alpha+\mu\alpha)} \tag{3-16}$$

where μ = displacement ductility factor and α = ratio between the post yield stiffness and initial stiffness, which usually ranges from 0 to 0.05 for most reinforced concrete members. For convenience, it is desirable to further simplify equation (3-16) to give

$$\xi_{eff} = 0.05 + 0.6\eta\left(1-\frac{1}{\mu}\right) \tag{3-17}$$

The response spectra adjustment factors for high damping in the short and long period ranges can also be obtained as

$$B_s = \left(\frac{\xi_{eff}}{0.05}\right)^{0.5} \quad \text{and} \quad B_l = \left(\frac{\xi_{eff}}{0.05}\right)^{0.3} \tag{3-18}$$

3.5 CLOSURE

A three-quarter scale ReCARD column was tested to verify the efficacy of the new retrofitting technique that was introduced as part of the current research. Another three-quarter scale CARD column and a further repair of the ReCARD specimen were tested under realistic seismic input for evaluating the sensitivity to variable amplitude displacement path and variable axial load. The conventional testing configuration was considered and modified. The problem with most of the current approaches is that they do not correctly model $P-\Delta$ effects. In an attempt to correctly mimic the secondary $P-\Delta$ moments that always exist due to the deflected shape of the column, a modification to the experimental setup was implemented. The so-called $P-\Delta$

apparatus consists of a secondary frame that is attached to a lower horizontal actuator which is slaved to the principal lateral loading actuator. In this way the vertical load can be applied in a truly vertical orientation.

SECTION 4
TEST SPECIMENS – DESIGN AND DETAILING

4.1 INTRODUCTION

This section presents a brief overview of the configuration and detailing for the specimens that were used in the laboratory testing. These consisted of an as-built column with insufficient lap splice length that was eventually retrofitted and a CARD specimen that was essentially a further repair of a specimen tested by Cheng and Mander (1997). The first retrofit (Test R0) and the repair (Test R1) of the inadequate lap splice column was tested under variable amplitude loading at increasing drift amplitudes. This was primarily done to check the efficiency of the retrofitting technique. Following this the CARD specimen and a second repair of the retrofitted specimen was tested under Quasi-Earthquake Displacement to investigate the effect of variable axial load on the fatigue life of such specimens. The details of the various specimens are given in the following.

4.2 AS BUILT COLUMN

One of the objectives of this research was to evaluate the experimental performance of a three-quarter scale model bridge column with inadequate lap splice after retrofit. The retrofit was performed on an almost exact replica of an existing bridge column in the field. Hence it was necessary that the column be constructed in the laboratory with identical details.

The as-built column shown in figure 4-1 was designed based on a 3/4 scale of a prototype column of diameter $813\,mm$. As shown in figure 4-1, the $3048\,mm$ tall and $610\,mm$ diameter model column was reinforced with 12 deformed #6 (nominal diameter = $19\,mm$) rebars which constituted a longitudinal steel ratio of 1.17% of the gross area of the column section. The top and lower $610\,mm$ of the column was reinforced with deformed #3 (nominal diameter = $9.53\,mm$) spirals at a pitch of $102\,mm$. At the central $1828\,mm$ part of the column the pitch was doubled.

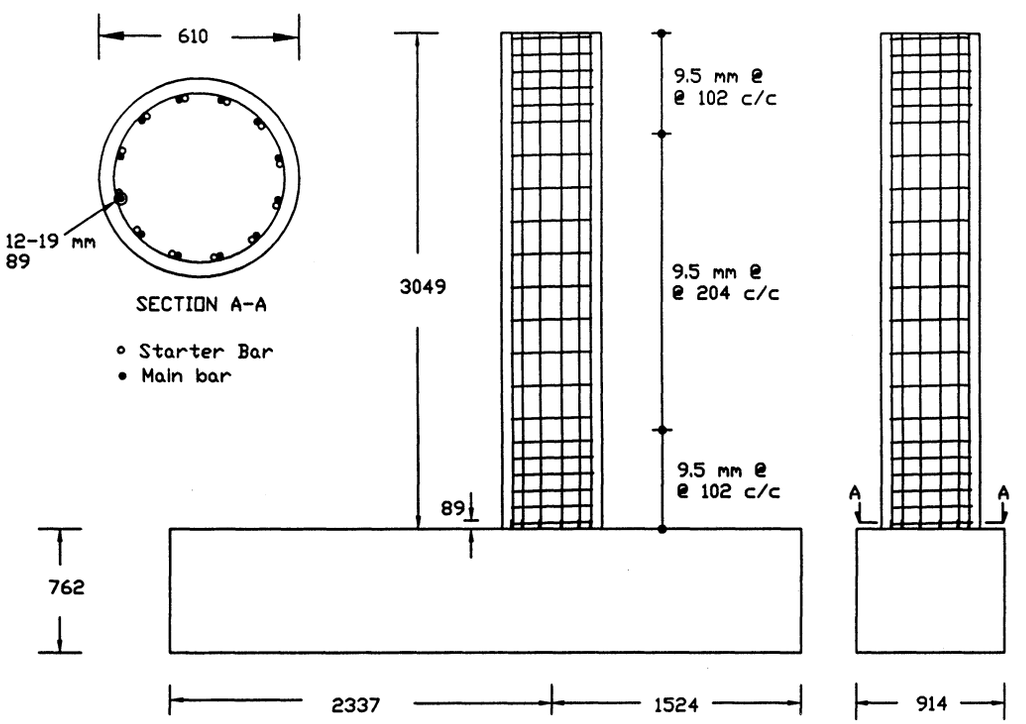

Figure 4-1 Construction Details of the As-built Column Specimen.

The longitudinal steel was lap spliced for $64\,mm$ at the base of the column Although such a small lap length is not expected even in a non-seismically designed column, it was chosen to reflect the most adverse situation and also enabled the use of the foundation beam constructed for earlier experiments by Cheng and Mander (1998).

4.3 Retrofit of the Inadequate Lap Splice Column

The as-built column with inadequate lap splice length was retrofitted in its undamaged condition in accordance with the ReCARD concepts developed in Section 2. The retrofitted column is shown in figure 4-2. The main feature of this retrofit include the provision of "fuse bars" in the potential plastic hinge zone so that the failure is governed by low cycle fatigue. The actual load path needed to be transferred from the existing longitudinal reinforcement to the fuse bars and finally down to the foundation. This requirement necessitated the provision of rectangular plates as shown in figure 4-2 which transferred the load from the main column bar to the fuse bar and back to the foundation via the welds. To prevent the existing longitudinal bars from carrying any tension, they were cut at mid-height with a portable band-saw. This was deliberately done so that these bars would only be effective in compression but not in tension.

The design details of the fuse bars and that of the plastic hinge closely follows the criterion developed in Section 2. The fuse bars were machined from $28.6\,mm$ diameter B7 threaded rods whose typical stress strain behavior is shown in figure 4-3. As can be seen from this figure, the steel does not have a particularly well defined yield plateau. The yield and ultimate stresses were measured as $f_y = 855\ MPa$ and $f_{su} = 990\ MPa$, respectively. The ultimate strain at ultimate stress was 0.05 and at fracture 0.225. The fuse bars were machined down to $17.8\,mm$ diameter to conform to the requirements of equation (2-2). The length of the fuse was set at $406\,mm$ which was equivalent to $L_f / D = 0.67$.

The design of transverse reinforcement was based on Dutta and Mander (1998). Figure 4-4 shows the plot for the theoretical volumetric ratio of transverse reinforcement required for concrete confinement, shear protection and antibuckling purposes. From the plot it is clear that

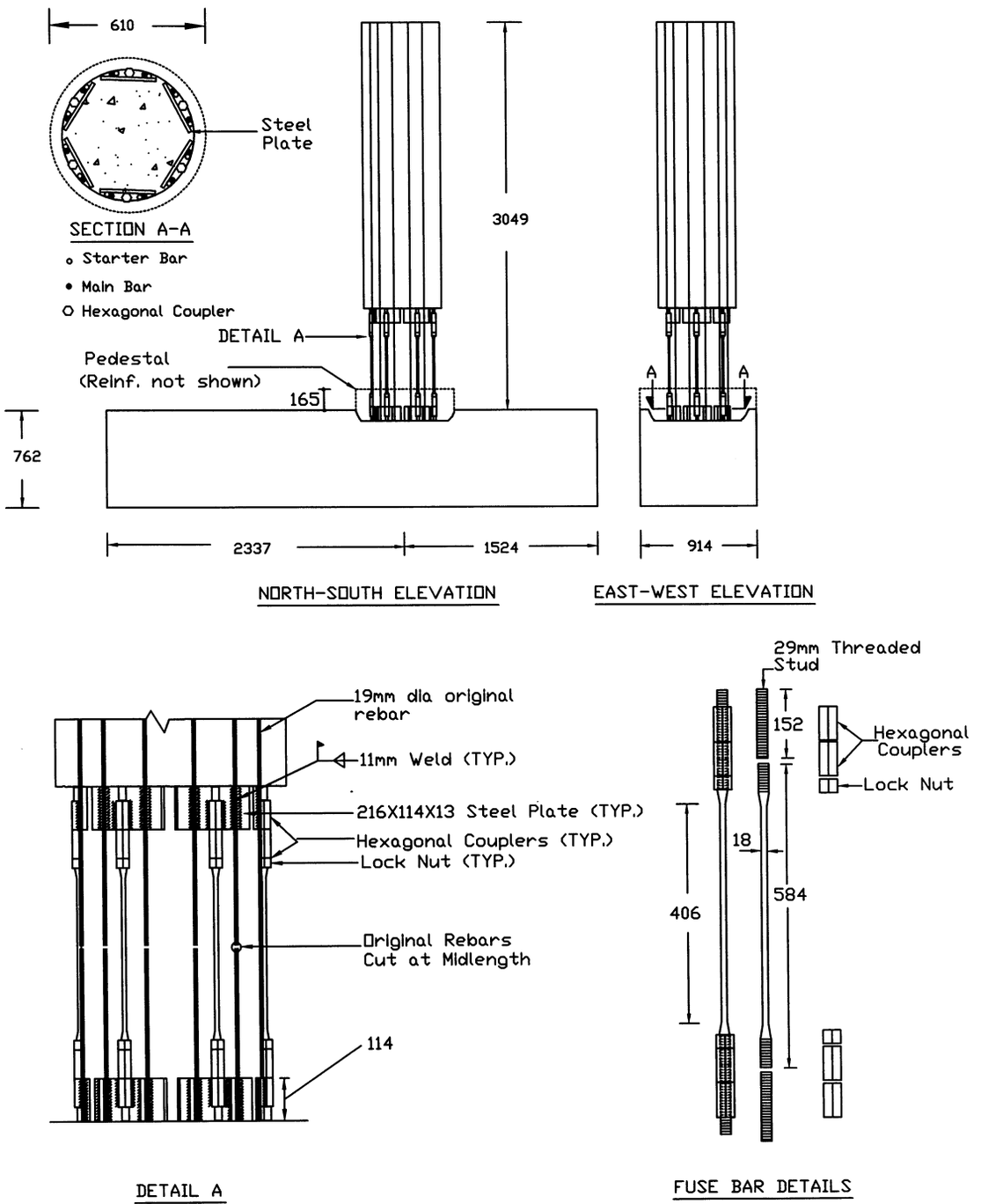

Figure 4-2 Construction Details of the Retrofit on the As-Built Lap Splice Column.

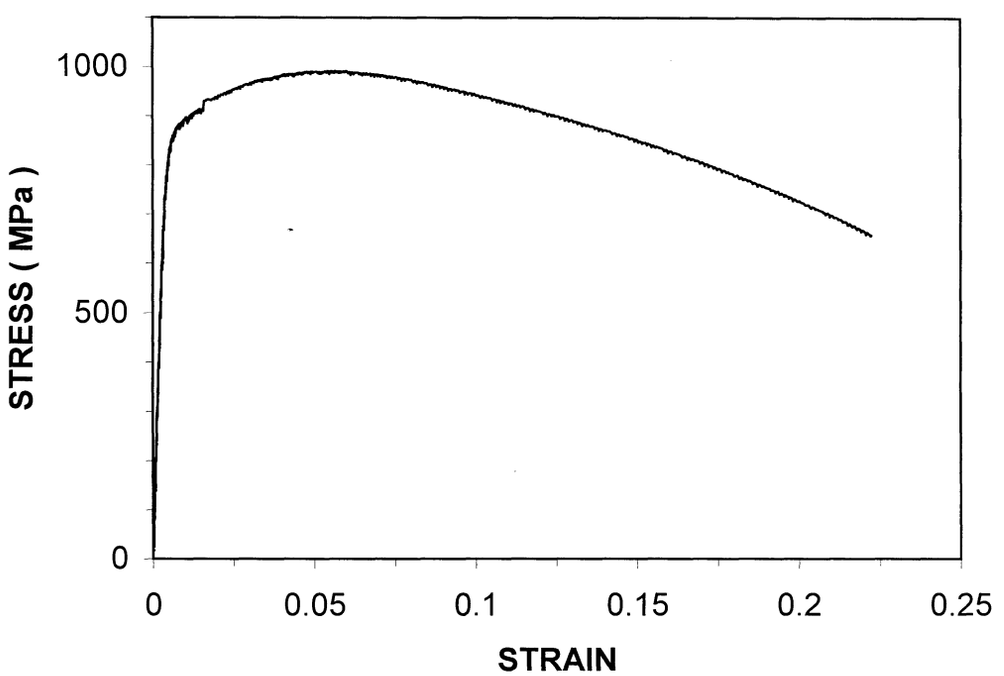

Figure 4-3 Stress-Strain Properties of the B7 Threaded Rods used as Fuse-Bars in the Retrofitted Specimen.

for the retrofitted column the volumetric ratio of transverse reinforcement corresponding to antibuckling is critical at $\rho_s = 0.015$.

Transverse reinforcement was provided in the form of $9.5\,mm$ galvanized 1×7 strand wire rope. The stress-strain property of the wire rope is shown in figure 4-5.

4.3.1 Retrofit and Repair Procedures

This subsection describes the retrofit and repair procedures for the original column. The initial retrofit column test is referred to as R0. As intended by design, the specimen was repaired and retested twice following the initial retrofit tests. These experiments are referred to as R1 and R2.

Retrofit (Test R0): This is the initial retrofit of the original as-built column that possessed a lap splice in the potential plastic hinge zone. About one month after casting the as-built column, the cover concrete around the perimeter of the column was removed by jack hammer from the top of the foundation beam for a height of $838\,mm$. After the hoop steel was exposed, it was removed (by gas cutting). In order to place the fuse-bar hardware, approximately $25\,mm$ of additional concrete was removed behind the longitudinal column bars. The starter bars were cut so that sufficient length remained for welding of the splice plates. Figure 4-6 presents a view of the column at this stage.

After the cover concrete and a portion of the core concrete were removed, the $216 \times 114 \times 113\,mm$ steel plates were inserted behind pairs of adjacent reinforcement and fillet welded with *E70XX* electrode. Care was taken to ensure the vertical clearance between the ends of the top and bottom plates was sufficient to secure the fuse-bar with the coupling arrangement.

Since the fuse-bars were to be assembled with hexagonal couplers both at the top and bottom, it was necessary that the other end of each coupler be screwed to the starter studs that

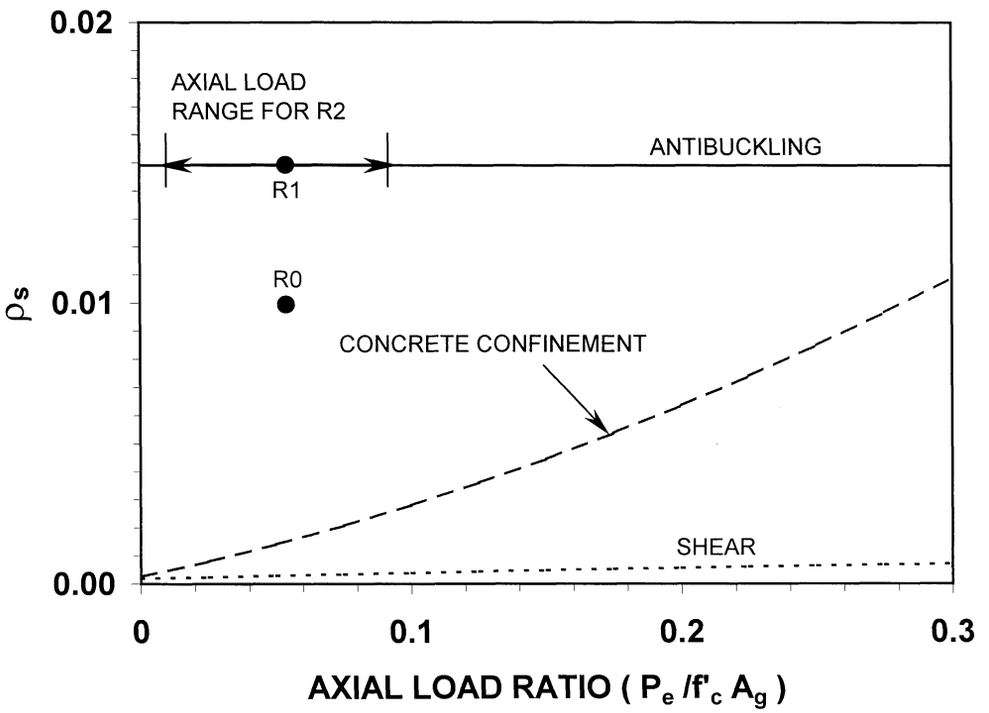

Figure 4-4 Design of Transverse Reinforcement for the Retrofitted Specimen after Dutta and Mander (1998).

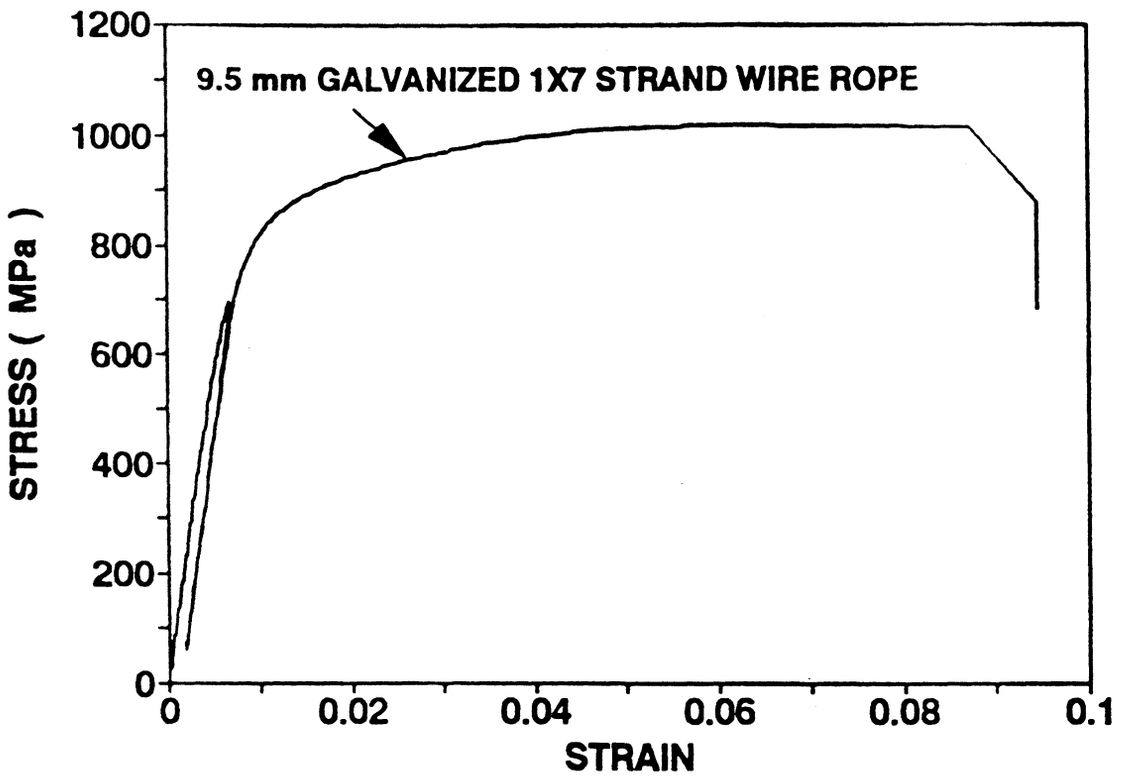

Figure 4-5 Stress-Strain Plot for the Galvanized Wire Rope used as Transverse Reinforcing.

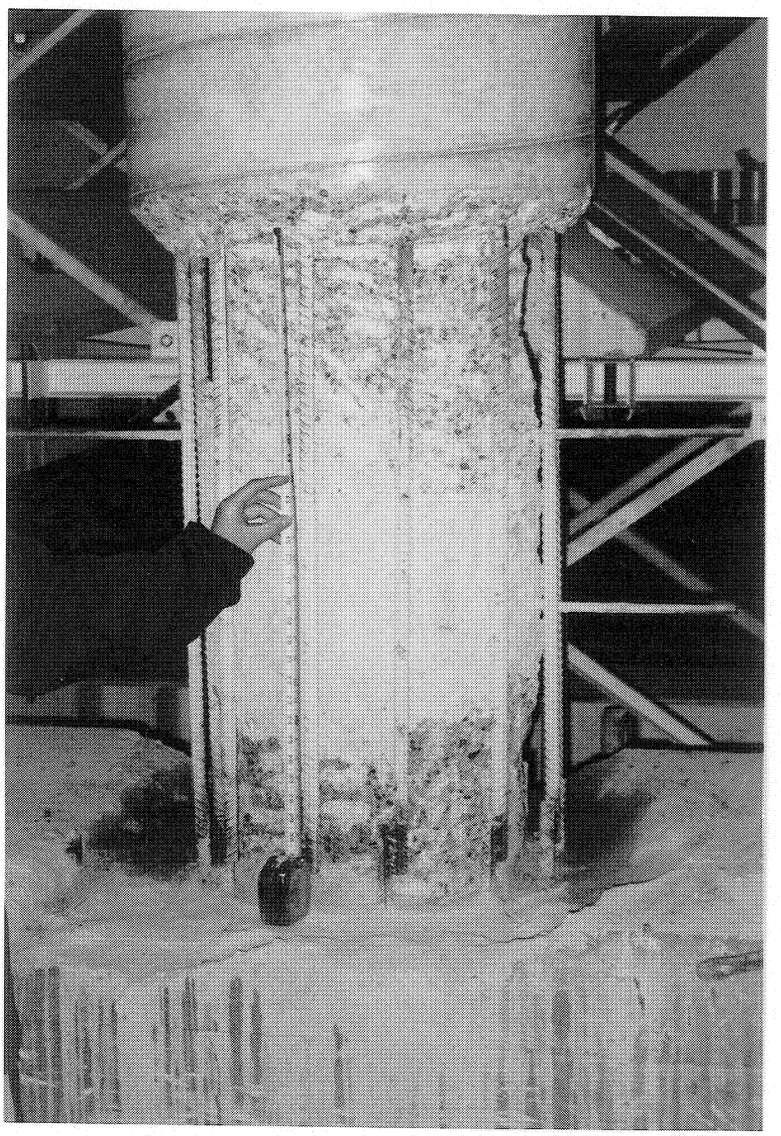

Figure 4-6 **Photographic View of the As-built Column after Removal of the Cover and Portion of the Core Concrete.**

in turn would be connected to the steel plates. Hence, 152 *mm B7* starter studs (diameter 28.6 *mm*) were attached at both ends of the fuse-bars via 76 *mm* hexagonal couplers. Another pair of couplers were screwed to the starter studs and then welded to the metal plates at the top and bottom. Care was taken so that the starter-coupler-fusebar assembly was properly aligned during the welding procedure. The fusebar was then lock-nutted to prevent any slackness of fit. The assembly procedure is schematically portrayed in figure 4-3 and figure 4-7 presents a view of the column after the completion of the assembly.

After the fuse-bars were welded, transverse reinforcement in the form of 9.5 *mm* galvanized 1×7 strand wire rope was wound around the fuse-bars. Although in accordance with the design it was necessary to maintain spacing of 38 *mm* for antibuckling considerations, it was decided that the spacing in the actual hinge zone measuring 152 *mm* on either side from the center of the fusebar should be relaxed to 58 *mm* to deliberately weaken the region. Conversely, to further strengthen the lower portion of the fusebar attachment, a pedestal (914×775) was cast up to 165 *mm* from the foundation (figure 4-2) and reinforced with additional rectangular hoop reinforcement consisting of 12.7 *mm* diameter deformed bars. These were welded to twelve longitudinal bars of the same diameter and of the same height as the pedestal and were distributed uniformly around the perimeter. Finally circular formwork in the form of proprietary cardboard tubing was assembled around the repaired hinge and high performance concrete was placed.

Concrete for the retrofit was cast in four pours. First the concrete in the pedestal was poured. The concrete proportions used for the pedestal are given in table 4-1. Next a strong layer extending some 51 *mm* from the top of the pedestal consisting of water, EMARCO-S77-CR and pea gravel in the ratio of 0.14:1:0.56 was cast. Concrete in the third level was the main portion expected to be damaged in an earthquake. In order to deliberately weaken this portion of the hinge zone a weaker strength concrete was poured for the next 457 *mm*. This weakening was achieved by adding 9.3 *ml / l* of Micro Air. Finally, for the top layer the same concrete mix as used in the second pour was used. Relevant information is included in table 4-2.

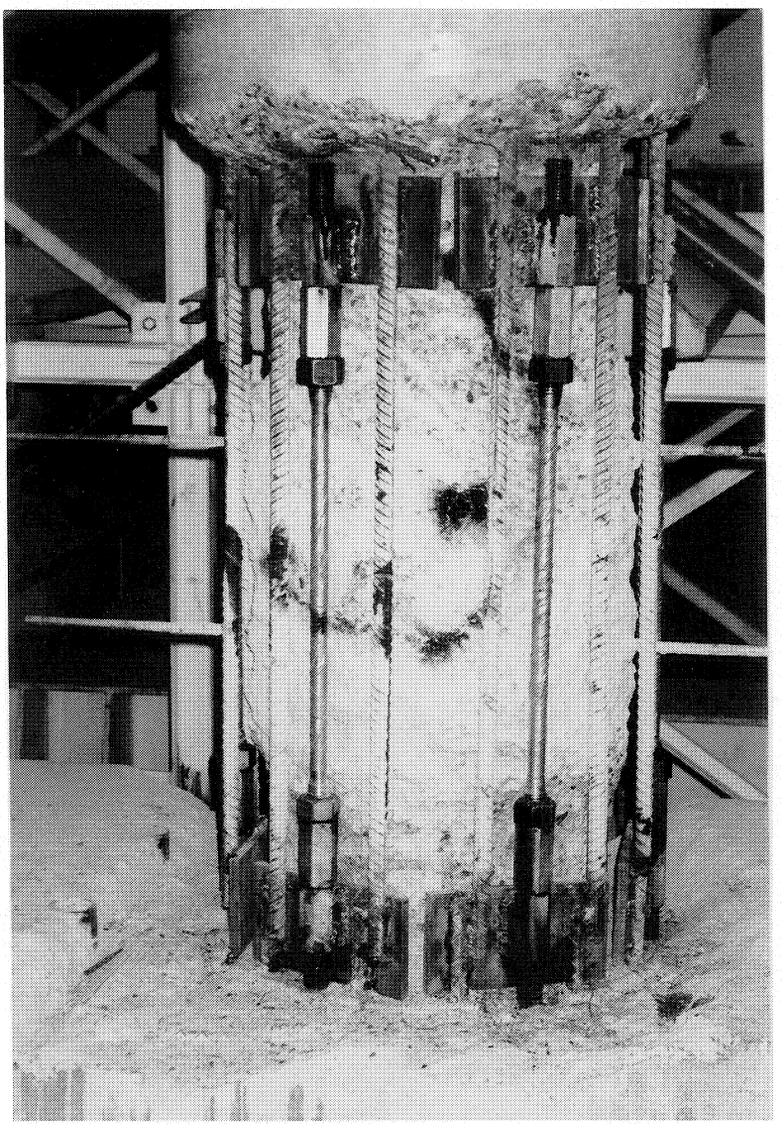

Figure 4-7 **Photographic View of the Column after the Assembly of the Plates and Fuse-Bars.**

Table 4-1 Mix Proportions for $1\,m^3$ of High-Strength Silica Fume Concrete Used for the Pedestal after Moknes and Jakobsen (1985).

Silica fume	32 *kg*
Plasticizer	6.14 *l*
Type III cement	416 *kg*
Fine aggregate (sand)	880 *kg*
Coarse aggregate (19 *mm*)	960 *kg*
Water	152 *l*

Water : Cement : Fine Aggregate : Coarse Aggregate = 0.34 : 1.0 : 1.96 : 2.14

Table 4-2 Concrete Mix Proportions in the Column Hinge Zone.

Batch	Water / EMARCO S77 - CR	Pea Gravel / EMARCO S77 - CR	Micro Air/Liter of Water (*ml*)	Pouring Height (*mm*)	7 Day Target Strength (*MPa*)
2	0.14	0.45	--	51	68
3	0.14	0.45	9.3	560	45
4	0.14	0.45	--	114	68

Repairs (Tests R1 and R2): Following the initial retrofit test (R0), the specimen was repaired and retested twice. On each occasion concrete in the sacrificial fuse zone was jack hammered up to 611 *mm* from the top of the pedestal and wire rope hoops were cut and removed. The damaged fuse-bars were replaced by a set of new fuse-bars and lock nuts tightened against the end of all couplers. Transverse reinforcement in the form of 9.5 *mm* galvanized 1×7 strand wire rope was wound around the hinge zone at a pitch of 38 *mm*. Figure 4-8 shows a typical view of the specimen at this stage. Finally, high performance concrete was poured in two layers with proportions corresponding to batches 2 and 3 in table 4-2.

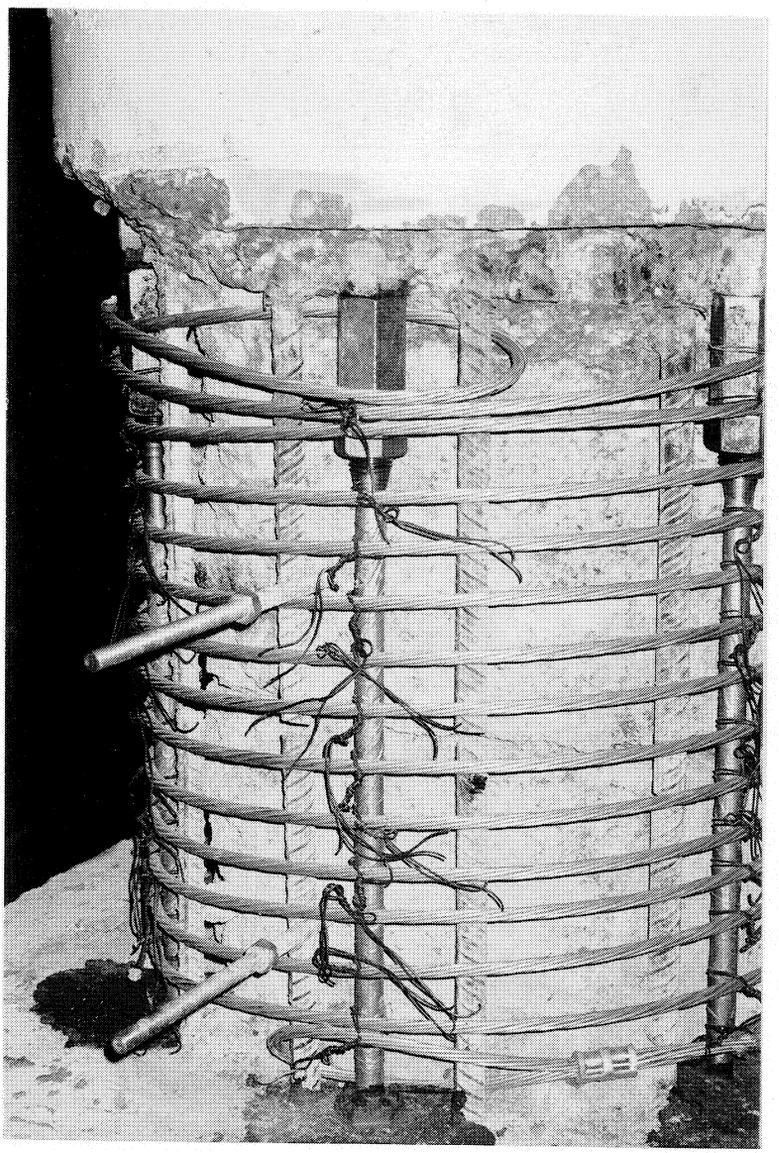

Figure 4-8 Typical Photographic View of the ReCARD Specimen during Repair.

4.4 PRESTRESSED CONCRETE REPLACEABLE HINGE CARD SPECIMEN

This subsection describes the repair preparations for retesting the three-quarter scale prestressed concrete column previously tested three times by Cheng and Mander (1997). The construction details for the specimen can be found in that reference. Based on lessons learned from those tests certain changes were incorporated into the specimen repair. The original three-quarter scale prestressed concrete column had a central core stub which was 279 *mm* diameter and reinforced with four 19 *mm* diameter deformed bars along with a 10 *mm* diameter spiral reinforcement wound with a pitch of 102 *mm*. The stub extended from the top of the foundation into the main portion of the column. This created a discontinuity at the column cap beam interface. However, the discontinuity should ideally be located at the mid-hinge height where the weakest zone is located. Therefore, the stub was cut 254 *mm* from the base of the column and seated on a concrete filled tube (310 *mm* in diameter, 343 *mm* in length). The lower end of the tube was secured by welding to the top rebars of the partially prestressed foundation beam. Figure 4-9 presents a view of the CARD specimen seated on the concrete-filled cast iron tube.

In the next phase a new set of fuse-bars was installed which were machined from 25.4 *mm* (Dywidag™) threadbars. In order to ensure that no damage propagated beyond the machined portion of the fusebar into the foundation, a pedestal (725 *mm* × 725 *mm*) with a height of 190 *mm* from the foundation beam was cast at the base of the column and reinforced with two levels of 19 *mm* diameter rectangular hoops. The concrete had the same mix proportions as listed in table 4-1. Finally, transverse reinforcement in the form of 9.5 *mm* galvanized 1×7 strand wire rope was wound around the plastic hinge with a variable pitch of 90 *mm* in the middle and 50 *mm* at the top and bottom. Details of construction are shown schematically in figure 4-10 and a view of the transverse and pedestal reinforcement is shown in figure 4-11.

The concrete used for the replaceable hinge zone was poured into hexagonal shaped plywood formwork in three distinct layers with proportions as listed in table 4-3. To further weaken the hinge zone, the hexagonal formwork was modified so that in the central portion of the hinge zone the overall width was 560 *mm*.

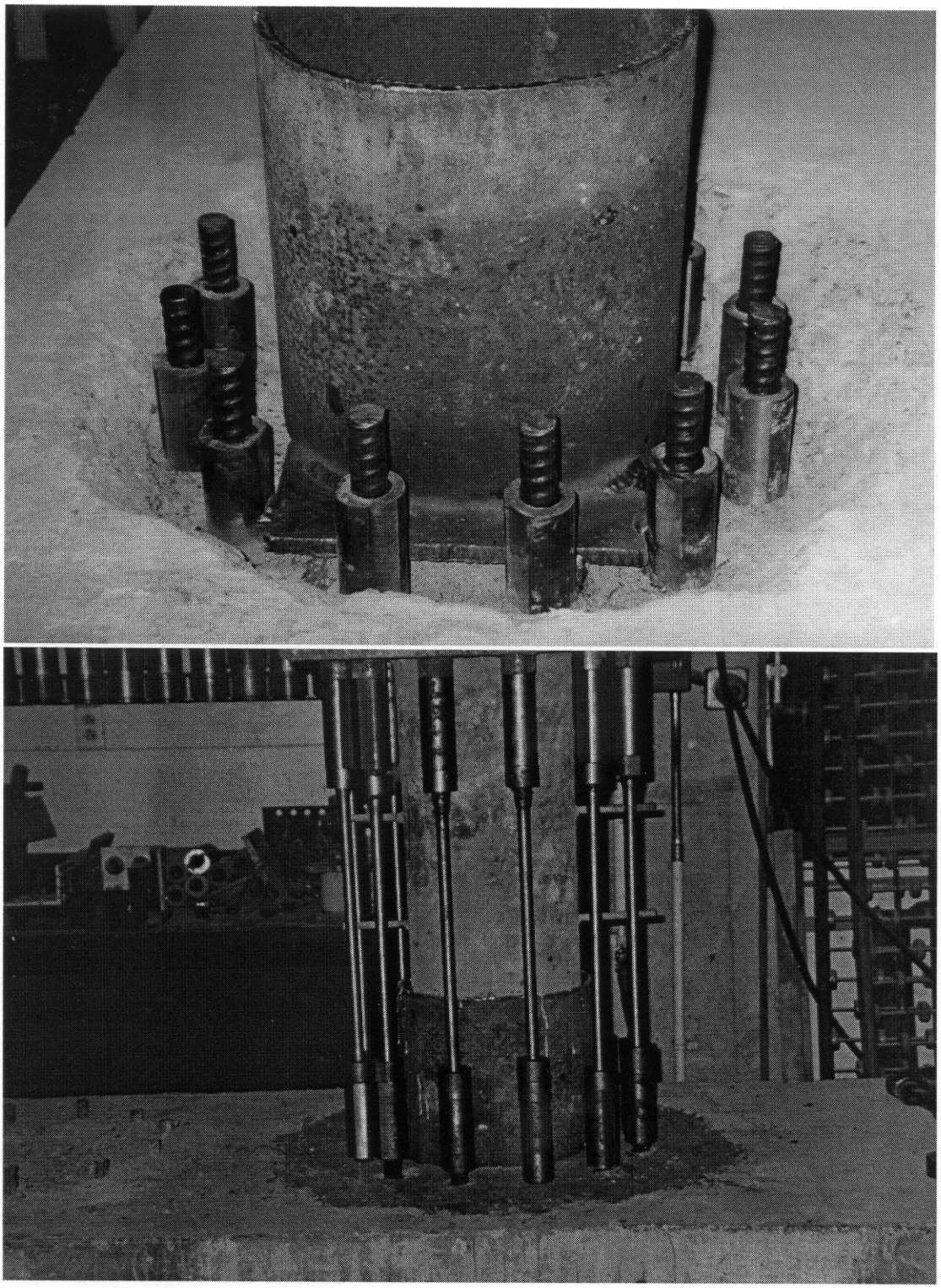

Figure 4-9 Photographic View of the CARD Specimen seated on the Concrete filled Cast Iron Tube.

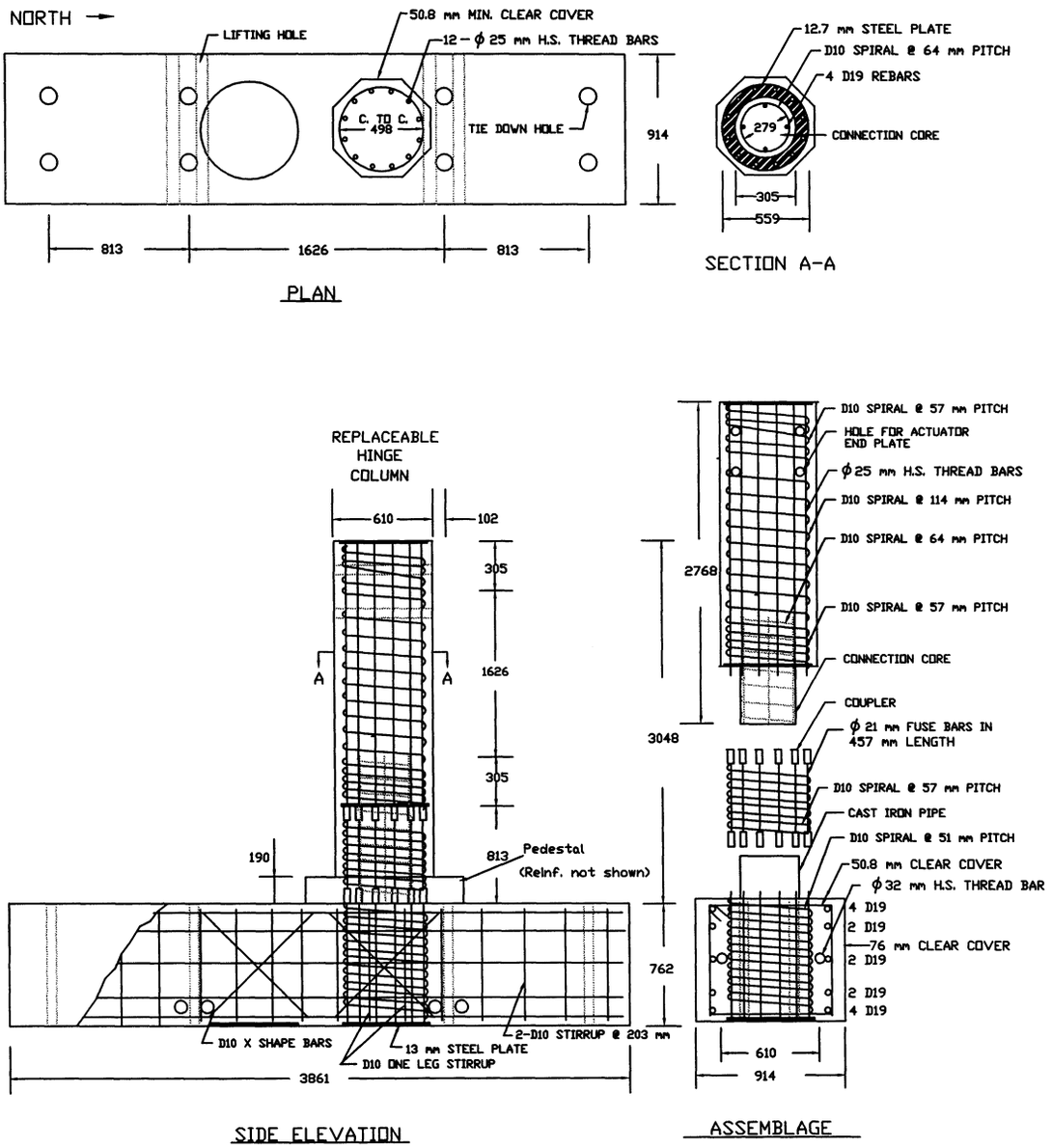

Figure 4-10 Construction Details of the Three Quarter Scale Prestressed Concrete CARD Specimen.

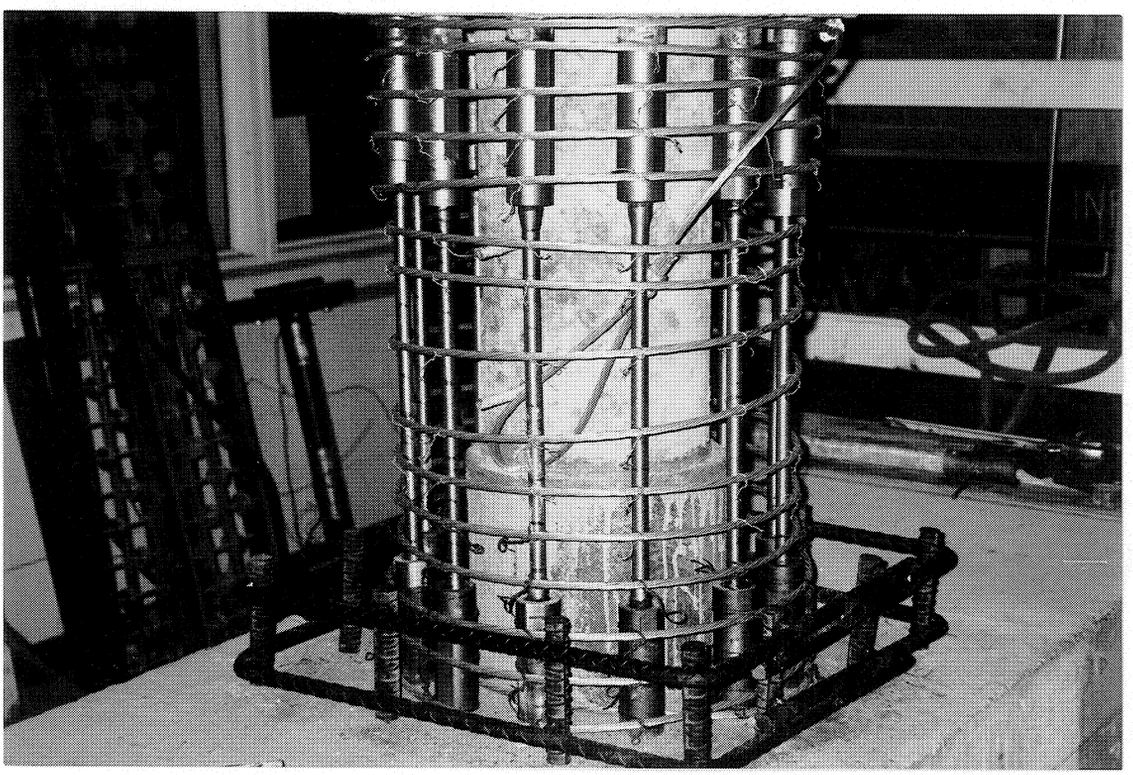

Figure 4-11 Photograph of the Hinge Zone of the ReCARD Specimen After the Placement of Transverse and Pedestal Reinforcement.

Table 4-3 Concrete Mix Proportions in the Replaceable Hinge Zone

Batch	*Water* / *EMARCO C77-CI*	*Pea Gravel* / *EMARCO C7-CR*	Pouring Height (*mm*)	28-Day Target Strength (*MPa*)
1	0.193	No	55	48
2	0.273	0.91	350	21
3	0.193	0.91	205	48

4.5 CLOSURE

This section provided a brief overview of the specimens that were tested as part of this research program. The construction details of the as-built lap splice column, its retrofit and a CARD specimen were discussed.

SECTION 5
EXPERIMENTAL RESULTS OF VARIABLE AMPLITUDE TESTS ON ReCARD SPECIMENS

5.1 INTRODUCTION

This section presents experimental results of the variable amplitude tests on the lap splice retrofit (Test R0) and its first repair (Test R1). The main purpose of these tests were to judge the efficiency of the retrofitting technique and verify the concept of repairability after a damaging earthquake.

5.2 EXPERIMENTAL PROTOCOL

Testing of the first retrofit (R0) and the repair (R1) was performed under displacement control where a command signal was provided by an analog function generator in the form of a positive sine wave which loaded the specimen first by pushing and then by pulling. The loading consisted of two cycles each at drift amplitudes of $\pm 0.5\%$, $\pm 1\%$, $\pm 2\%$, $\pm 3\%$, and $\pm 4\%$. The specimen was tested at two quasi-static rates of cycling referred to as "slow" and "fast". Initially slow cycling at a 0.017Hz test frequency (60 s period) was used. In the latter stages of testing a fast loading at a 0.033Hz test frequency (30 s period) was used. The drift level for the fast cycle was maintained at $\pm 4\%$ until the end of testing. A constant vertical (gravity) load of 716 kN was applied to the specimen throughout each phase of testing. The sampling rate for the data acquisition system was set at 3Hz and 6Hz for slow and fast loading respectively, both rates providing 180 data samples per cycle of loading.

5.3 VISUAL OBSERVATIONS

The strong upper portion of the column remained undamaged at all stages of loading. Thus all damage was forced into the sacrificial reinforced concrete (fuse-bar) hinge zone. The

flexure fatigue failure modes were dominant in all the tests. The following presents a descriptive outline of the events that occurred at various drift levels for each test.

Test R0 (First test after retrofitting the lap splice zone with fuse-bars)

Drift Level	*Events*
0.5%	One flexural crack initiated at the center of the hinge zone on both sides.
1%	Additional hairline flexural cracks appeared at the interface between middle and lower layers of concrete.
2%	Two new flexural and several vertical cracks opened on both sides.
3%	The existing cracks extended. Figure 5-1 shows a view of the specimen at the end of the 2% and 3% drift subtest.
4%	The concrete cover on both sides started spalling.
4%(fast)	Buckling of the fuse-bars was first observed in the north side in the first cycle of loading. Bar fracture due to low cycle fatigue occurred in the first quarter of the fourth cycle (south) and immediately on reversal (north). Figure 5-2 shows a view of the column at the end of testing.

Test R1 (Retest following first repair after initial testing and damage sustained by Test R0)

Drift Level	*Events*
0.5%	One flexural crack initiated at the center of the hinge zone on both sides. A flexural crack on the north side appeared at the interface of middle and lower layers of concrete. Figure 5-3 shows a view of the specimen at this stage.
1%	The flexural crack at the center widened.
2%	Several inclined cracks appeared on both sides as indicated in figure 5-4.
3%	The concrete cover on the north side started spalling.
4%	Concrete cover continued spalling. Diagonal cracks opened on both east and west sides. Longitudinal reinforcement in the south side fractured during the second cycle at 4% drift.

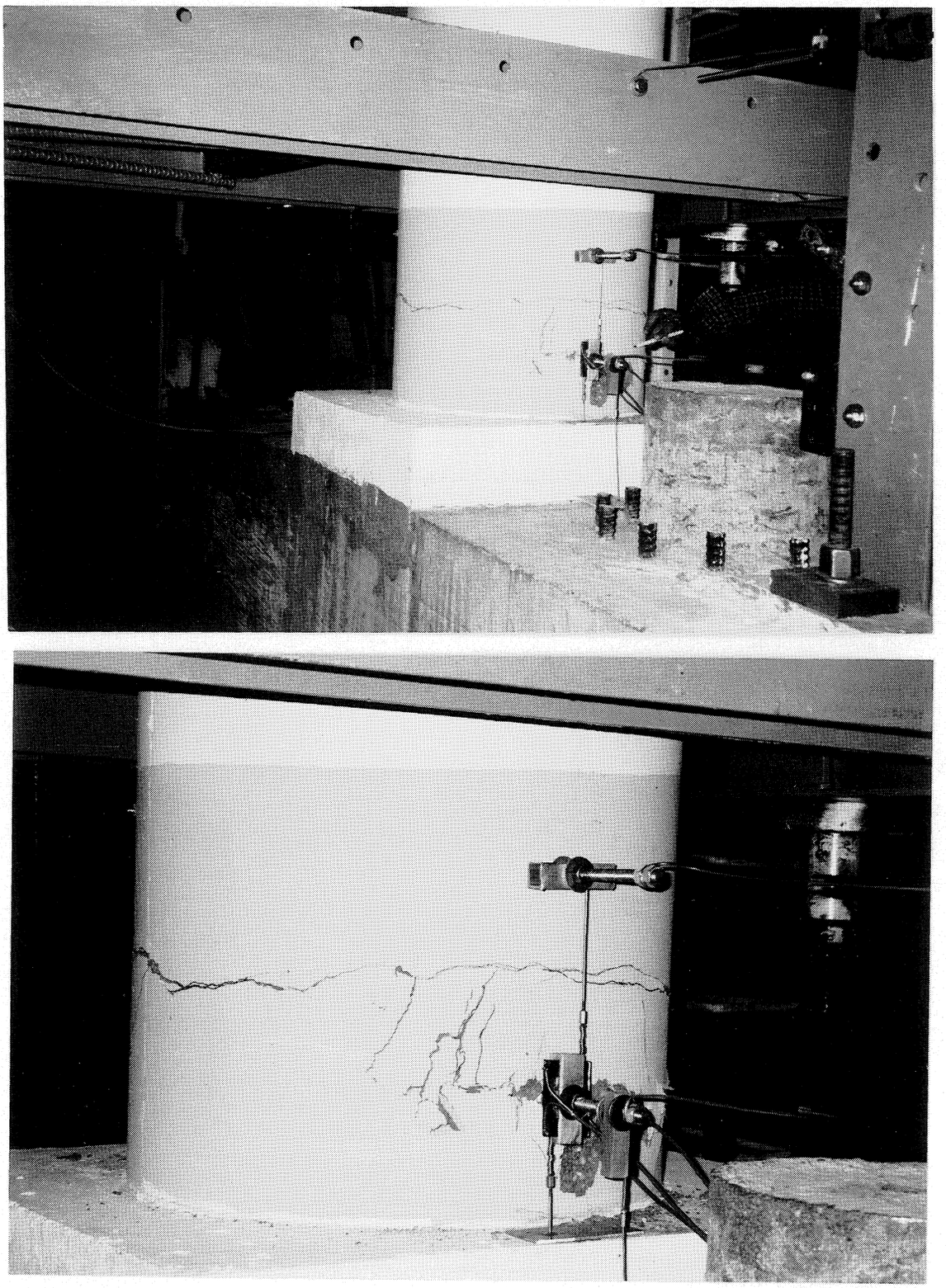

Figure 5-1 Photographic View of the Specimen R0 at the Conclusion of 3% Drift Level.

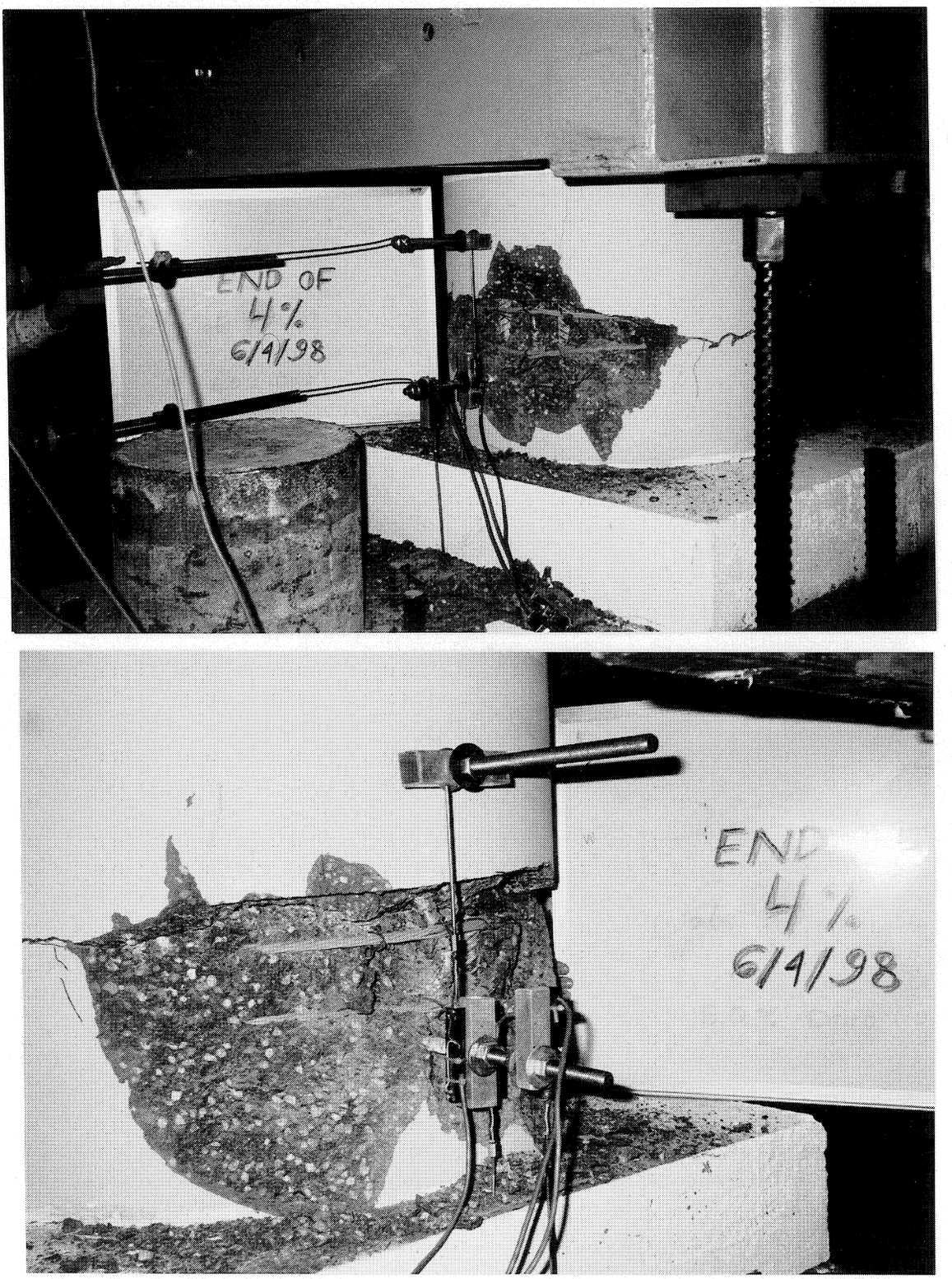

Figure 5-2 Photographic View of the Specimen R0 at the Conclusion of Test.

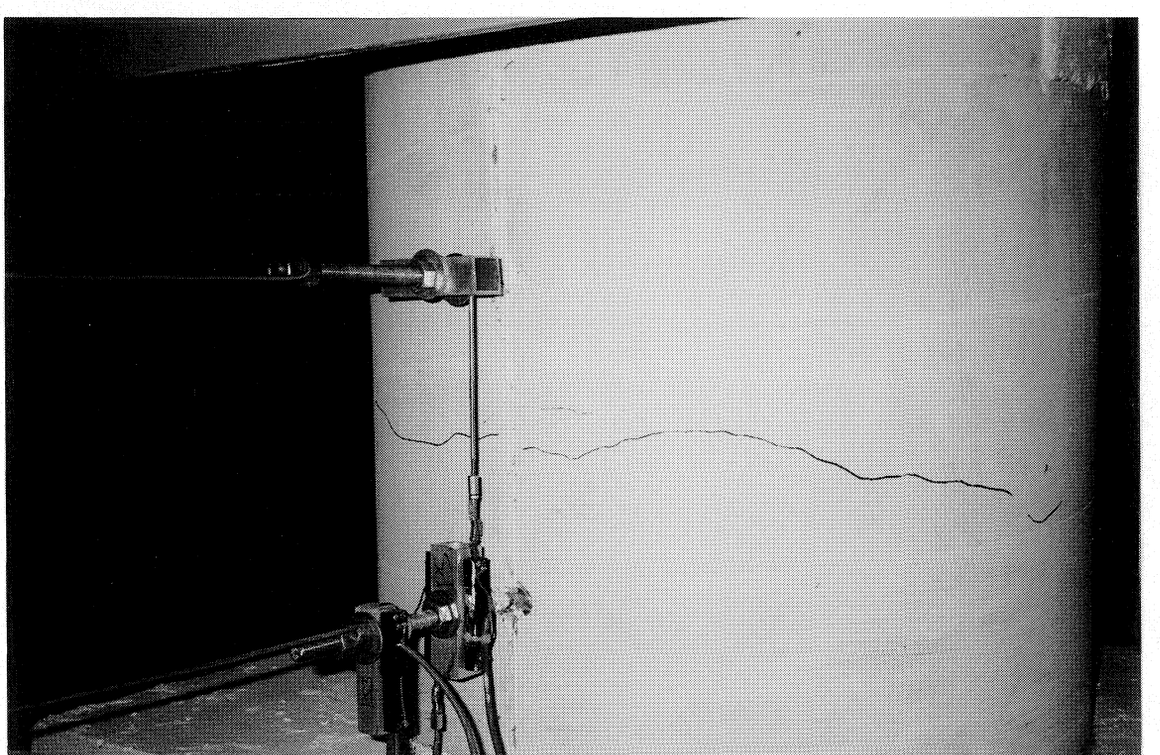

Figure 5-3 Photographic View of the Specimen R1 at the end of 0.5% Test.

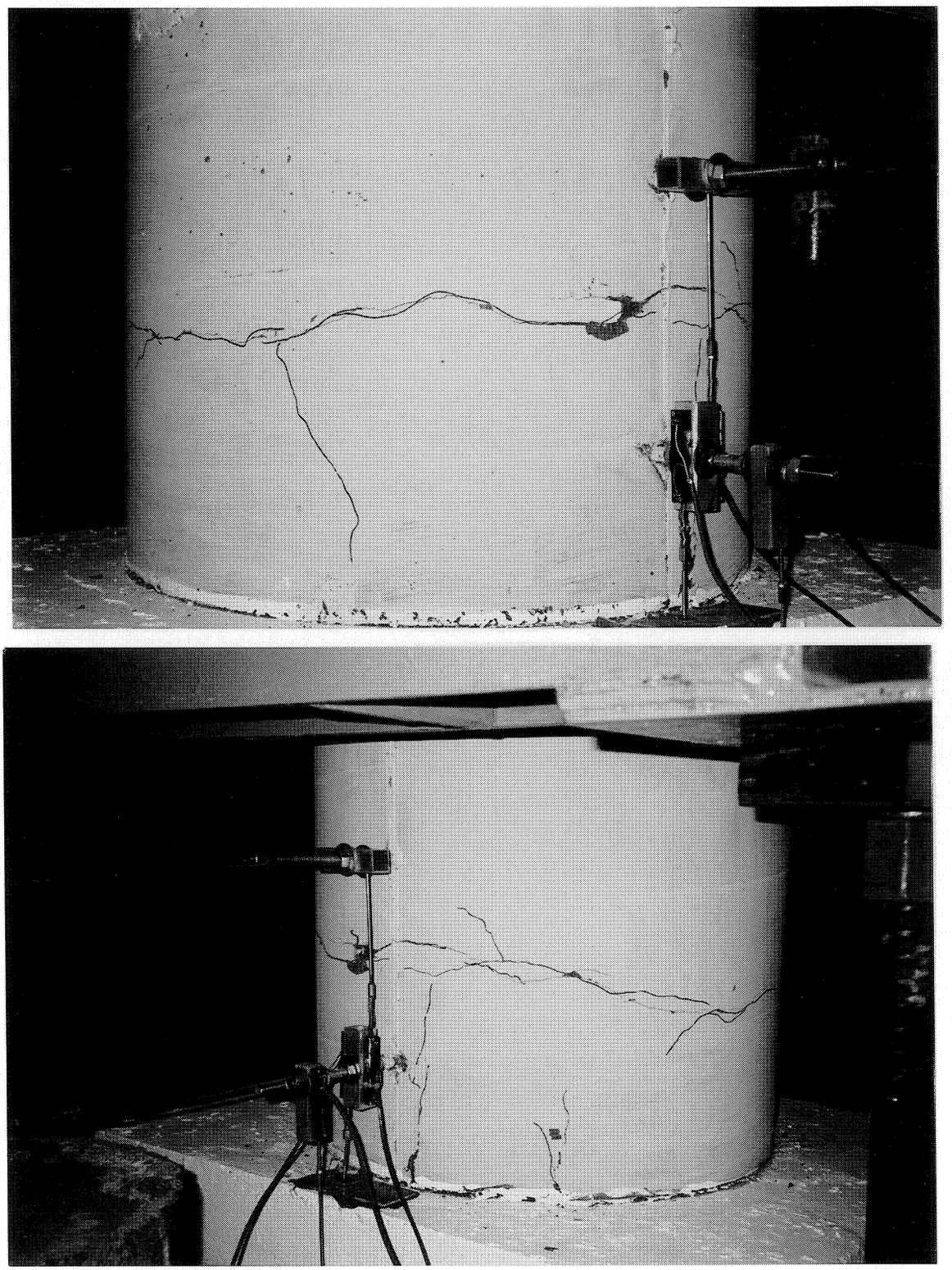

Figure 5-4 Photographic View of Specimen R1 at the end of 2% Drift Sub-test.

4%(fast) at — Buckling of the longitudinal reinforcement was observed during the second cycle 4% (fast) in the north side. Longitudinal rebar in the north side fractured in the fourth cycle. Figure 5-5 shows the specimen at the end of testing.

5.4 Hysteretic Performance

The lateral force versus column displacement results from the tests R0 and R1 are plotted in figure 5-6. The "reversed Z" dotted line in each graph represents the nominal flexural strength of the specimen accounting for the $P-\Delta$ effect. Note that the nominal flexural strength is based on measured material properties. Both columns behaved in a ductile manner showing good energy dissipation.

In the slow loading tests, both specimens behaved essentially elastic until reaching $\pm 1\%$ drift and then entered into the plastic range at $\pm 2\%$ drift. The lateral force in both columns reached a maximum (about 0.3 base shear capacity) in the first cycle of 2% drift for all columns. Degradation in the force level was observed due to spalling of the cover concrete and buckling of the longitudinal rebars. For both columns there was a sudden drop in the force level when bars fractured at 4% drift.

5.5 Strength Degradation and Energy Absorption

Figure 5-7(a) presents the peak forces for all columns with respect to the applied cumulative total drifts. The total forces are defined here as the average of the push and pull loading directions in one complete reversal cycle. The first repair (R1) had a premature bar fracture indicating lower force levels.

The normalized cumulative energy (defined in equations 3-12 and 3-13) versus the cumulative plastic drift for each test is plotted in figure 5-7(b). The dashed line represents the efficiency of the specimen with respect to EPP behavior. This is used as a reference to compare

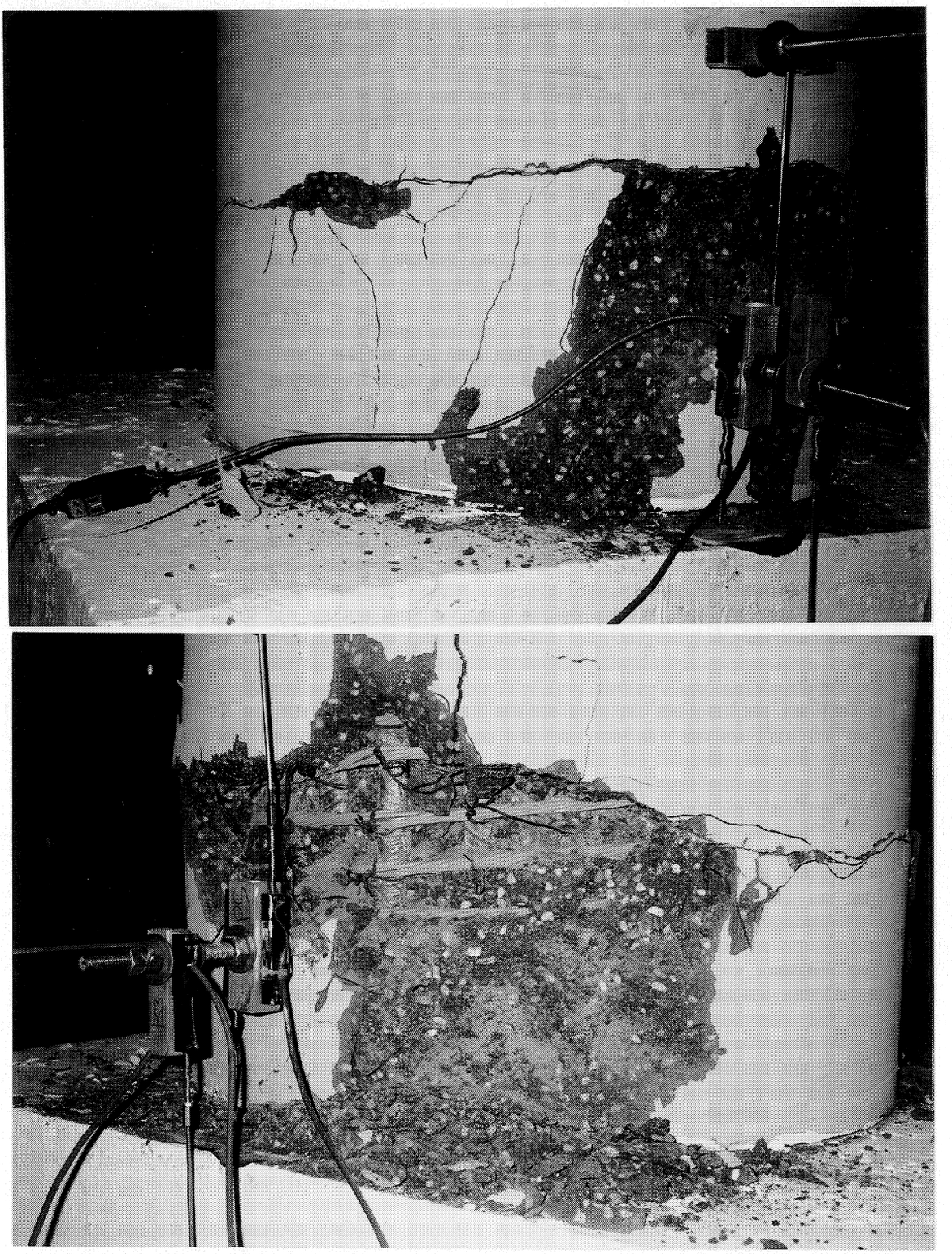

Figure 5-5 Photographic View of the Specimen R1 at the Conclusion of Test.

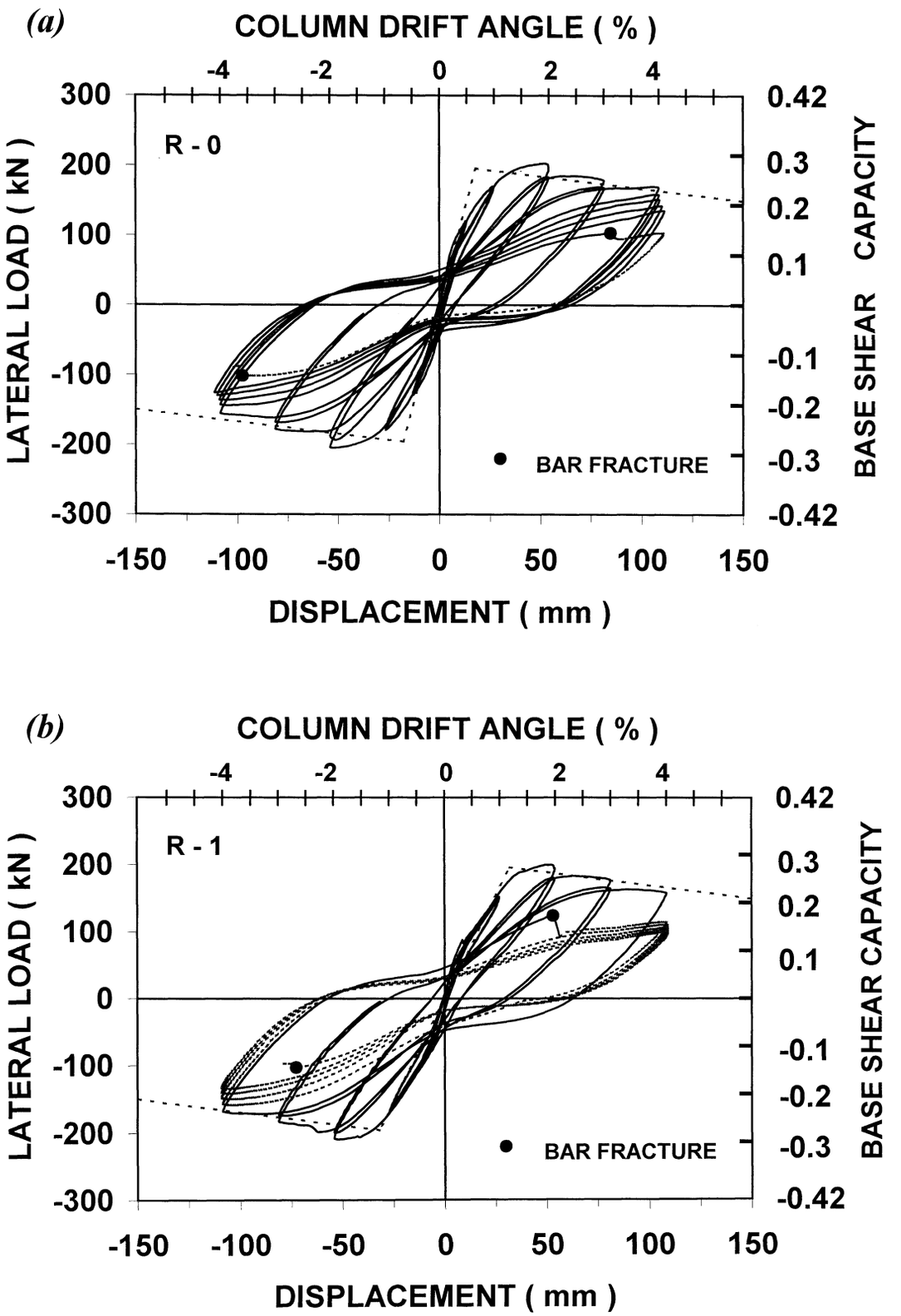

Figure 5-6 Force Displacement Hysteresis Loops for (a) Test R0 and (b) Test R1.

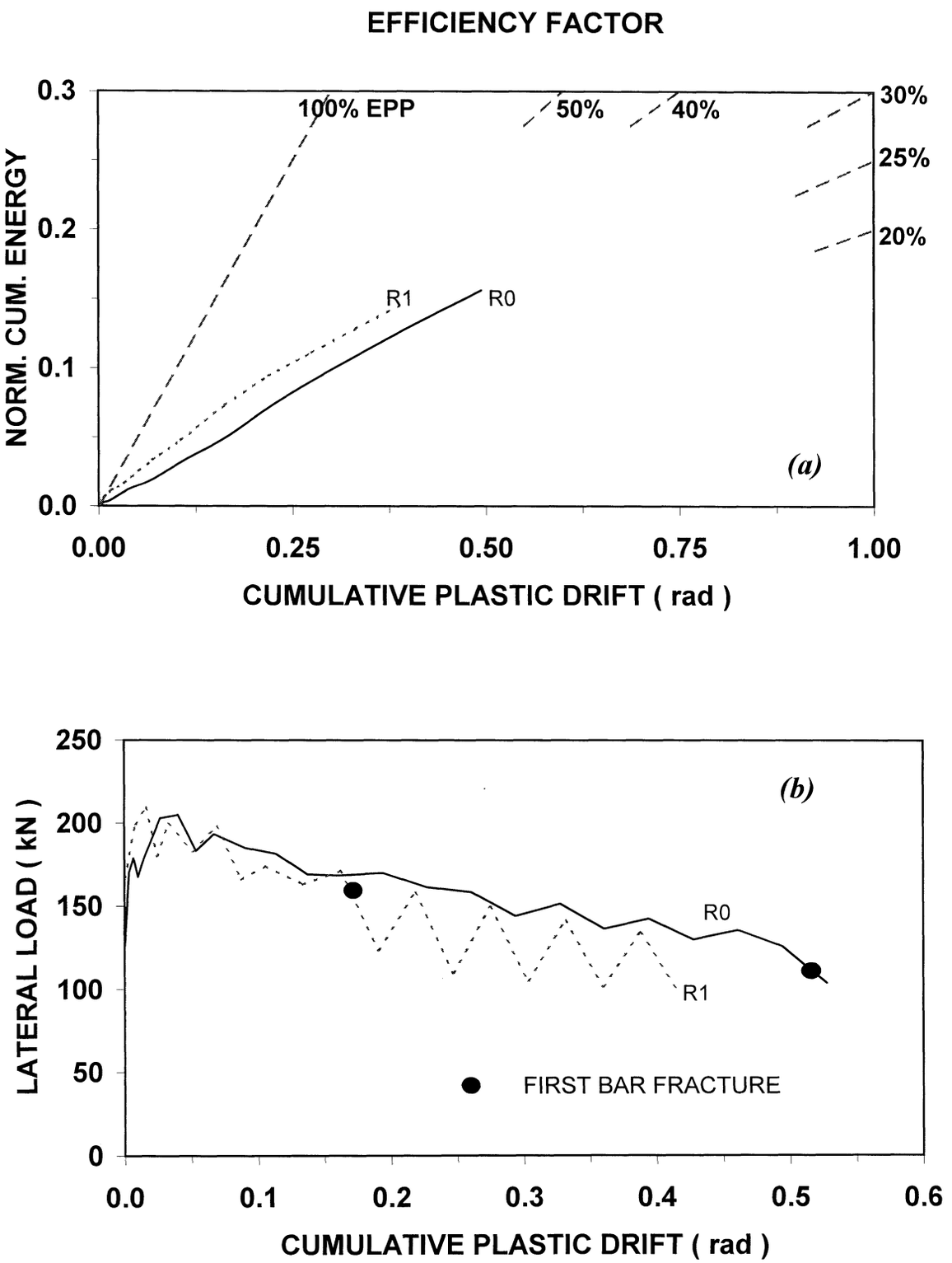

Figure 5-7 Showing (a) Efficiency Factor, (b) Variation of Peak Lateral Load (c) Damping Ratio and (d) Spectral Adjustment Factors.

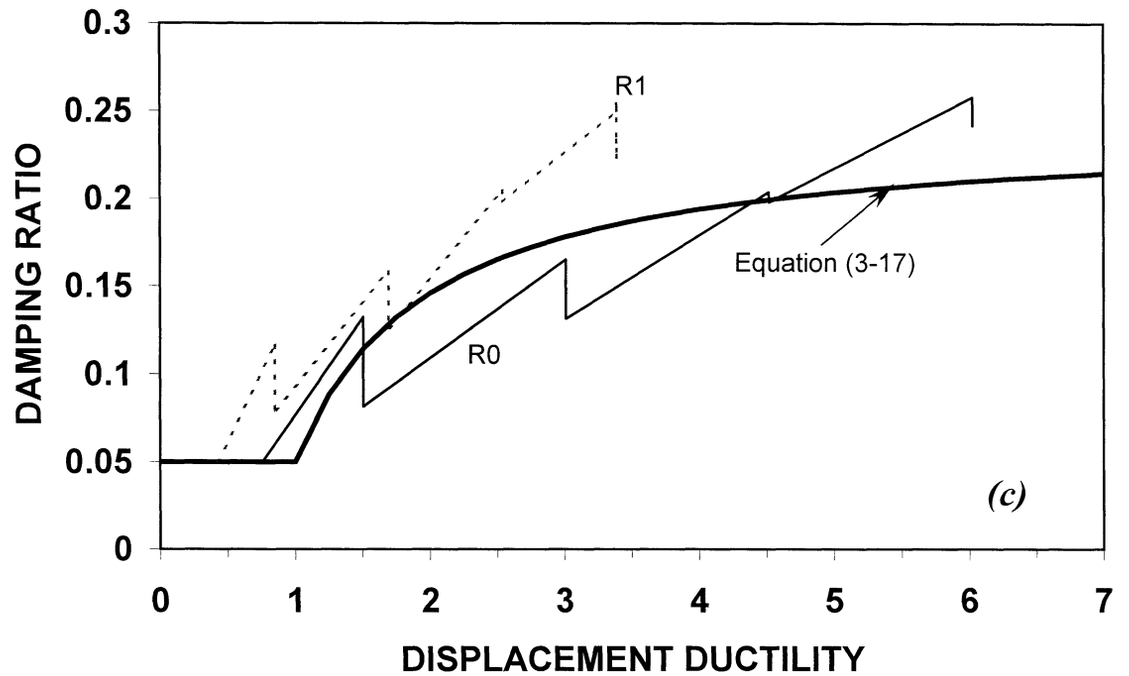

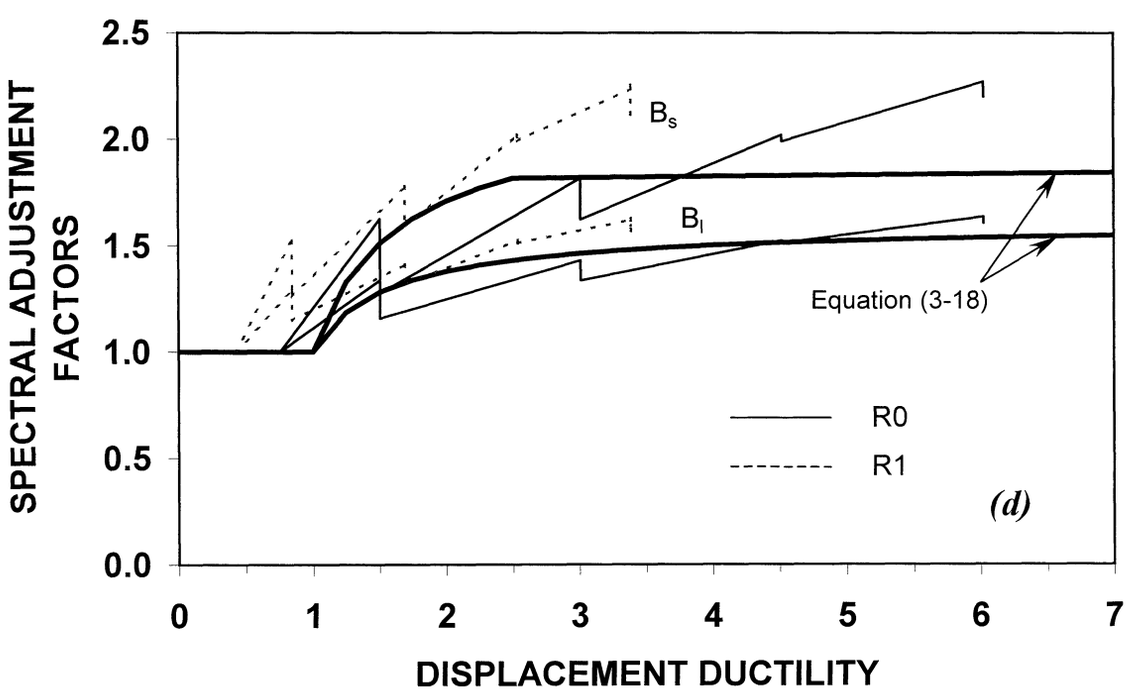

Figure 5-7 Continued.

energy absorption efficiency for each specimen. The procedure for determining the rate of energy absorption is the same as described in Section 3.4. For both specimens, overall energy absorption efficiency was about 27%.

The equivalent damping ratio (determined by equation 3-15) with respect to displacement ductility factor for each specimen is presented in figure 5-5(c). A prediction of theoretical damping calculated by equation (3-17) is also presented. The spectral adjustment factors are shown in figure 5-5(d).

5.6 Discussion

This section presented the variable amplitude test results on the retrofitted lap splice column and its first repair. As was evident from the test results, the retrofitted specimens performed very well and showed satisfactory energy dissipation characteristics. This was a marked improvement over the test results of Cheng (1997) as shown in figure 2-4. The repaired specimen performed as well as the original retrofit, thereby proving that such a technique can be reused repeatedly without any significant detrimental effect on performance.

SECTION 6
QUASI-EARTHQUAKE DISPLACEMENT EXPERIMENTATION

6.1 INTRODUCTION

This section presents the development of the Quasi-Earthquake Displacement (QED) experimental technique. This experimental technique uses a non-linear time-history computational simulation to predict seismic displacements and forces in a prototype structure. These earthquake-induced actions are scaled to permit laboratory experiments on reduced-scale subassemblages of the prototype structure. The QED experimental objective for this research was to verify the behavior of bridge piers built with sacrificial hinges to random displacement input such as that typically experienced under earthquake loading. The effect of variation of axial load on the column was also an issue that was investigated during this research.

6.2 PREVIOUS RESEARCH

Testing of structures subjected to randomly generated displacement is not new. Igarashi et al. (1993) and Seible et al. (1994) used an online technique to test a three-story in-plane shear walls and a five-story full scale masonry building. In this technique the structure was subjected to a ground motion, its stiffness evaluated and fed into a computer program, the restoring force output from which was input to the actual structure and the loop retraced. Kunnath et al. (1997) while experimenting on one-quarter scale bridge piers used generated displacement output from the inelastic analysis program IDARC as an input signal to the test specimens. The sequence of chosen earthquake ground motions represented various combinations of a major earthquake, a minor aftershock and finally a major event. However, none of the above research studied the influence of axial load variation that can play a important role when significant inelastic behavior is expected in the structural concrete element. This research uses a similar technique as the one used by Kunnath et al. (1997) with further modifications to account for axial load changes. Two

specimens were tested – a CARD specimen which essentially was a fourth repair of the column tested by Cheng and Mander (1997) and a further repair (Test R2) of the three-quarter scale lap splice column. Details of the experimental program are presented next.

6.3 Quasi-Earthquake Displacement (QED) Experimentation

A fourth repair of the CARD specimen tested by Mander and Cheng (1997) and a further repair of the ReCARD specimen was tested under a random displacement pattern to simulate the effects of real ground motion. The Quasi-Earthquake Displacement (QED) experimentation technique was introduced as a method of testing. This requires the prototype (full scale) bridge to be modeled by any reasonable inelastic analysis program and subjected to a dynamic input. Such input should ideally characterize a foreshock, a main shock and an after shock. The real magnitude of the forces and deformations obtained from the computer program can then be appropriately scaled and used on the model structure.

The QED technique was used for the testing the CARD and ReCARD specimens. The hybrid setup discussed in section 3.3 was used for application of the lateral and vertical load on the specimen with the angle of inclination chosen as $\theta = 28.2°$ based on laboratory constraints (refer to figure 6-1 for a schematic of the test setup). However, since the inclined actuator was to operate on displacement control it was necessary to know the exact displacement signal that it was to follow. For this purpose a prototype bridge was modeled using the inelastic analysis program Drain-2DX and subjected to a random ground motion input. The results from the computer simulation were used as input to the three-quarter scale specimens after applying proper scale factors. The details of the model is discussed next.

Full Scale Computer Model: The prototype structure was modeled as part of a long multiple span concrete slab on steel girder bridge (figure 6-2a). Each span was assumed as $28\,m$ in length and $10\,m$ in width. The soffit of the superstructure was assumed to be $7\,m$ above the rigid piled foundation. For simplicity, the effective deck weight (girders, concrete deck, guard rails) was assumed as $7\,kPa$.

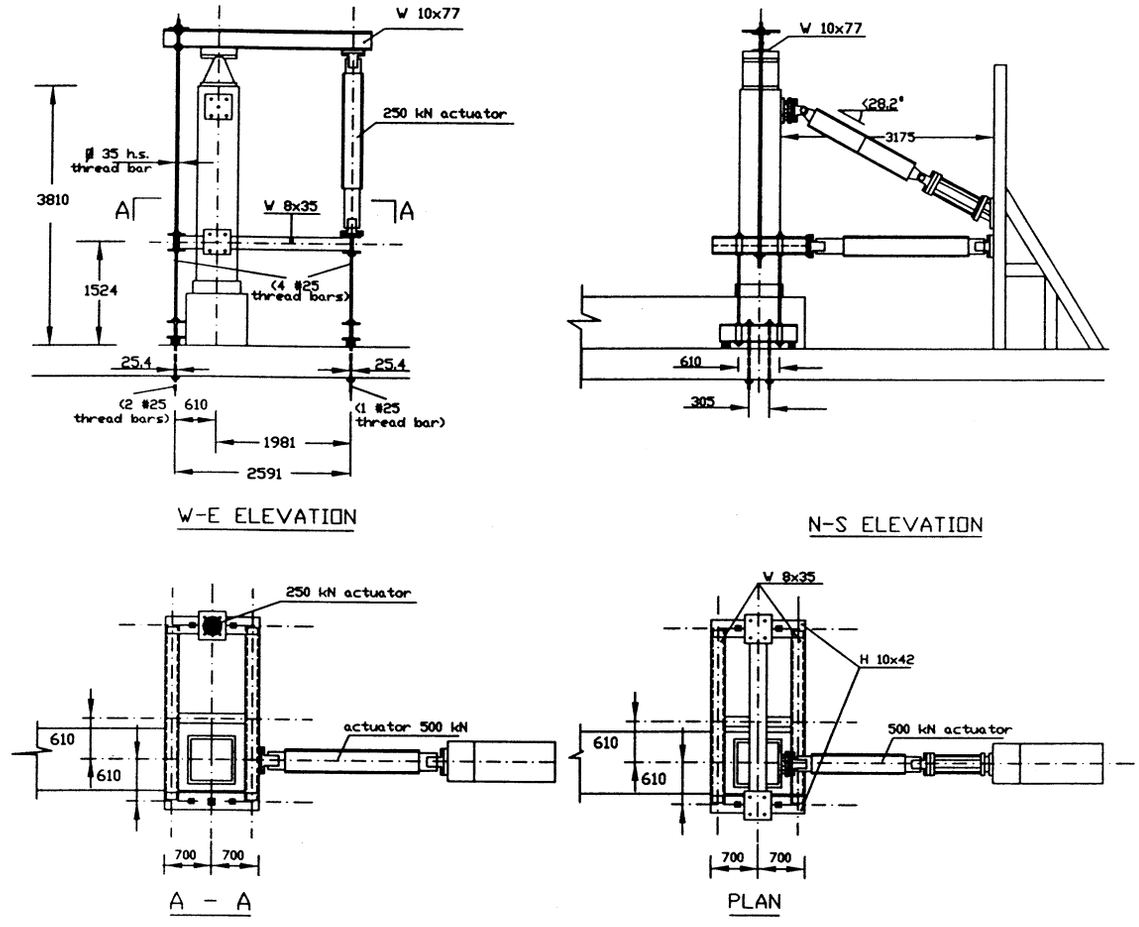

Figure 6-1 Test Setup for the QED Experimentation.

Tributary gravity weight:

$$W_y = 10\,m \times 28\,m \times 7\,kPa = 1960\,kN$$

Transverse inertia weight:

$$W_x = 2 \times W_y = 3920\,kN$$

The transverse inertia weight was chosen as double the gravity weight to deliberately magnify the lateral displacement. The model also assumed two columns at the bent, each of diameter = $0.8\,m$.

Cross sectional area of each column:

$$A = \frac{\pi}{4} \times D^2 = \frac{\pi \times 0.8^2}{4} = 0.502\,m^2$$

Column self weight:

$$W_{self} = A \times H \times \rho = \frac{\pi \times (0.8\,m)^2}{4} \times 7\,m \times 2.4\,t/m^3 \times 9.81\,m/s^2 = 88\,kN$$

where A = area of the column, H = effective height of the column, ρ = density of concrete.

Average axial load in each column:

$$P = 0.5\,W_y + W_{self} = 0.5 \times 1960\,kN + 88\,kN = 1068\,kN$$

Total stiffness of pier bent:

Assuming the columns fixed at each end

$$K = \frac{24 \times E_c \times I_{cr}}{H^3} = \frac{24 \times \pi \times E_c \times D^4}{64 \times H^3}$$

where H = effective column height taken as $7\,m$, D = column diameter, E_c = Young's modulus of concrete calculated as $E_c = 4700\sqrt{f_c'(MPa)} = 4700\sqrt{40} = 30000\,MPa = 30 \times 10^6\,kPa$ and I_{cr} = cracked concrete moment of inertia with $I_{cr} = \frac{\pi \times D^4}{64} \times 0.5 = 0.01\,m^4$. Thus,

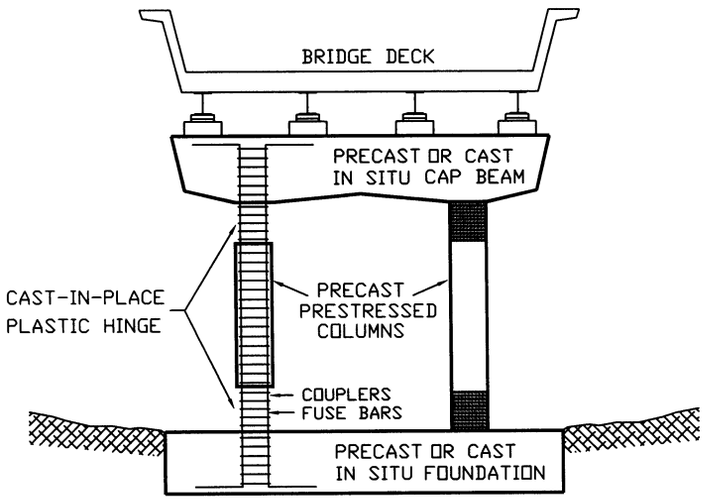

(a) Prototype Bridge Pier

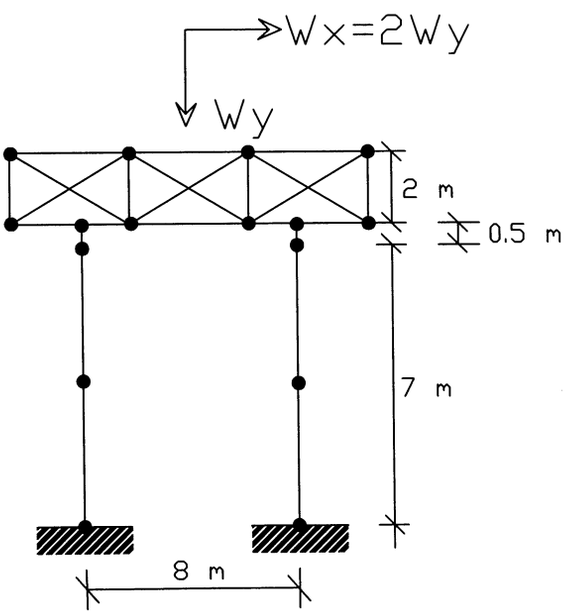

(b) DRAIN-D2DX Computer Model

Figure 6-2 Prototype Bridge Pier and the Computational Model used for Non-Linear Time History Analysis.

$$K = \frac{24 \times 30 \times 1000000 \times 0.01}{7^3} = 20991\ kN/m$$

The two-dimensional model of the prototype bridge, shown in figure 6-2(b), was composed of discrete beam-column elements having both flexural and axial stiffness in the DRAIN-2DX program. Flexural yielding was concentrated in plastic hinges located at the element ends. The post-yield stiffness was assumed to be 2% of the initial elastic stiffness. The gross moment of inertia of the columns in the model was multiplied by a factor of 0.5 to account for cracking. The soffit of the superstructure was modeled to be stronger than the pier bent so that an energy dissipation mechanism with plastic hinges at the ends of the columns was developed.

The model was tested under variable axial load and variable flexure in four stages. On the first three stages the algorithm presented in figure 6-3 was followed. The final stage of testing consisted of constant amplitude cycling at a drift amplitude of ±3.5%.

First Stage. The specimen was subjected to a sine wave with a drift amplitude of ±0.5%. Following the conclusion of the experiment, the experimental stiffness of the specimen was scaled up to 100% and used to represent the initial stiffness of the column in the computer model of the prototype bridge. Next TAFT (July 21, 1952, Lincoln School Tunnel S69E record) ground motion was selected to represent the foreshock. The horizontal component was scaled to give a PGA of 0.2g and the vertical component was scaled by the same factor as the horizontal. This earthquake motion was used to evaluate the dynamic response to the prototype bridge. After output axial force-time and displacement-time histories were generated, they were scaled to 75% and applied to the specimen.

Second Stage. The stiffness of the model was determined at the end of the previous experiment (the TAFT earthquake). The model stiffness was scaled up for the 100% prototype and used as input to the computational model. Dynamic nonlinear analysis was performed using

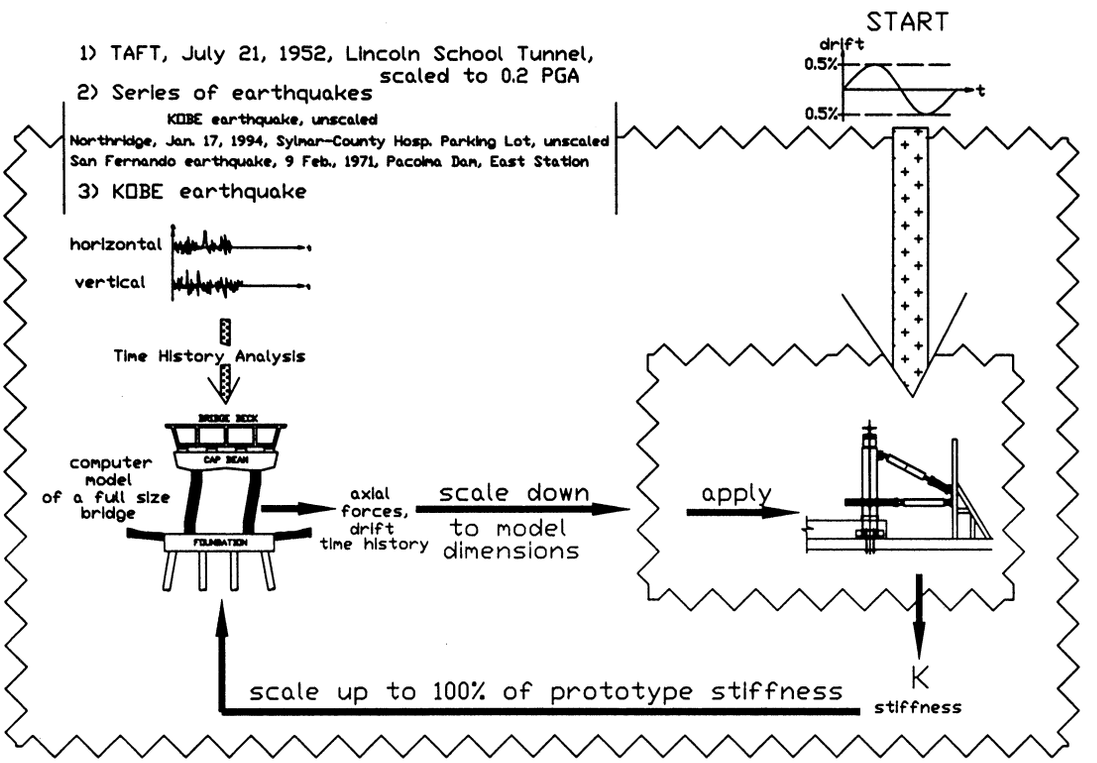

Figure 6-3 Algorithm used for the Testing of Prestressed Concrete CARD Specimen during the QED Experimentation.

various ground motion records of moderate and higher intensity, namely the Great Hanshin (January 25, 1995 Kobe Station N-S record), Northridge (January 17, 1994 Sylmar Hospital 90° record), and San Fernando (February 19, 1971 Pacoima Dam S16E record) earthquakes. Following the computer analysis the axial force-time and displacement-time histories were scaled and combined into one input segment and applied to the 3/4 scale model specimen in the laboratory. For each segment of earthquake, the responses of both the left and right piers were considered in the final combination.

Third Stage. The complete algorithm was repeated again for a Great Hanshin earthquake (January 25, 1995 Kobe Station) record.

Fourth Stage. The specimen was subjected to a constant amplitude ±3.5% drift cyclic test until failure occurred through low cycle fatigue of the longitudinal reinforcement.

The prestressed concrete CARD specimen was tested with the generated random displacement pattern from the computer program DRAIN-2DX. Figures 6-4, 6-5 and 6-6 show the displacement and axial load signals applied to the column during the first three stages of testing. Due to the difficulties in implementing the output rate in the servo controlled actuator, the displacement signals were slowed down respectively by factors of 5, 10 and 20 for the Taft, series of earthquake (second stage) and Kobe records.

Similar to the prestressed concrete CARD specimen the first phase of this test consisted of two cycles at 0.5% drift amplitude. Due to the similar stiffnesses of the ReCARD and CARD specimens the same displacement history was run for the ReCARD specimen. In this way it was considered possible to easily establish similarities and/or differences between the two specimens.

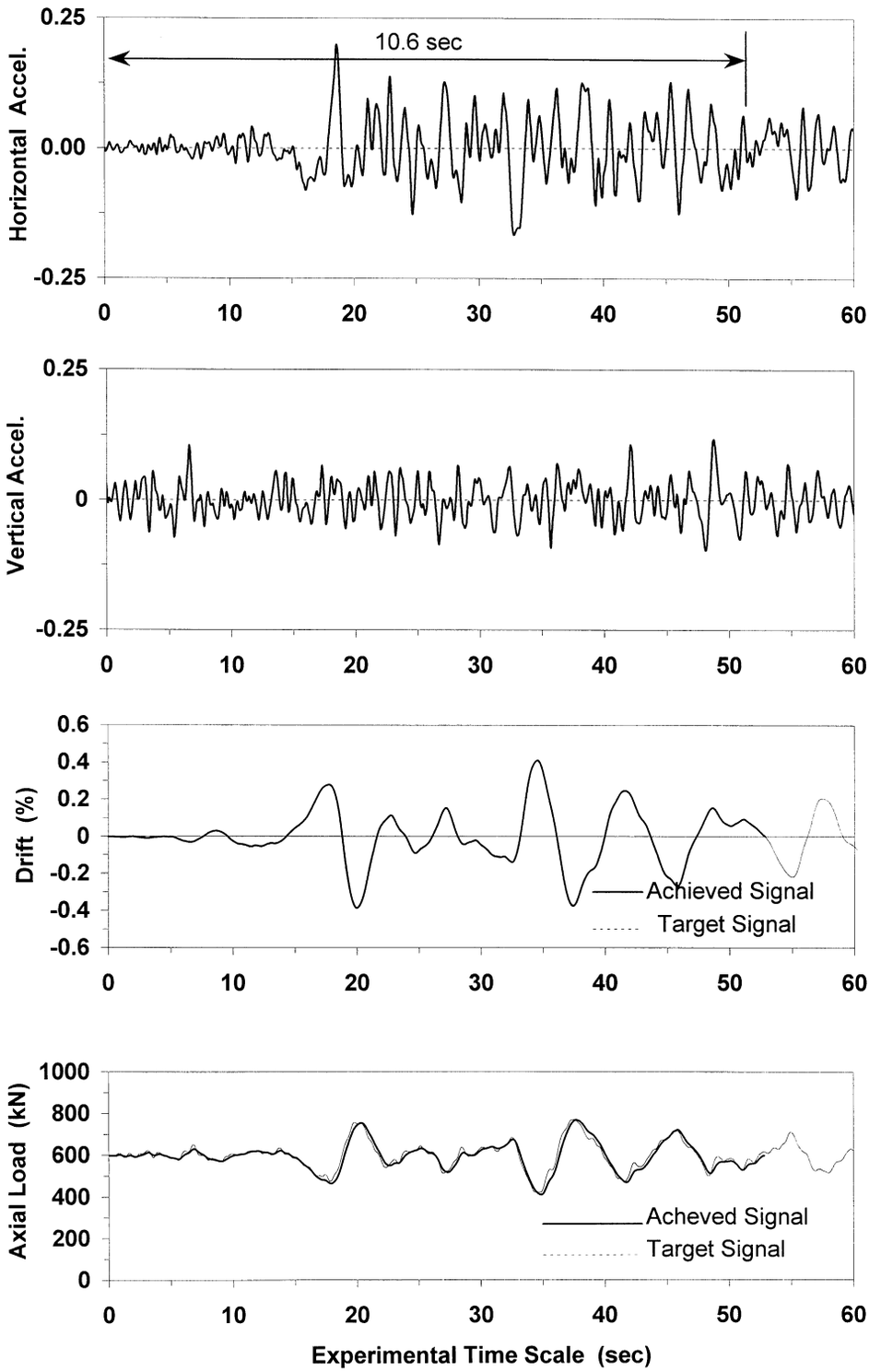

Figure 6-4 **Horizontal and Vertical Components of Acceleration used for generating the Target Drift and Axial Load Signals for the Taft (Lincoln School Tunnel S69E Record) Earthquake.**

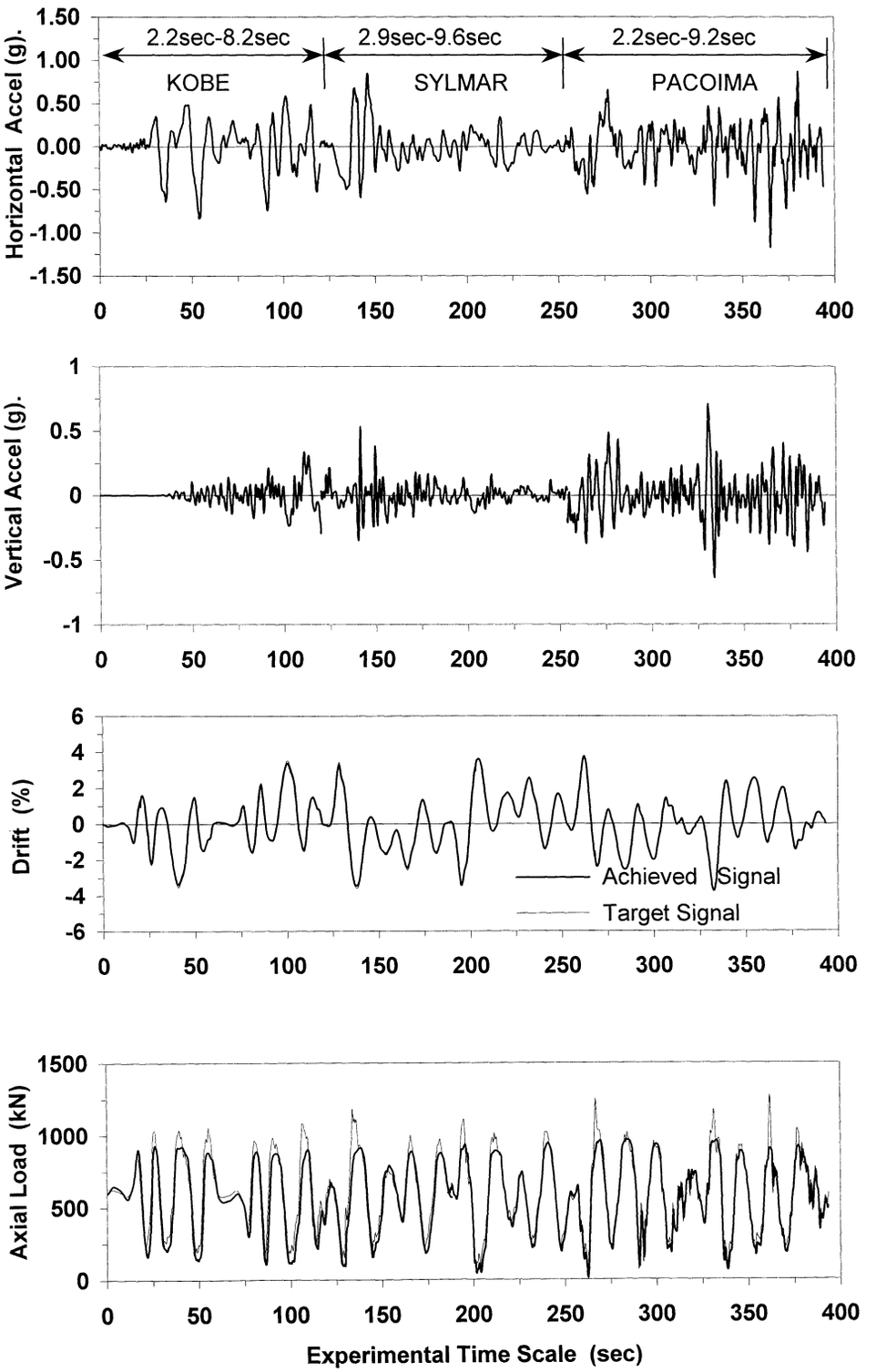

Figure 6-5 **Horizontal and Vertical Components of Acceleration used for generating the Target Drift and Axial Load Signals for the Series of Earthquakes.**

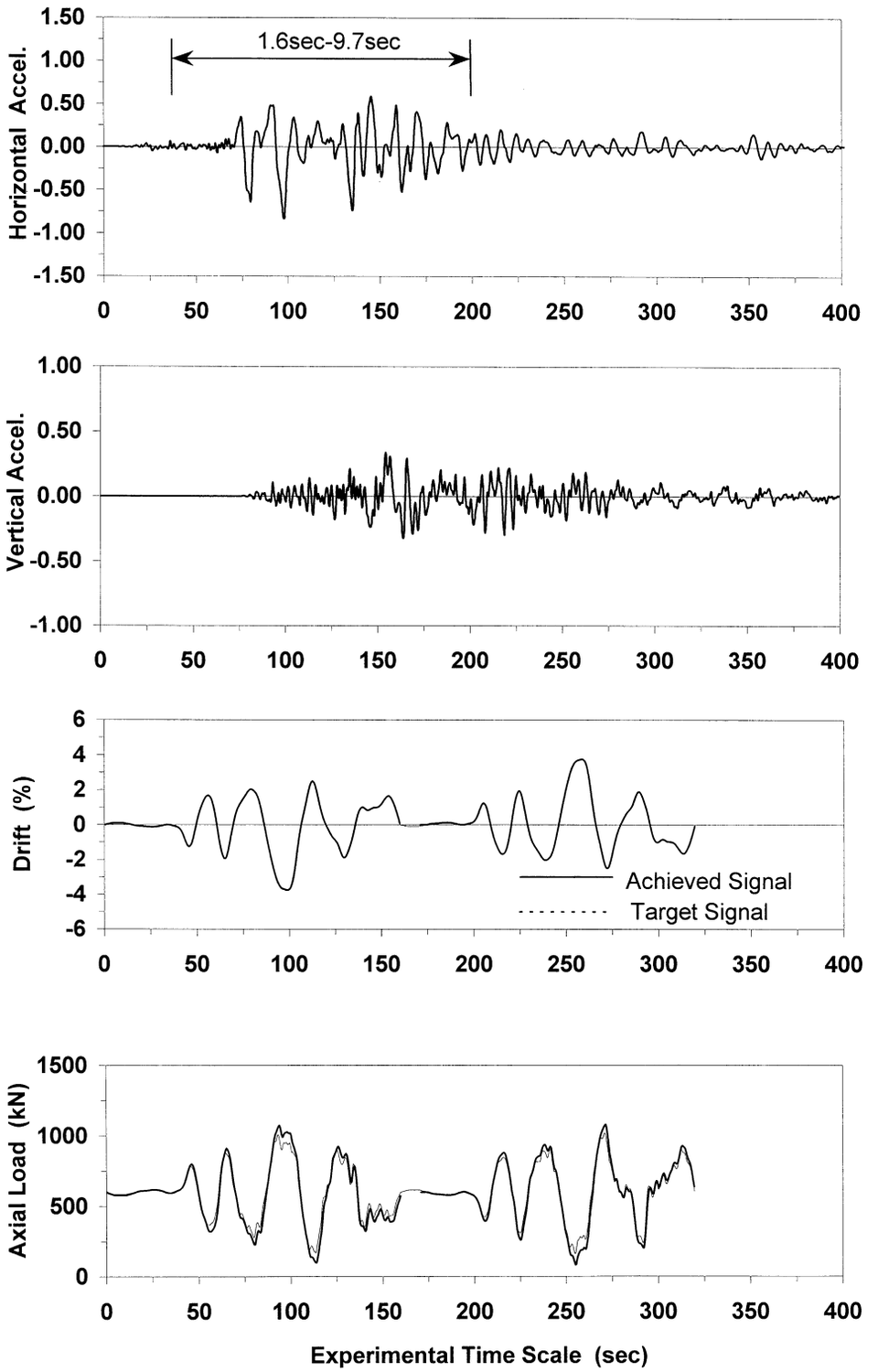

Figure 6-6 **Horizontal and Vertical Components of Acceleration used for generating the Target Drift and Axial Load Signals for the Kobe (Kobe Station N-S Record) Earthquake.**

6.4 CLOSURE

Quasi-Earthquake Displacement (QED) Experimentation was introduced as a means by which the seismic behavior of bridge piers subjected to seismic excitation can be verified. This technique uses a non-linear time history computational simulation to predict seismic displacements (and forces) in the prototype structure. These earthquake-induced actions are then scaled to permit laboratory experiments on reduced scale subassemblages of a prototype structure. Random displacement and axial load input segments obtained through computer analysis are then combined and applied to the experimental specimens. QED experimentation is useful for evaluating seismic behavior of experimental specimens by applying pseudo-dynamic forces and displacements.

SECTION 7
RESULTS OF QED EXPERIMENTATION

7.1 INTRODUCTION

Two 3/4 scale model bridge columns built with replaceable hinges were tested under combined axial load and flexure using the QED method. Real earthquake motions with large impulse and vertical acceleration components were used. Figures 6-4, 6-5 and 6-6 show the displacement and axial load signals applied to the column during the first three stages of testing. The results of the testing are discussed in what follows.

7.2 PRESTRESSED CONCRETE CARD SPECIMEN

Visual Observations: The strong upper portion of the column remained undamaged at all stages of loading. Thus all the damage was forced into the sacrificial reinforced concrete hinge zone. The flexure-fatigue mode was dominant. The following presents a description of observations at various stages of the test.

Phase	Events
0.5%	No visible distress to the column.
Taft 0.2g	Two major horizontal cracks and a number of inclined cracks appeared in the north and south side.
Series	Concrete cover on both sides started spalling. Figure 7-1 shows the specimen at the end of this stage.
Kobe	Cracks widened and the cover concrete continued to spall (figure 7-2).
3.5% drift	Bar fracture due to low cycle fatigue occurred in the eleventh cycle (south side). Figure 7-3 shows a view of the column at the termination of testing.

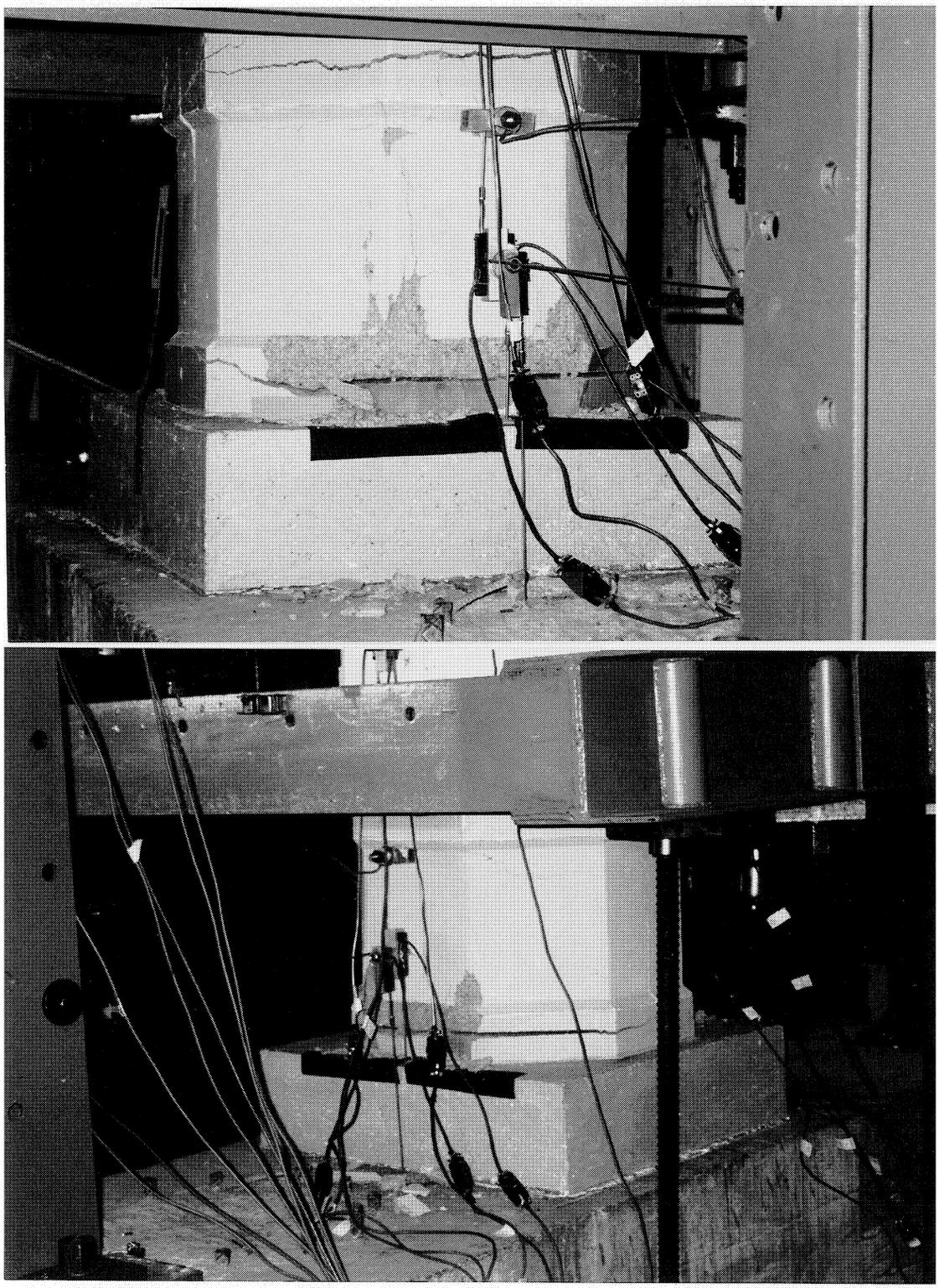

Figure 7-1 Photographic View of the CARD Specimen after the Conclusion of QED Testing with Series of Earthquake Records representing the Mainshock.

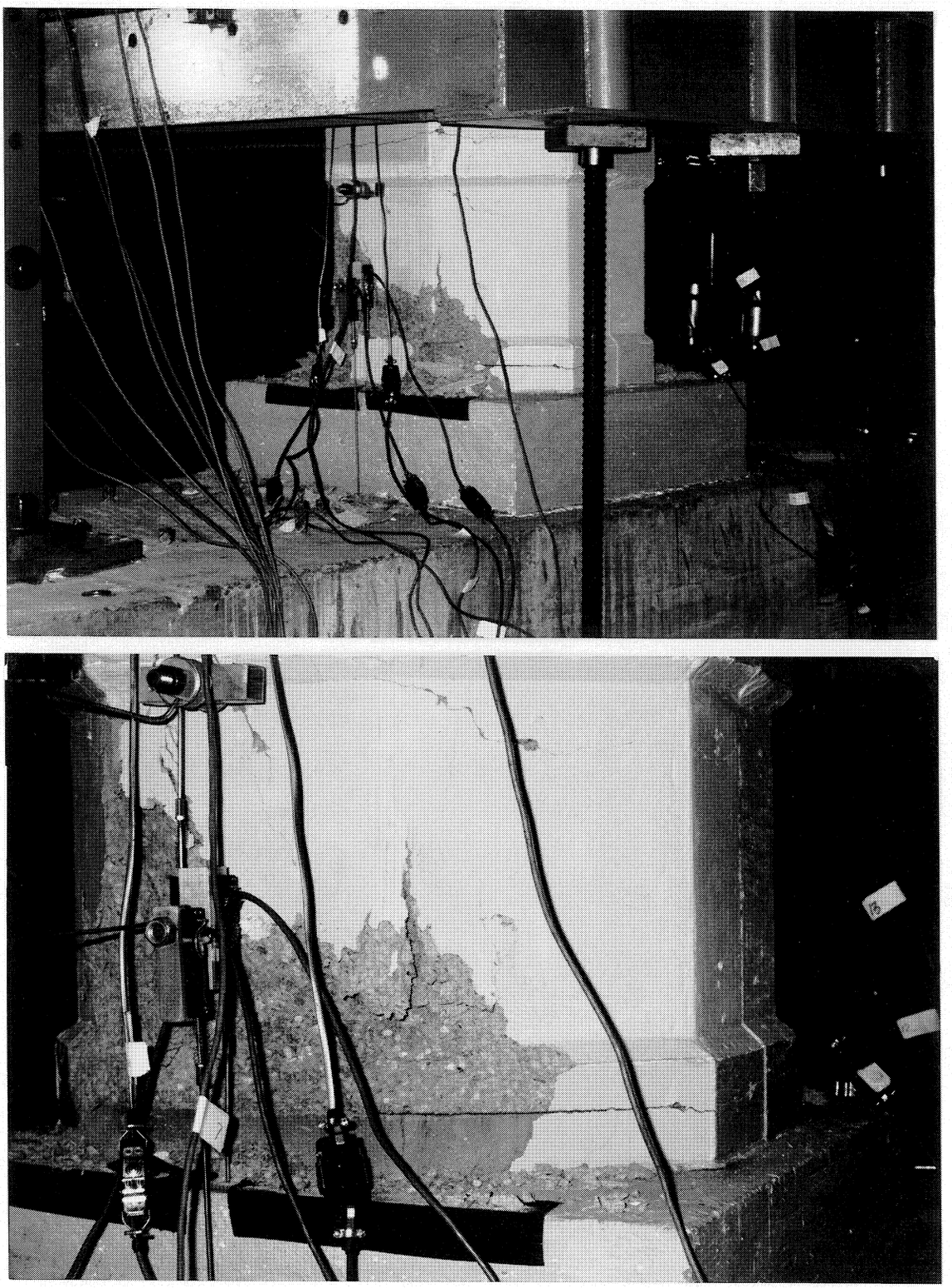

Figure 7-2 Photographic View of the CARD Specimen after the Conclusion of QED Testing with Kobe Earthquake Record representing the Aftershock.

Figure 7-3 Photographic View of the CARD Specimen after the Termination of the Final Constant Amplitude Testing.

Hysteretic Performance: The force-displacement hysteresis for the CARD specimen for each of the four stages of testing are plotted in figure 7-4. As can be seen, the column displayed satisfactory energy dissipation characteristics and maintained a steady lateral resistance until the fracture of the longitudinal bar due to low cycle fatigue. The moment curvature history for the random earthquake testing phase along with strain profiles at the indicated points are plotted in figure 7-5. Note that readings from potentiometers PW6 and PE6 (see figure 3-7) were used.

The final failure of the specimen was a result of fatigue fracture in the longitudinal fuse-bars. Fatigue fracture is dependant on the magnitude of strain amplitude. This is shown in figure 7-5)b). Since the primary effect of variation of axial load is to produce asymmetric strain profiles, it is apparent that it is also to effect the fatigue life of the specimen. This issue is addressed in Section 8.

7.3 ReCARD Specimen

Similar to the prestressed concrete CARD specimen, the first phase of this test on ReCARD specimen consisted of two cycles at 0.5% drift amplitude. However, the similarity between the stiffnesses of this specimen and the CARD specimen obviated any further analysis and enabled the axial load signals of figure 6-4, 6-5 and 6-6 to be applied with alteration.

Visual Observations: As was the case with the prestressed concrete CARD specimen, the strong upper portion of the column remained undamaged at all stages of loading with the damage being concentrated in the sacrificial fuse-bar zone. The following presents a description of observations at various stages of the test.

Phase	Events
0.5%	One hairline crack appeared at the center of the plastic hinge on the north side.
Taft 0.2g	Two major horizontal cracks and a number of inclined cracks appeared in the north and south side at the location where the original bars were cut.
Series	Concrete cover on both sides started spalling. Figure 4-7-1 shows a view of the

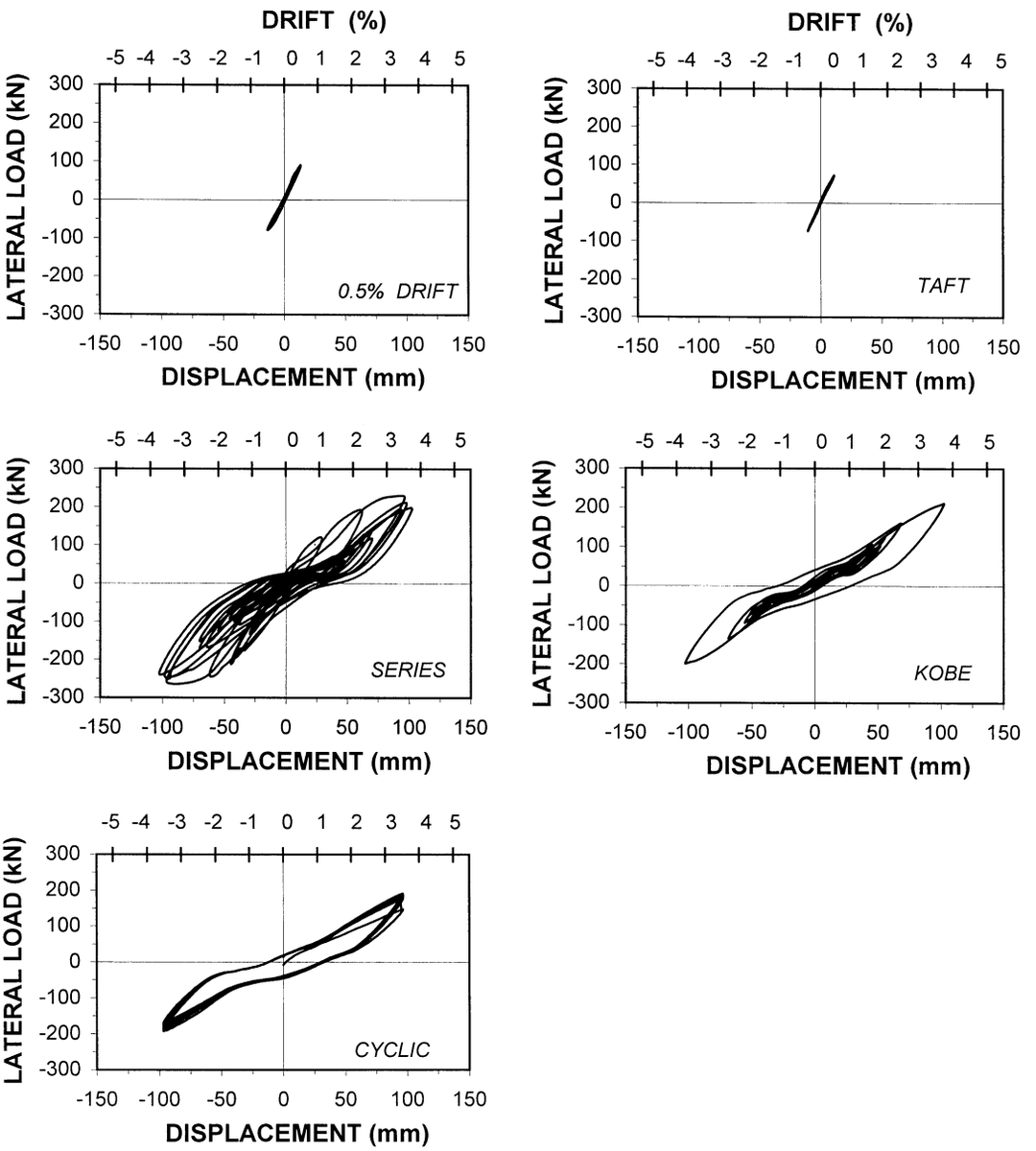

Figure 7-4 Force Displacement Hysteresis Loops for the CARD Specimen.

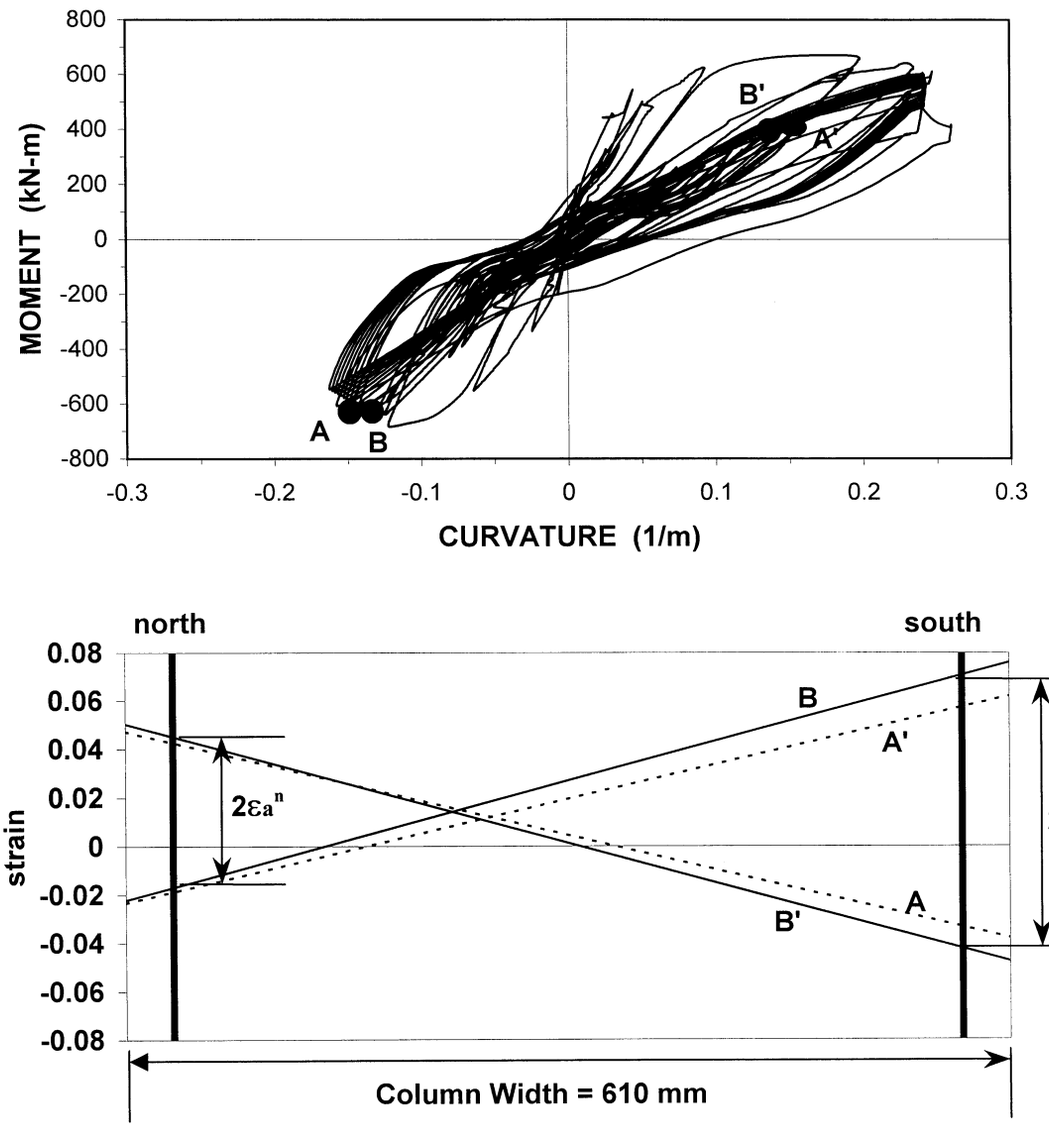

Figure 7-5 **(a) Moment Curvature Plot for the CARD Specimen and (b) Strain Profiles at points indicated in figure 7-5(a).**

specimen at the end of this stage.

Kobe — Cracks widened and the cover concrete continued to spall. First bar fracture occurred. Figure 7-7 shows a view of the column at the termination of testing.

Hysteretic Performance: The force-displacement hystereses for the ReCARD specimen are plotted in figure 7-8. Satisfactory energy dissipation characteristics as well as maintenance of a steady lateral resistance were observed until the fracture of the main rebar due to low cycle fatigue. The moment curvature history is plotted in figure 7-9. Only a pair of points are plotted since the potentiometer readings at high strain amplitudes were not consistent, apparently due to malfunctioning.

The overall hysteretic performance of the two specimens are compared in figures 7-10(a) and (b). As can be seen, the specimens display unequal strength in the two opposite directions. This is due to the variation of axial load and can be explained with the aid of a nominal axial load-moment interaction diagram for the two columns as shown in figures 7-11(a) and (b). The maximum and minimum axial loads in the P-M interaction diagrams correspond to the values attained during the QED experiments. It is observed from these results that the nominal lateral resistance (nominal moment divided by the lever arm) along with $P-\Delta$ effects constitute an envelope that closely traces the experimentally observed values. Excellent energy dissipation and maintenance of steady lateral resistance is observed from both the specimens.

7.4 CLOSURE

This section presented the results of testing of 3/4 scale CARD and ReCARD specimens subjected to Quasi-Earthquake Displacement (QED) experimentation. The behavior of bridge piers retrofitted with replaceable hinges responding in flexure to variable amplitude displacement and axial load input was closely investigated during this research.

The 3/4 scale reinforced concrete CARD and ReCARD specimens was tested under

realistic seismic input. The strong upper portion of both the columns remained undamaged at all stages of loading. All damage was forced into the sacrificial reinforced concrete hinge zone. The flexure-fatigue failure mode was dominant. Satisfactory hysteretic performance in terms of steady strength degradation and energy dissipation was observed.

The seismic resistance of these test specimens was more than adequate for several earthquakes. Therefore, the detailing would be satisfactory for a strong foreshock, mainshock, and aftershock.

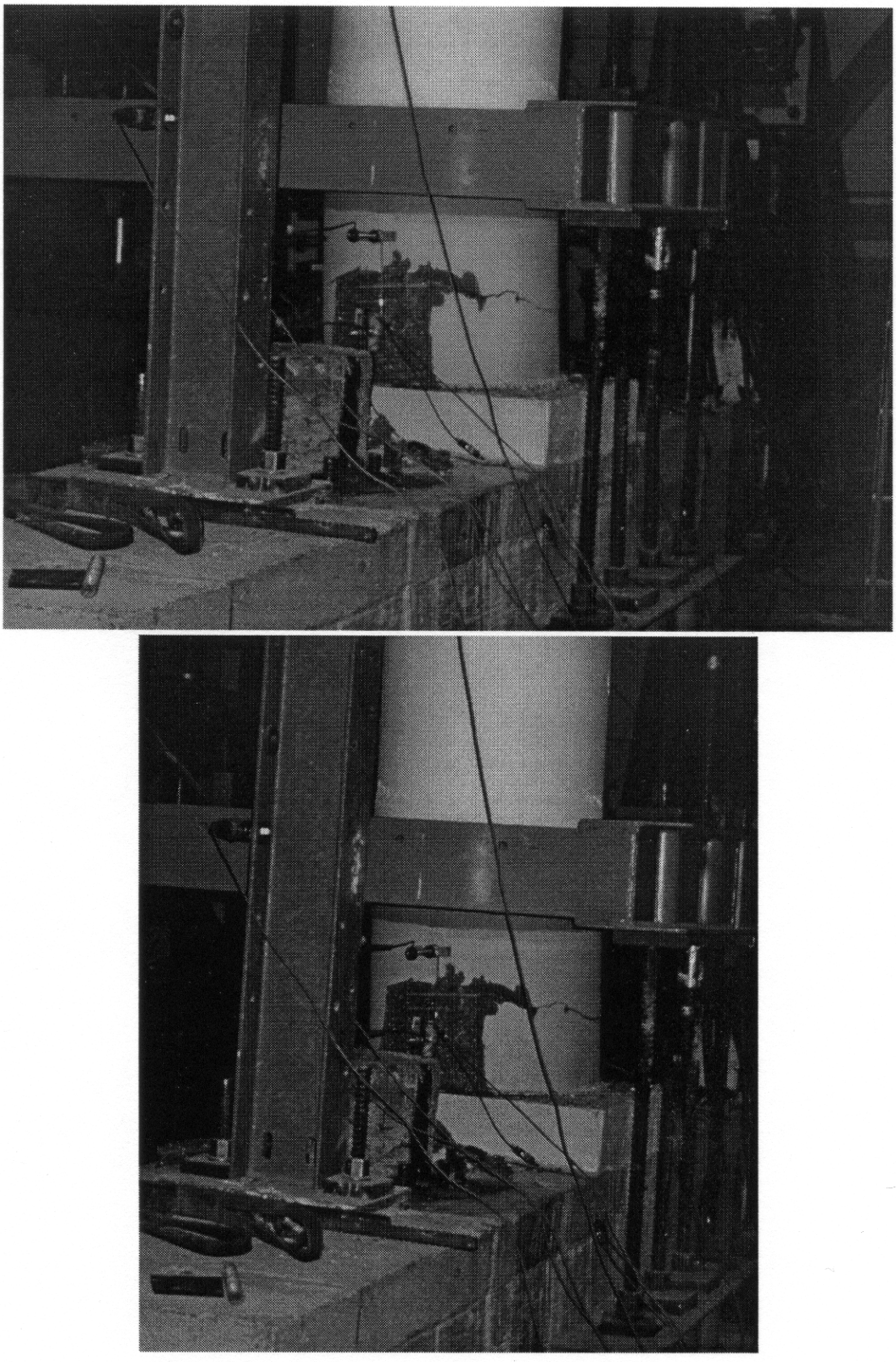

Figure 7-6 Photographic View of the ReCARD Specimen after the Conclusion of the QED Testing with Series of Earthquake Records representing the Mainshock.

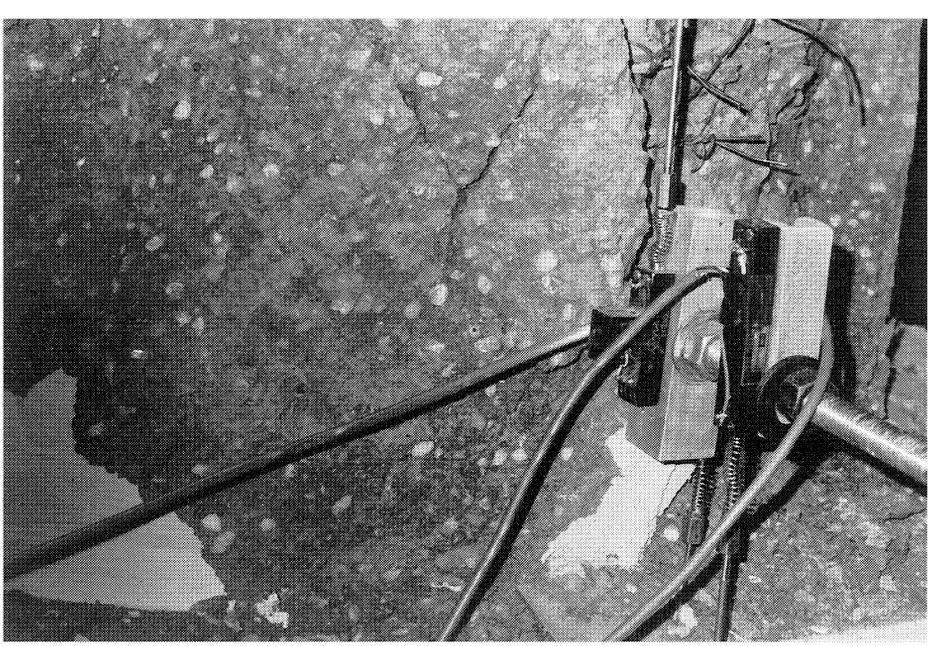

Figure 7-7 Photographic View of the ReCARD Specimen after the Conclusion of the QED Testing with Kobe Earthquake Record representing the Aftershock.

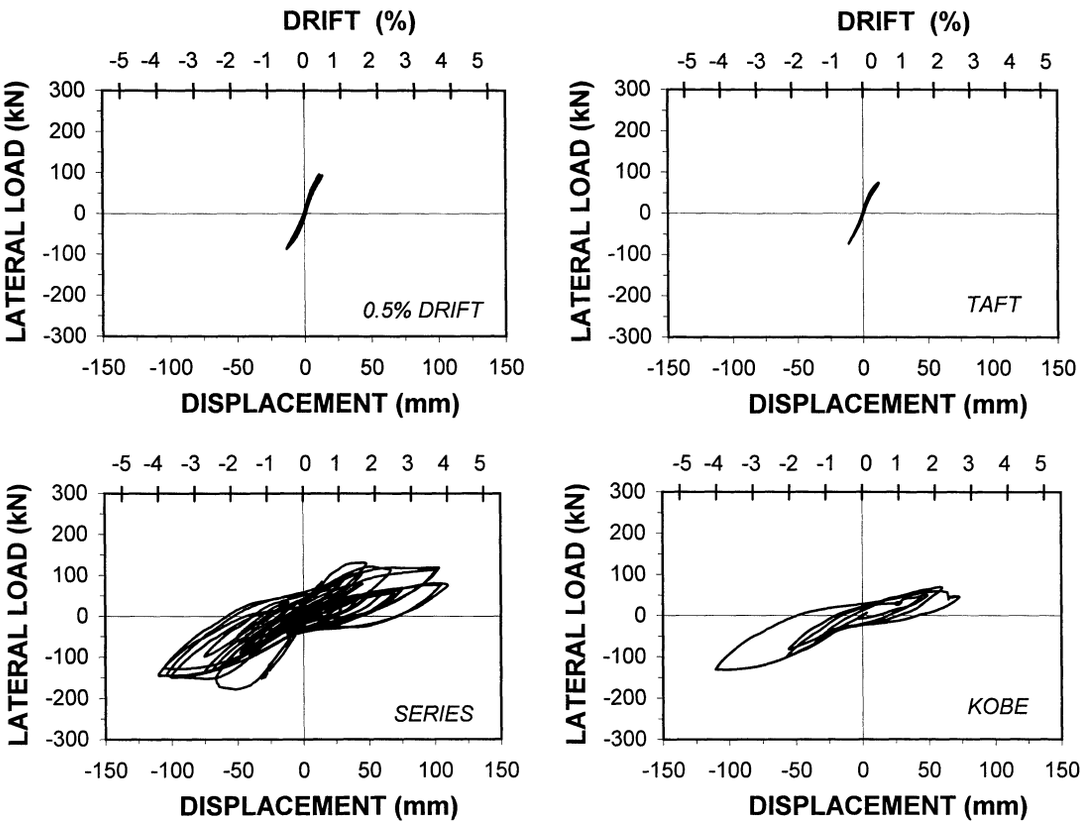

Figure 7-8 Force Displacement Hysteresis Loops for the ReCARD Specimen.

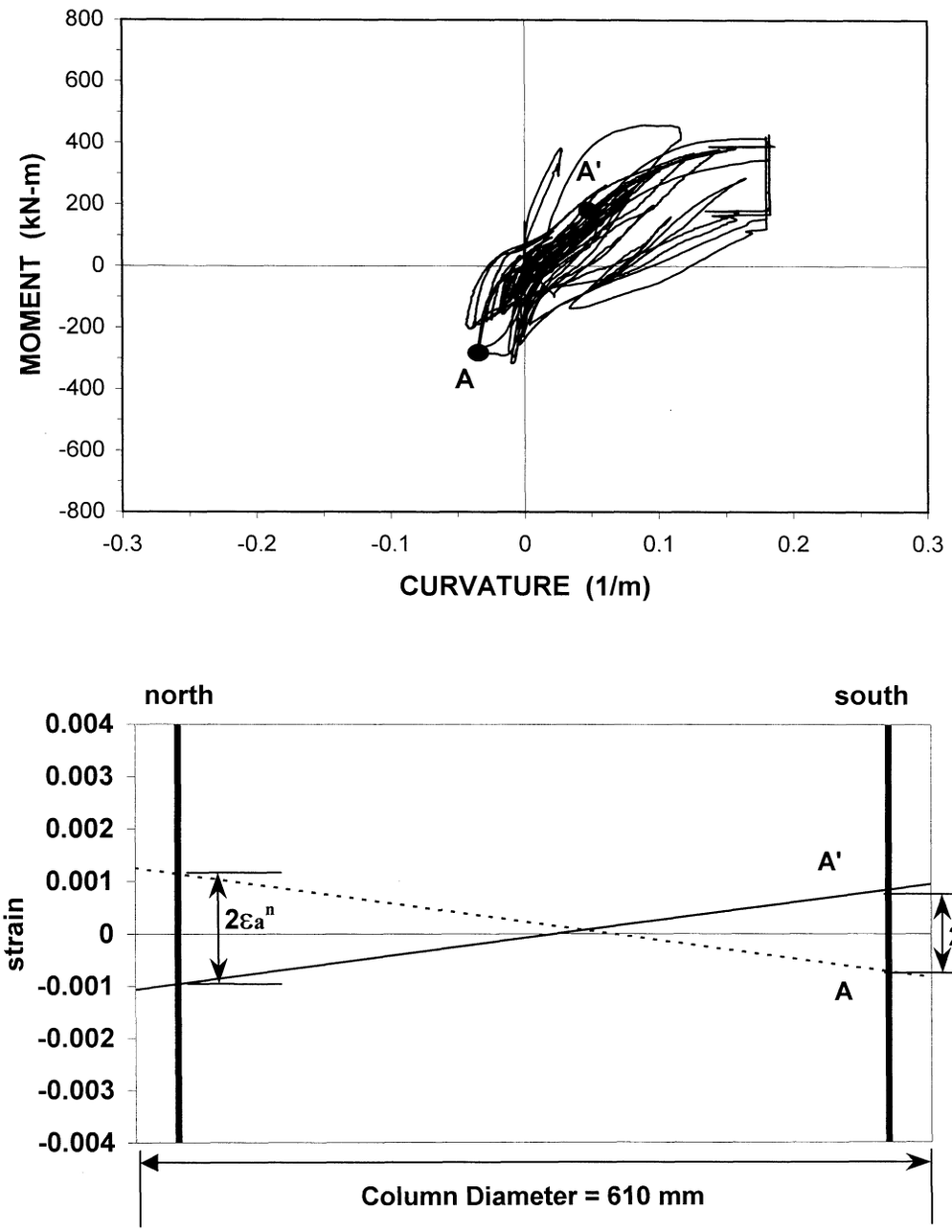

Figure 7-9 **(a) Moment Curvature Plot for the ReCARD Specimen, (b) Strain Profiles at Points indicated in Figure 7-9(a).**

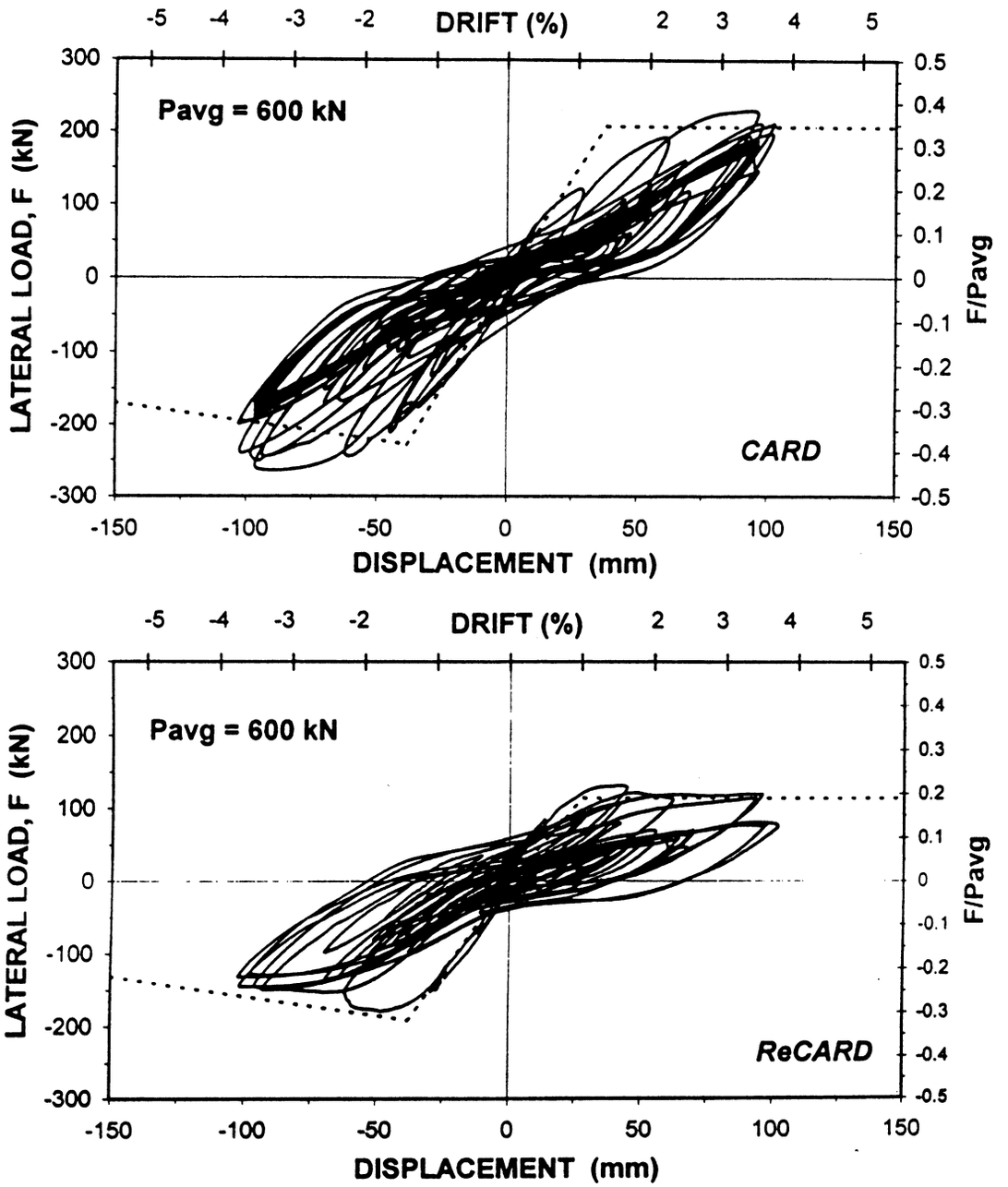

Figure 7-10 Force Displacement Hysteresis Loops for the CARD and ReCARD Specimens.

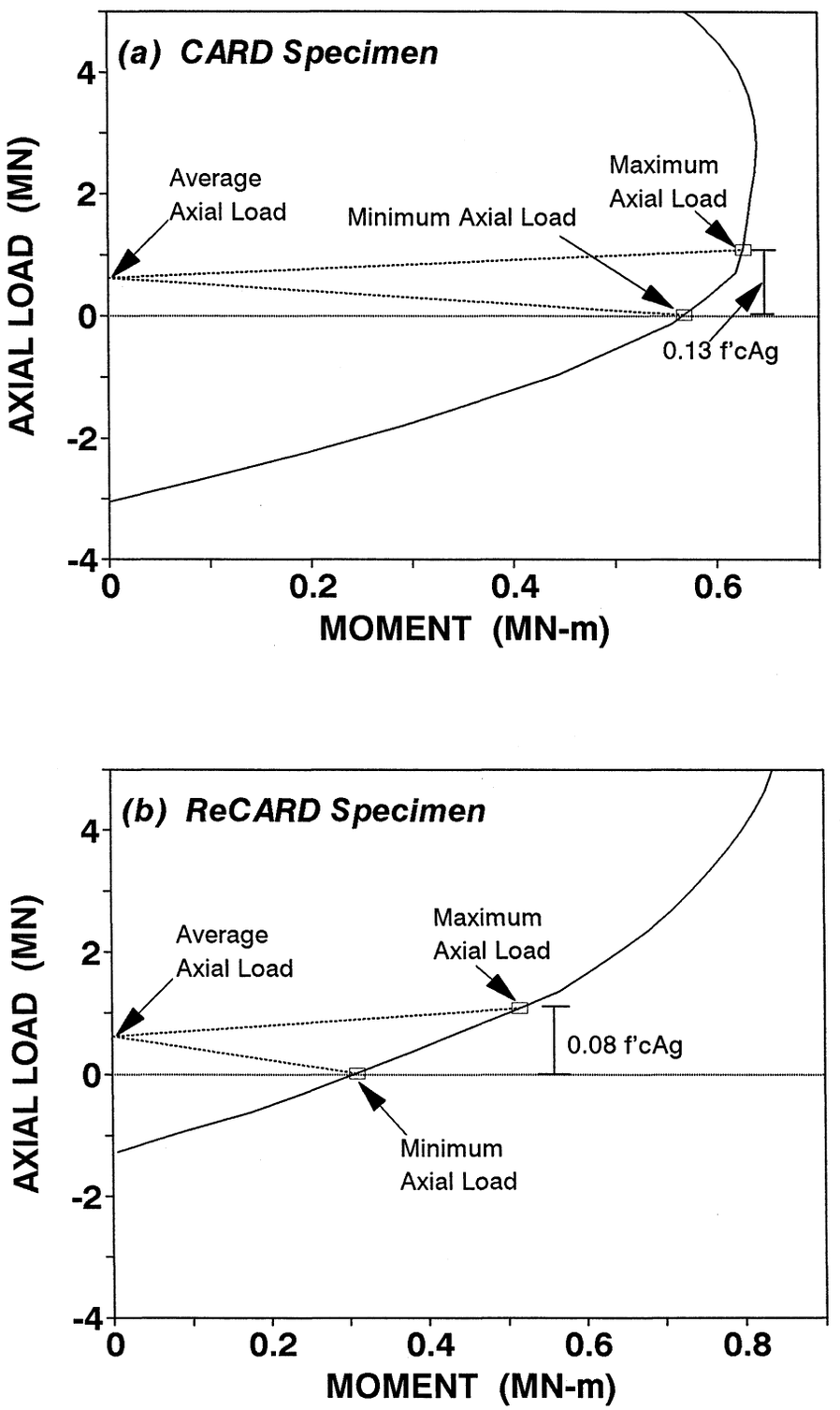

Figure 7-11 Nominal P-M Interaction Diagrams for the CARD and ReCARD Specimens.

SECTION 8
COMPARISON OF THEORETICAL AND EXPERIMENTAL FATIGUE LIFE

8.1 INTRODUCTION

This section compares the theoretical and experimental fatigue life of the 3/4 scale specimens that were tested as part of this current research program. Since the failure mode of the longitudinal reinforcement in these columns was by design that of low cycle fatigue, expressions for fatigue life are derived from such criteria and contrasted with experimental observations.

8.2 THEORETICAL FATIGUE LIFE UNDER SYMMETRICAL LOADING

Symmetrical loading may be thought of as a case that produces equal compression on either side (i.e. same depth to the neutral axis) when the structural element is cyclically loaded. A constant (or variable) amplitude loading with a steady gravity load that targets the same drift amplitude in both the positive and negative direction (push-pull or vice versa) can be thought of as a symmetrical loading case. The strain diagram for such a sectional shape is shown in figure 8-1.

In a recent study on the low cycle fatigue behavior of reinforcing steel, Mander et al. (1994) showed that the plastic strain amplitude (ε_{ap}) is given in terms of the fatigue life (N_f cycles to failure) by the relation

$$\varepsilon_{ap} = 0.08 \left(2 N_f\right)^{-0.5} \tag{8-1}$$

and a replot of the results in terms of total strain amplitude gives a simple relation in the form

$$\varepsilon_a = 0.08 \left(2 N_f\right)^{-0.333} \tag{8-2}$$

where $2N_f$ = number of reversals to the appearance of first fatigue crack, ε_a = total strain and

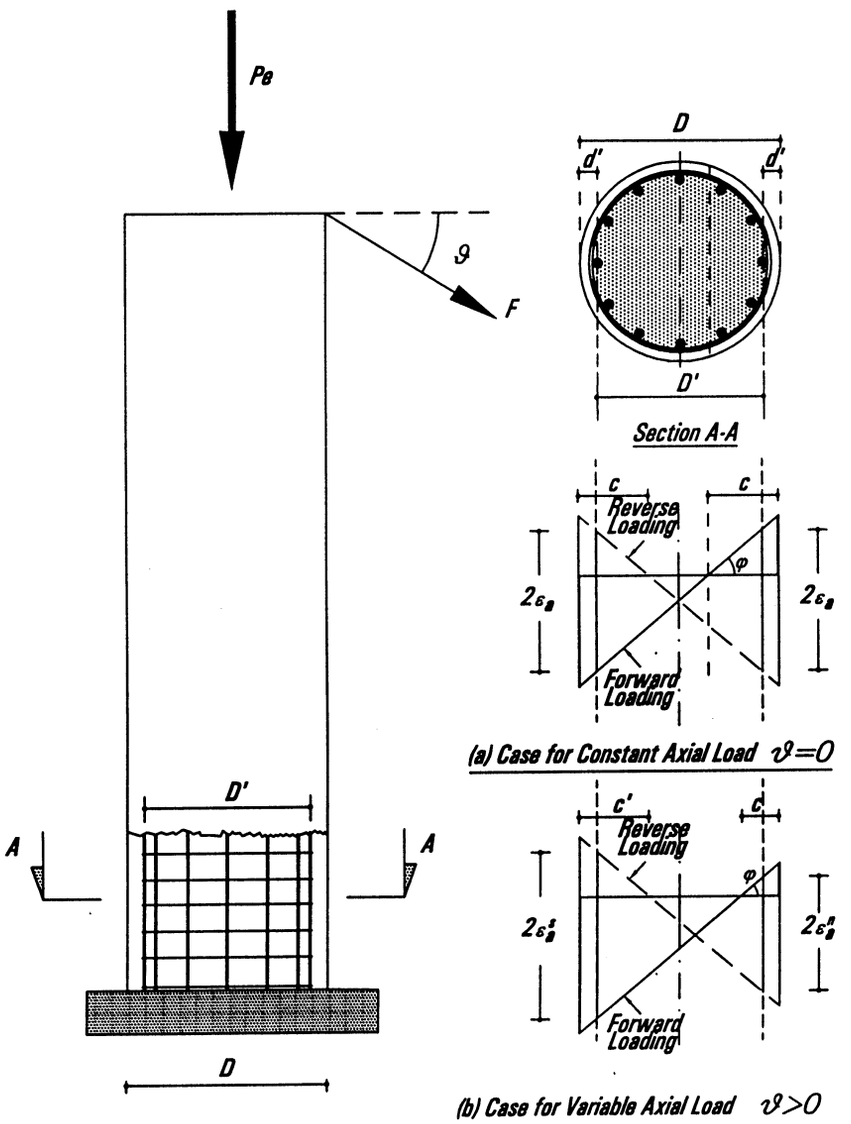

Figure 8-1 **Strain Diagram for a Circular Section under Constant and Variable Axial Loading.**

ε_{ap} = plastic strain at the level of the reinforcing bars.

Using a simple strain transformation and elements of moment area theorem it was shown by Dutta (1995) that the plastic drift amplitude θ_p for specimens failing by low cycle fatigue fracture of the longitudinal reinforcement is given by

$$\theta_p = 0.113 \frac{L_f}{D'} (N_f)^{-0.5} \tag{8-3}$$

where L_f = length of the plastic hinge (or length of the fuse zone) and D' = pitch circle diameter. By rearranging equation (8-3), the theoretical number of cycles to first fatigue crack can be determined as

$$N_f^{theory} = \frac{0.013}{\theta_p^2} \left(\frac{L_f}{D'} \right)^2 \tag{8-4}$$

In case of variable amplitude cyclic loading, θ_p may be thought of as the maximum plastic drift to which the element is cycled.

8.3 Theoretical Fatigue Life under Asymmetrical Loading

Asymmetrical loading may be defined as a case that produces unequal compression on the two opposite sides when the element is cyclically loaded. All realistic earthquake loading can be thought of as asymmetric loading. Since the depth to the neutral axis for the forward and reverse loading are not the same, it is necessary to alter the theoretical fatigue life expression of equation (8-4) to reflect this effect.

Consider the strain diagram of figure 8-1 for the variable axial load case. It is assumed that the neutral axis depth c in the forward direction is less than the corresponding one (c') in the reverse direction. From the same figure it can also be seen that the total strain amplitude on the heavily strained side $2\,\varepsilon_a^s$ is given by

$$2\,\varepsilon_a^s = 2\,\varepsilon_a^* = \phi(D - c - d') + \phi(c' - d') = \phi(D - 2d' - \Delta c) \tag{8-5}$$

where ϕ = curvature, d' = effective cover, $\Delta c = c' - c$ and remaining symbols are easily identifiable from figure 8-1. It can be concluded that for a symmetric loading scenario at the same level of curvature, $\Delta c = 0$ and hence equation (8-5) simplifies to

$$2\,\varepsilon_a = \phi(D - 2d') \tag{8-6}$$

Thus the total strain amplitude at the level of the reinforcing bars for asymmetric loading expressed as a ratio of the corresponding amplitude for symmetric loading can be written as

$$\frac{\varepsilon_a^*}{\varepsilon_a} = \frac{\phi D(1 - 2d'/D \pm \Delta c/D)}{\phi D(1 - 2d'/D)} = 1 \pm \frac{\Delta c/D}{1 - 2d'/D} \tag{8-7}$$

where the $\pm$ sign is used to denote the fact that the asymmetric loading produces larger compressive stresses in the direction for which the neutral axis depth is larger and vice versa. This also signifies that the fatigue life will be less for the reinforcing bars on the heavily compressed side, whereas on the less compressed side of the column fatigue life will increase.

If it is assumed that the change in the neutral axis Δc only affects the compressive force in the concrete (C_c), it can be concluded that the difference in the axial loads in the forward and reverse direction is equivalent to the change in the compressive force of the concrete. Thus

$$\Delta P = \Delta C_c = (\alpha f_c')(\beta \Delta c)\, B_{av} \tag{8-8}$$

where α, β = stress block factors and B_{av} = average width. Solving for Δc in equation (8-8)

$$\frac{\Delta c}{D} = \frac{\Delta P}{\alpha \beta f_c' B_{av} D} \tag{8-9}$$

Since bridge columns are lightly loaded, the neutral axis depth ratio (c/D) for such columns is usually around 0.3. For such a depth, B_{av} can be conservatively taken as $\pi D/4$. Thus

$$\frac{\Delta c}{D} = \frac{\Delta P}{\alpha \beta f_c' (\pi/4D^2)} = \frac{\Delta P}{\alpha \beta f_c' A_g} \tag{8-10}$$

where A_g = gross cross sectional area. Substituting this in equation (8-7)

$$\frac{\varepsilon_a^*}{\varepsilon_a} = 1 \pm \frac{\Delta P / \alpha \beta f_c' A_g}{1 - 2d'/D} \tag{8-11}$$

Since the strain amplitudes ε_a and ε_a^* can be expressed as in equation (8-2) in terms of the number of cycles to fatigue fracture N_f and N_f^*, equation (8-11) can also be expressed in an alternative form as

$$\frac{N_f^*}{N_f} = \left(1 \pm \frac{\Delta P / \alpha \beta f_c' A_g}{1 - 2d'/D} \right)^{-3} \tag{8-12}$$

It is evident that equation (8-12) is critical when the positive sign is considered.

For convenience assume $\alpha = \beta = 0.85$ and $1 - 2d'/D = 0.8$, then the modified number of cycles to fatigue failure (N_f^*) for a column with variable axial load (ΔP) compared to the standard case (N_f) where the axial load is constant ($\Delta P = 0$) is given by

$$N_f^* = \frac{N_f}{\left(1 + 1.73 \frac{\Delta P}{f_c' A_g} \right)^3} \tag{8-13}$$

8.4 Effective Number of Cycles to Failure

The effective number of cycles to failure can be derived using Miner's linear damage accumulation criteria. For a symmetrical loading with increasing drift amplitudes it was shown by Dutta et al. (1998) that the effective number of cycles in terms of the total drift is given by

$$N_f^{exp} = \sum_{i=1}^{n} \left(\frac{\theta_i}{\theta_{max}} \right)^3 \tag{8-14}$$

where θ_i = <u>total</u> drift amplitude for the i-th cycle and θ_{max} = maximum drift.

8.5 COMPARISON WITH EXPERIMENTAL RESULTS

Test R0 and R1: The theoretical number of cycles to fatigue failure expressed by equation (8-4) can be compared to the experimentally obtained cycles to failure (equation 8-14). Alternatively, the inferred plastic strain amplitude using the moment-area theorem can also be compared to equation (8-1) as

$$\varepsilon_{ap} = \frac{(\Delta_u - \Delta_e)}{2(H - \overline{y}_f)} \frac{D'}{L_f} \qquad \textbf{(8-15)}$$

where Δ = applied ultimate displacement, Δ_y = elastic displacement, $\overline{y}_f$ = distance from the top of the foundation to the center of the fuse bar and H = height of the column.

The results expressed in table 8-1 and figure 8-2 show that the theoretical prediction matches very well for the retrofit. However, it exceeds the experimental value for the first repair. This is because the second failure was not exactly true flexural fatigue. Based on a post-test inspection it was apparent that a fatigue notch inadvertently existed in the bar due to faulty machining of the fuse. Evidently the pre-existing flaw was instrumental in leading to a premature fracture. The explanation is reasonable since the fracture of the bar in the north side is again close to the theoretical prediction.

CARD Specimen: This was the first specimen that was tested under the quasi-earthquake loading scheme. The theoretical number of cycles to failure is as obtained using equation (8-4). The corrected value accounting for axial load effects is also evaluated and listed in table 8-2.

Alternatively, the reduction in fatigue life due to variable load effects can be deduced from experimental strain data using a graphical approach. As was discussed previously and evidenced in the strain profiles of figure 7-5(b), the most important effect of the variation of the axial load is to produce asymmetric strain profiles under the forward and reverse loading. If it is presumed that the critical (maximum) strain amplitude ε_a^* is on the south (failure) side of the specimen, then an average strain amplitude ε_a^{avg} can be defined as

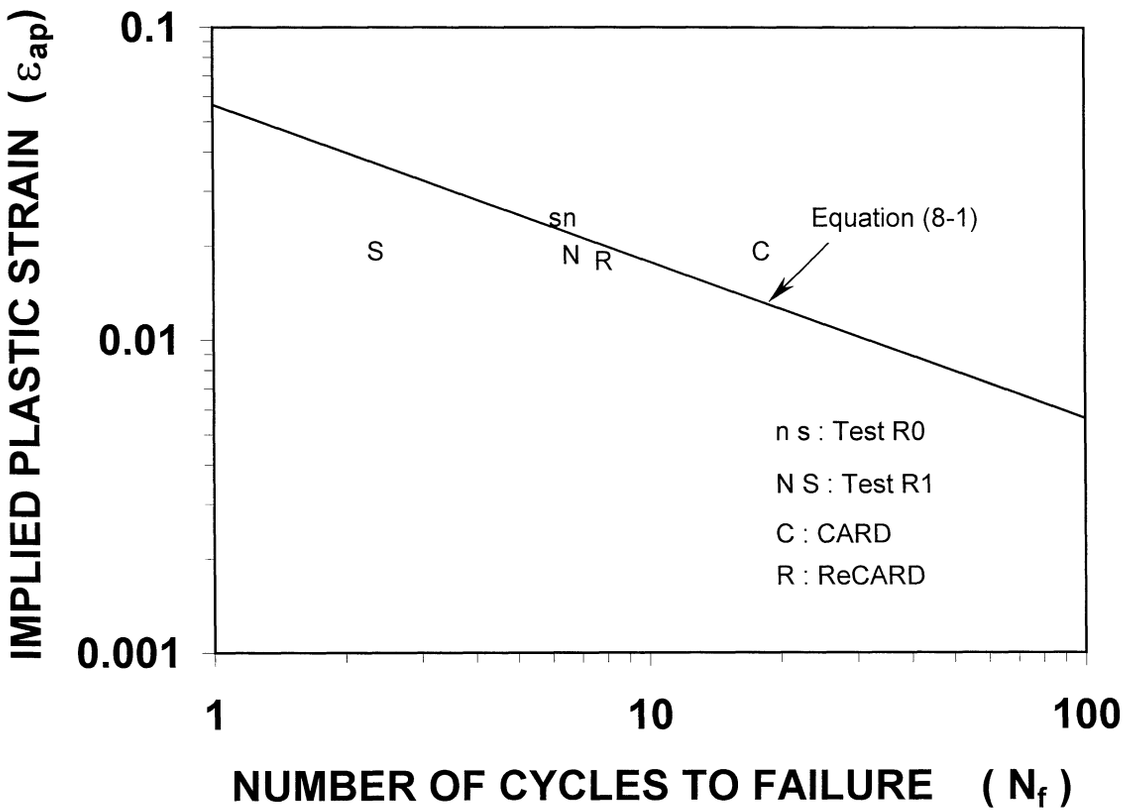

Note: N and S stand for north and south sides respectively.

Figure 8-2 Fatigue Plots for the Test Specimens.

$$\varepsilon_a^{avg} = \frac{\varepsilon_a^N + \varepsilon_a^S}{2} \tag{8-16}$$

where ε_a^N and ε_a^S = strain amplitudes on the north and south side of the column, respectively.

The critical (maximum) strain amplitude thus corresponds to the total strain on the southern side. Hence

$$\varepsilon_a^* = \varepsilon_a^S \tag{8-17}$$

The ratio of the average strain and the critical strain can be related to the reduced fatigue life using equation (8-2) as

$$\left(\frac{\varepsilon_a^N + \varepsilon_a^S}{2\,\varepsilon_a^S} \right)^3 = \frac{1}{8}\left(1 + \frac{\varepsilon_a^N}{\varepsilon_a^S} \right)^3 \tag{8-18}$$

from which

$$\frac{N_f^*}{N_f} = \left(\frac{\varepsilon_a^{avg}}{\varepsilon_a^*} \right) = \frac{1}{8}\left(1 + \frac{\varepsilon_a^N}{\varepsilon_a^S} \right)^3 \tag{8-19}$$

where the symbols are as explained previously.

From the experimentally observed strain profiles in figure 7-5(b), $\varepsilon_a^N / \varepsilon_a^S$ = 0.52. Thus, according to the equation (8-19), the expected number of cycles to fatigue failure for the variable axial load test is $N_f^* = 0.44\,N_f$. This value is shown in parentheses in table 8-2.

The experimental results can also be plotted in a graph as shown in figure 8-2 where the implied plastic strain corresponds to

$$\varepsilon_{ap}^* = \frac{(\Delta_u - \Delta_e)}{2\left(H - \overline{y}_f\right)} \frac{D'}{L_f}\left(1 + 1.73\,\frac{\Delta P}{f_c' A_g} \right) \tag{8-20}$$

obtained by combining equations (8-11) and (8-15). The number of cycles to failure corresponds

to N_f^*.

Test R2: The number of cycles to failure can be calculated in the same manner as was done for the CARD specimen. The number of cycles are modified to account for axial load effects. Details are given in table 8-3.

It is apparent that the variation of axial load affects the fatigue life of the ReCARD specimen as well. However, the strain ratio approach was not applied here due to apparent errors in the potentiometer readings.

Table 8-1 Comparison of Experimental and Theoretical Number of Cycles to First Bar Fracture.

Specimen	Experimental N_f	Theoretical N_f
R0	6.3	6.9
R1	2.3 (6.8*)	6.9

* Represents the experimental number of cycles to the second bar fracture.

Table 8-2 Comparison of Experimental and Theoretical Cycles to Fatigue Failure for the CARD Specimen.

Earthquake/Cycle Suite	Experimental N_f^{expt}	Theoretical	
		N_f	N_f^*
Series of Earthquake	6.6	19.7[a]	10.7[b](8.7[c])
Kobe	1.2		
Cycle	10.3		
Total at Failure $\sum$ =	18.1		

a: For the calculation of N_f, $D' = 497.8\,mm$, $L_f = 406.4\,mm$, $\theta_p = 0.021$.
b: For the calculation of N_f^*, $\Delta P/f_c' A_g = 0.13$
c: Graphical Solution

Table 8-3 Comparison of Experimental and Theoretical Cycles to Fatigue Failure for the ReCARD Specimen.

Earthquake/Cycle Suite	Experimental N_f^{expt}	Theoretical	
		N_f	N_f^*
Series of Earthquake	6.6	19.7	13.4[a]
Kobe	1.2		
Total at Failure $\sum$ =	7.8		

a: For the calculation of N_f^*, $\Delta P/f_c' A_g = 0.08$

8.6 Comparison of Fatigue Life of ReCARD Retrofits with a Conventional Steel Jacket Retrofit

It is of interest to compare the fatigue life of the proposed replaceable hinge retrofitting strategy that uses fuse-bars in accordance with the ReCARD philosophy with a conventional steel jacket retrofit.

The fatigue life of the steel jacket retrofit can be found by using a modified form of equation (8-3). The parameter L_f is replaced by L_p to give

$$\theta_p = 0.08 \frac{L_p}{D'} (2N_f)^{-0.5} \qquad \textbf{(8-21)}$$

where L_p = equivalent plastic hinge length. According to Chai, Priestley and Seible (1991), the equivalent plastic hinge length of a steel jacketed column is given by

$$L_p = L_{gap} + 12\, d_b \qquad \textbf{(8-22)}$$

where L_{gap} = the gap between the end of the steel shell and the cap beam (the gap is normally $50\,mm$) and d_b = diameter of the longitudinal reinforcing bars.

Consider a typical $1500\,mm$ diameter column reinforced with $\#11\,(35\,mm)$ diameter longitudinal rebars. If the column has $50\,mm$ cover and $12\,mm$ diameter hoops, then

$$D' = 1500 - 2 \times (50 + 12) - 35 = 1341\,mm$$

and

$$L_p = 50 + 12 \times 35 = 470\,mm$$

thus

$$L_p / D' = 470 / 1341 = 0.35$$

This is contrasted with a ReCARD design where $L_f / D' = 0.67$ is recommended.

Suppose now for a given design the plastic rotational capacity $\theta_p = 0.02\,rad.$ was chosen. Then, according to equation (8-4) the number of cycles to failure would be 15 and 4 for the ReCARD and the steel jacket solutions, respectively. Not only is the probability of obtaining a rebar fracture in the steel jacket considerably greater than the ReCARD equivalent, but it should be emphasized that once fractured the steel jacket retrofit cannot be easily repaired.

A plot of plastic rotation versus fatigue life shown in figure 8-3 shows that the ReCARD solution gives a consistently higher fatigue life compared to the steel jacket retrofit over the entire range of possible plastic hinge rotations.

8.7 Discussion of Results

It is clear from the previous section that the theoretical predictions match reasonably well with the experimentally observed results. The effect of variation in axial load is clear from the results of Test R2. Although the theoretical results are slightly higher than the experimentally observed values, it should be realized that this is indeed very common in all fatigue-life results. Considering this, the results can be considered satisfactory.

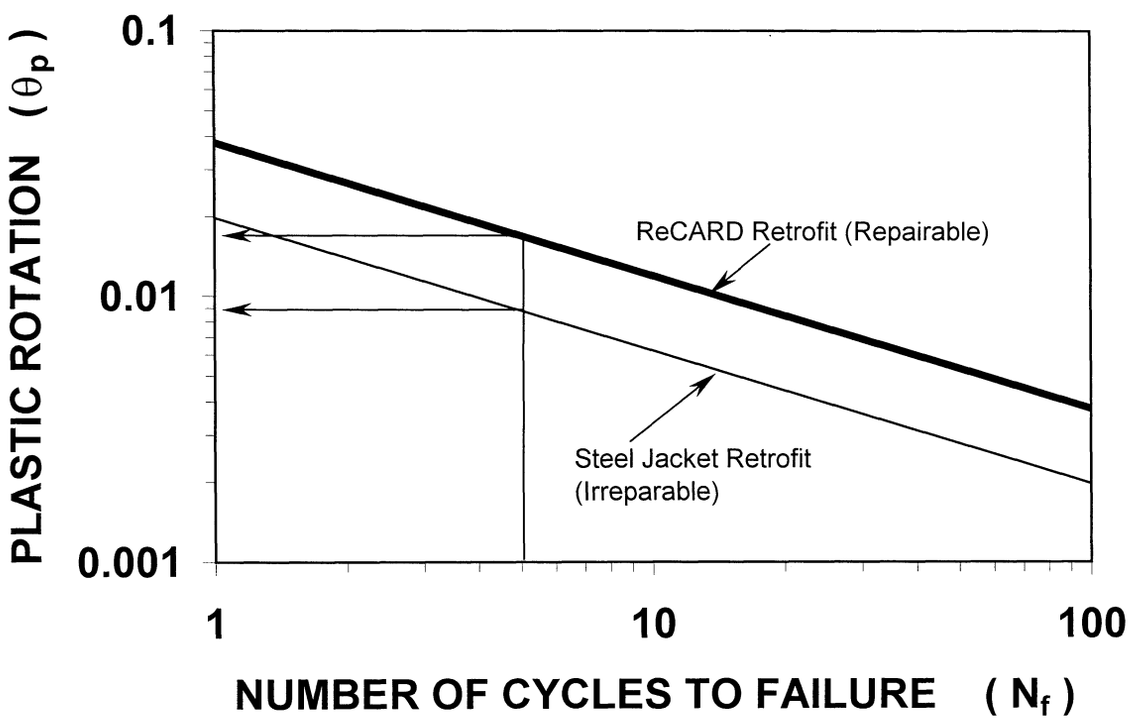

Figure 8-3 Comparison of the Fatigue Life for the ReCARD and Steel Jacket Retrofit.

SECTION 9
SUMMARY AND CONCLUSIONS

9.1 SUMMARY

This report has been concerned with two issues. First, the Control and Repairability of Damage (CARD)design philosophy developed by Cheng and Mander (1997) for new structures has been extended to incorporate seismic retrofitting of existing non-ductile bridge columns. Like the CARD approach the Retrofit Control and Repairability of Damage (ReCARD) approach developed herein uses specially machined fuse-bars which are installed in the potential plastic hinge zone. Under reversed cyclic lateral loading all seismically induced damage is restricted to the fuse-bar zone—all other regions, including the foundation or cap beam connection and the column itself, remain elastic and undamaged. In addition damage in the fuse-bar zone is repairable.

The second objective of this report was to investigate the effect of experimental load path including the effect of axial load variations arising from frame action plus vertical ground motions on the seismic performance and fatigue life of columns constructed using either CARD or ReCARD philosophies.

The Quasi-Earthquake Displacement (QED) experimental technique was proposed in this research as a means for testing structures subjected to seismic input in quasi-static conditions. QED uses a non-linear time-history computational simulation to predict seismic displacements and forces in a prototype structure. These earthquake-induced actions are scaled to permit laboratory experiments on reduced scale subassemblages of the prototype structure.

For testing the efficacy of the proposed retrofit methodology, a 3/4 scale column representative of as-built columns typically found in practice, was constructed in the laboratory and retrofitted in accordance with the ReCARD principles proposed herein. Special fuse-bars

that permit full repair and restoration following an earthquake were installed at the potential damage zones. The results of the tests showed that the strong upper portion of the specimens remained undamaged at all stages of loading. All damage was forced into the sacrificial reinforced concrete hinge zones. The flexure-fatigue failure mode was dominant. In terms of hysteretic performance, the models demonstrated good energy dissipation characteristics and maintained a steady lateral resistance until the fracture of a longitudinal bar occurred due to low cycle fatigue.

9.2 CONCLUSIONS

The following conclusions are drawn from the this research:

1. The ReCARD approach for retrofitting bridge columns introduced as part of this research is suitable for deficient columns with inadequate lap splice or poor confinement at the potential plastic hinge zones. The proposed methodology is a significant departure from the currently used techniques since it allows for repeated usage and is apparently unaffected by past seismic history. On the contrary, other methods like steel or composite jacketing may suffer from major deficiencies including: (i) reduced fatigue life due to a short hinge zone; and (ii) jacket retrofits do not allow for easy repairability after an earthquake. Moreover, the bridge owner may be unaware as to the extent of damage incurred to the main column since damage may be hidden by the presence of the jacket.

2. $P-\Delta$ effects which are not properly accounted for in currently used experimental setups can be properly modeled using some modifications. This allows the full strength of the specimen to be mobilized under simulated seismic loading.

3. The effect of sensitivity to realistic earthquake input was investigated. Results show that axial load affects the fatigue life of columns. This aspect may become important for building columns where the axial load variations are likely to be relatively high.

4. Due to the provision of fuse-bars, the fatigue capacity of reinforced concrete bridge columns designed in accordance with either the CARD or ReCARD philosophies is governed by fatigue life of fuse-bar. The fatigue capacity can be tuned to the fatigue demand by providing an appropriate length of fuse-bars. The recommendation that $L_f = 0.67\,D$, where L_f = length of a fuse and D = diameter of the column of Cheng and Mander (1997) seems reasonable.

SECTION 10

REFERENCES

AASHTO (1994), *AASHTO LRFD Bridge Design Specifications*, 1st ed., American Association of State Highway and Transportation Officials, Washington, D.C.

AISC (1995), *Load and Resistance Factor Design*, 2nd. ed., American Institute of Steel Construction, Chicago, IL.

Chai, Y.H., (1996) "An Analysis of the Seismic Chracterestics of Steel Jacketed Circular Bridge Columns", Earthquake Engineering and Structural Dynamics, Vol. 25, pp. 149-161.

Chai, Y.H., Priestley, M.J.N. and Seible, F., (1991), "Seismic Retrofit of Circular Bridge Columns for Enhanced Flexural Performance", ACI Structural Journal, Vol. 88, No. 5, pp. 572-584.

Cheng, C.T., (1997), *New Paradigms for the Seismic Design and Retrofit of Bridges*, Ph.D. Dissertation, Department of Civil Engineering, State University of New York at Buffalo, Buffalo, New York.

Cheng, C.T. and Mander, J.B., (1997), *Seismic Design of Bridge Columns Based on Control and Repairability of Damage*, Technical Report NCEER-97-0013, National Center for Earthquake Engineering Research, State University of New York at Buffalo, Buffalo, New York.

Dutta, A., (1995), *Fatigue Analysis of Non-Ductile Concrete Columns*, M.S. Thesis, Department of Civil Engineering, State University of New York at Buffalo, Buffalo, New York.

Dutta, A. and Mander, J.B., (1998), *Capacity Design and Fatigue Analysis of Confined Concrete Columns*, Technical Report MCEER-98-0007, Multidisciplinary Center for Earthquake Engineering Research, State University of New York at Buffalo, Buffalo, New York.

Igarashi, A., Seible, F. and Hegemier, G.A., (1993), *Development of the Generated Sequential Displacement Procedure and the Simulated Seismic Testing of the TCCMAR 3-Story Inplane Walls*, TCCMAR Report No. 3.1(b)-2.

Kunnath, S., El-Bahy, A., Taylor, A. and Stone, W., (1997), *Cumulative Seismic Damage of Reinforced Concrete Bridge Piers*, Technical Report NCEER-97-0006, National Center for Earthquake Engineering Research, State University of New York at Buffalo, Buffalo,

New York.

Mander, J.B., Cheng, C.T., (1997), *Seismic Resistance of Bridge Piers Based on Damage Avoidance Design*, Technical Report NCEER-97-0014, Multidiciplinary Center for Earthquake Engineering Research, State University of New York at Buffalo, Buffalo, New York.

Mander, J.B., Panthaki, F.D., and Kasalanati, A., (1994), "Low Cycle Fatigue Behavior of Reinforcing Steel," Journal of Materials in Civil Engineering, ASCE, Vol.6, No.4, pp.453-467.

Mander, J.B., Priestley, M.J.N. and Park, R.,(1983), *Behavior of Ductile Hollow Reinforced Concrete Columns,* Bulletin of the New Zealand national Society for Earthquake Engineering, Vol.16, No.4, Dec-83, pp.273-290.

Mander, J.B., Priestley, M.J.N. and Park, R., (1984), *Seismic Design of Bridge Piers,* Department of Civil Engineering, University of Canterbury, Report 84-2, Feb-84, 483 pp.

Priestley, M.J.N, Seible, F. and Calvi, G. M., (1996), *Seismic Design and Retrofit of Bridges*, John Wiley and Sons, Inc., New York.

Seible, F., Hegemier, G.A., Priestley, M.J.N., Kingsley, G.R., Kurkchubasche, A.G., Igarashi, A. and Weeks, J.S., (1994), *The US-TCCMAR Full-Scale Five Story Masonry Research Building Test*, Report No. 94-1.

Sheikh, S.A. and Yeh, C.C., (1990), "Tied Concrete Columns Under Axial Load and Flexure", Journal of the Structural Division, ASCE, Proceedings, Vol. 116, No. 10, pp. 2780-2801.

Xiao, Y. and Rui, M. (1997), "Seismic Retrofit of RC Circular Columns Using Prefabricated Composite Jacketing", Journal of Structural Engineering, Vol. 123, No. 10, pp. 1357-1364.

Yuk Lung Wong, (1990), *Squat Circular Bridge Piers Under Multi-Directional Seismic Attack*, Ph.D. Thesis, Department of Civil Engineering, University of Canterbury, Christchurch, New Zealand.

MULTIDISCIPLINARY CENTER FOR EARTHQUAKE ENGINEERING RESEARCH

A National Center of Excellence in Advanced Technology Applications

University at Buffalo, State University of New York
Red Jacket Quadrangle ▪ Buffalo, New York 14261-0025
Phone: 716/645-3391 ▪ Fax: 716/645-3399
E-mail: mceer@acsu.buffalo.edu ▪ WWW Site: http://mceer.buffalo.edu

University at Buffalo *The State University of New York*

ISSN 1520-295X